University of Sheffield

Investigation of Diabetes-Induced Histological Changes in the Peripheral Sensory Neurons

Thesis Submitted for the Degree of Doctor of Philosophy

Reham Mansour Filfilan

Supervised by

Dr. Mohammed Nassar

The University of Sheffield

School of Bioscience

2024

Acknowledgement

Abstract

Diabetic peripheral neuropathy (DPN) is the most common type of neuropathy, which is characterised by the degeneration of the peripheral nerves. The symptoms of DPN begin distally, in the lower limbs, then progress proximally to the upper limbs, producing the characteristic "stockings and gloves" distribution. Patients with DPN experience positive symptoms, including tingling, pinprick sensation, and pain, which affect 30% of diabetic patients, while up to 50% experience negative symptoms, such as numbness and a loss of sensation. These sensory deficits increase the risk of developing foot ulcers and gangrene; of the patients who are affected by these problems, 25% are at risk of developing amputation. This highlights the significant impact of sensory loss on the quality of life of DPN patients. However, the precise mechanism underlying sensory deficit remains unclear. Dorsal root ganglia (DRG) contain the sensory neurons and are particularly vulnerable to damage due to diabetes. In this study, we investigated histological changes in the sensory neurons in the lumbar DRG of 32-week-old db/db mice, focusing on changes that might cause sensory deficit related to DPN. Sympathetic sprouting into the DRG has been linked to pain in nerve injury models. Thus, we investigated whether the sympathetic sprouting occurred in the db/db mice, which might contribute to pain in DPN. No sympathetic sprouting was detected in the DRG of the db/db mice. However, a slight increase in the TH-positive neurons, accounting for 3.69% and 4.42% in the L4 and L5 DRG, respectively, were found. Then, we further investigated previous data from our lab, which showed a reduction in the large-diameter neurons in cultured DRG from the db/db mice. Here, we examined changes in the number and soma size of large-diameter neurons (labelled neurofilament 200) and small-diameter neurons (labelled peripherin) in the db/db mice (*in vivo*). Our findings revealed a 12.46% reduction in large-diameter neurons, with a decrease in the size of their soma diameter. No change was observed in small-diameter neurons. In addition, we were the first to characterise the presence of cytoplasmic vacuoles in large-diameter neurons, with vacuolated neurons being 11.27% more prevalent in the db/db mice. The number of vacuoles increased in diabetic mice, ranging between 5 and 8 per neuron. However, the origin of these vacuoles could not be determined using cellular markers. The findings of this study offer insights into the structural changes within the specific population of the DRG sensory neurons, which are particularly vulnerable in DPN. These large-diameter neurons are responsible for detecting

touch and vibration, so their loss might explain sensory deficit in DPN, and so contribute towards a therapeutic approach that targets these neurons to minimise sensory deficit.

Declaration

I declare that this thesis is the result of my own work carried out in the School of Bioscience, University of Sheffield, between October 2020 and October 2024, and has been composed entirely by myself. All supporting literatures, resources, and collaborative contributions have been acknowledged clearly. It is not substantially the same as any work that has already been submitted before for any degree of other qualification at the University of Sheffield or other institution.

Signature:

Reham Mansour Filfilan

October 2024

List of abbreviations

53BP1	P53-binding protein1
AD	Alzheimer's Disease
AGE	Advanced Glycation End-products
ALS	Amyotrophic Lateral Sclerosis
AOI	Area of interest
ATG	autophagy-related genes
ATG12	Autophagy-Related 12
ATP5A	ATP-synthase subunit alpha
BMI	Body-mass index
BSA	Bovine Serum Albumin
Calr	Calreticulin
CAP	Capsaicin
CCD	Chronic compression DRG
CCI	Chronic compression injury
CGRP	Calcitonin gene-related peptide
CMA	Chaperone-mediated autophagy
CNC	Chronic nerve compression
CNS	Central nervous system
CV	conduction velocity
DAPI	6-diamidino-2-phenylindo
DBH	Dopamine-B-hydroxylase
DM	Diabetes mellitus
DN	Diabetic neuropathy
DNA	Deoxyribonucleic acid
DPN	Diabetic peripheral neuropathy
DREZ	dorsal root entry zone
DRG	Dorsal root ganglia
ER	Endoplasmic Reticulum
ERAD	Endoplasmic Reticulum-associated protein degradation
GA	Golgi Apparatus
GLUT	Glucose Transporter
GM130	Golgi matrix protein 130
HD	Huntington's disease
HFD	High-fat-diet
HIF1A	Hypoxia-inducible factor 1-alpha
IASP	International Association of the Study of Pain
IDF	International Diabetic Federation
IENFDs	Intraepidermal nerve fibre densities
IHC	Immunohistochemistry
IL-1B	interleukin 1B
LAC	lactate
LC3B	Microtubule-associated proteins 1A/1B light chain 3B

Lepr	Leptin receptor
MCT	Monocarboxylate transporter
NCV	Nerve conducting velocity
NDD	Neurodegenerative diseases
NDS	Neuropathy Disability Score
NeuPSIG	Interest Group on Neuropathic Pain
NF	Neurotropic Factor
NF200	Neurofilament 200
NGF	Nerve Growth Factor
NIF	Neuronal intermediate filament
NOD	Non-Obese Diabetic
Non-VNs	Non-vacuolated neurons
NSPL2	Neuroendocrine specific protein like 2
NSS	Neuropathy Symptom Score
OCT	Optimal cutting Temperature
OS	Oxidative Stress
PBS	Phosphate Buffered Saline
PD	Parkinson's Disease
PDN	Painful diabetic neuropathy
PKC	Protein Kinase C
PNL	partial nerve ligation
PNS	Peripheral nervous system
PO	Post operation
PRPH	Peripherin
PYR	Pyruvate
Rab-7	Ras-related protein 7
RAGE	Receptor for advanced glycation end-products
ROS	Reactive oxygen species
RT	Room temperature
scRNA-seq	Single-cell RNA sequencing
SCs	Schwan cells
SEM	Standard error of mean
SGCs	Satellite Glial Cells
S-LANSS	Leeds Assessment of Neuropathic Symptoms and Signs
SMP	Sympathetically mentioned pain
SNL	Spinal nerve ligation
SOD	Superoxide dismutase
SP	Substance P
SSL	Segmental spinal ligation
STZ	Streptozotocin
SV2A	Glycoprotein 2-alpha
T1DM	Type 1 diabetes mellitus
T1DN	Type 1 diabetic neuropathy
T2DM	Type 2 diabetes mellitus
T2DN	Type 2 diabetic neuropathy
Tau	Microtubule binding protein tau

TCAs	Tricyclic
TDP-43	TAR DNA-binding protein-43
TH	Tyrosine hydroxylase
TNF-a	Tumour necrosis factor a
TRPa	Transient Receptor Potential-activated
UPR	Unfolded Protein Response
VGSC	Voltage Gated Sodium Channel
VNs	Vacuolated Neurons

Table of Contents

List of Figures

List of Tables

Chapter 1: General Introduction

1.1 Diabetes Mellitus

Diabetes Mellitus (DM) is a chronic metabolic disorder that is marked by persistent hyperglycaemia (elevated blood glucose levels), dysisnulinemia (abnormal insulin levels), and various complications (Sapra A, 2023). There are two main types of DM: *Type 1 DM (T1DM)*, also known as insulin-dependent DM; and *Type 2 DM (T2DM)*, also known as non-insulin-dependent DM (Figure 1.1) (Ibrahim and Megahed, 2013). DM affects a substantial proportion of the global population and is considered a global pandemic that requires global intervention to address its risk factors (Kavakiotis *et al.*, 2017). The International Diabetes Federation (IDF) estimated that 536 million individuals would have diabetes by 2021, and this figure is estimated to reach 643 million by 2030 and 783 million by 2045 (Magliano and Boyko, 2021; Sun *et al.*, 2022). In 2050, a third of the anticipated 9.7 billion living individuals will have either T1DM or T2DM (Boyle *et al.*, 2010). DM is associated with macrovascular complications, which primarily affect the large blood vessels and increase the risk of cardiovascular diseases. It is also associated with microvascular complications, which affect small blood vessels, including those in the retina (retinopathy), the kidneys (nephropathy), and the nervous system (leading to neuropathy) (Fowler, 2008). DM is considered a risk factor for the development of diabetic neuropathy (DN) (Akter *et al.*, 2020; Entezari *et al.*, 2022). The long-term complications of DM significantly impact morbidity, mortality, and quality of life (Pelletier *et al.*, 2012).
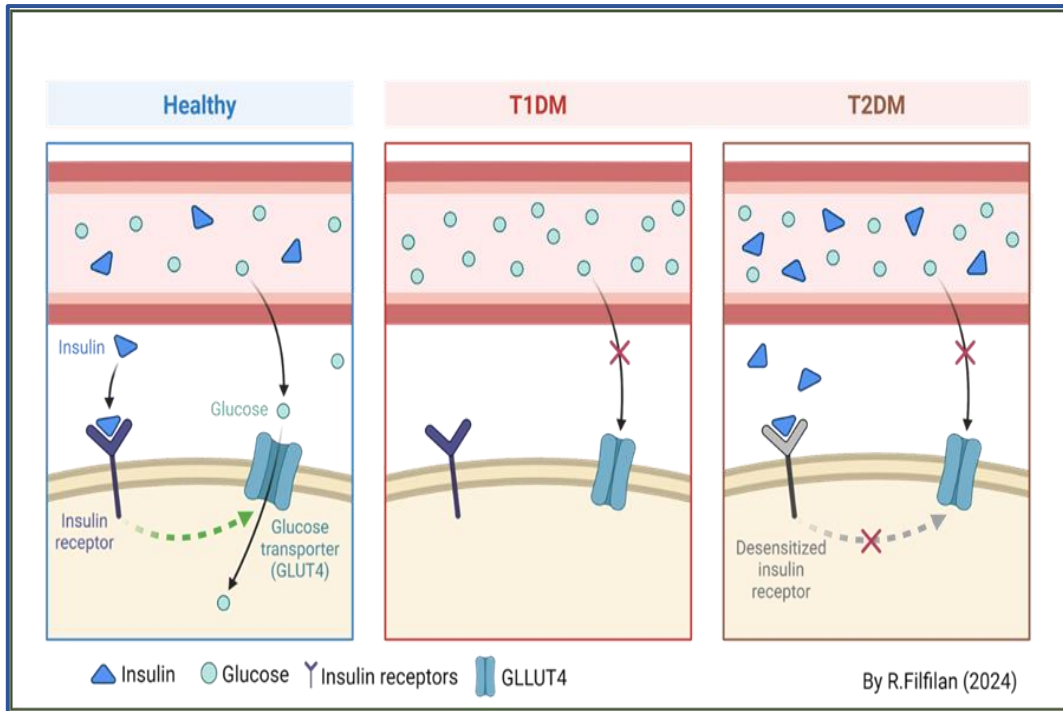
Figure 1.1 Comparison between insulin production in healthy, T1DM and T2DM individuals

(A) In a healthy individual, insulin is produced by pancreatic βcells (blue triangle) to allow glucose (light blue circle) uptake by glucose transporter cells 4 (GLUT4, turquoise). (B) In T1DM individuals, insulin production is disrupted, resulting in the accumulation of glucose in the bloodstream. (C) In T2DM individuals, insulin is produced, but insulin receptors are desensitised, resulting in glucose failing to bind to GLUT4 receptors, which decreases glucose uptake. (Created with BioRender).

1.2 Diabetic Neuropathy

Diabetic Neuropathy (DN) is the most common complication of diabetes, which causes persistent nerve damage (Samakidou et al., 2021). It is estimated that 30-50% of diabetic individuals suffer from neuropathy (Edwards *et al.*, 2008). DN affect different classes of nerves, i.e. sensory, motor, and autonomic nerves, where the symptoms vary between types. There are several types of DN, including *Diabetic peripheral neuropathy (DPN)*, which is the most common and characterised by nerve damage to long axons in the hands and lower limbs (Peltier, Goutman and Callaghan, 2014). *Entrapment neuropathy,* which is characterised by compression of median, ulnar, and peroneal nerves, causes tingling and pain (Madani and Doughty, 2020). Diabetic autonomic neuropathy (DAN), which affects parasympathetic and sympathetic nerves that innervate the heart and blood vessels (Li *et al.*, 2011). *Radiculopathy*, which affects the nerves of the lumbosacral plexus and sacral plexus, causes weakness in the upper leg and thigh, which leads to symptoms of pelvic and femoral pain (Thaisetthawatkul and Dyck, 2020). *Multifocal or multiplex neuropathy*, which affects the nerves of the brachial plexus, causes weakness in the proximal upper limbs with no sensory loss (Beadon and Léger, 2020) (Figure 1.2).
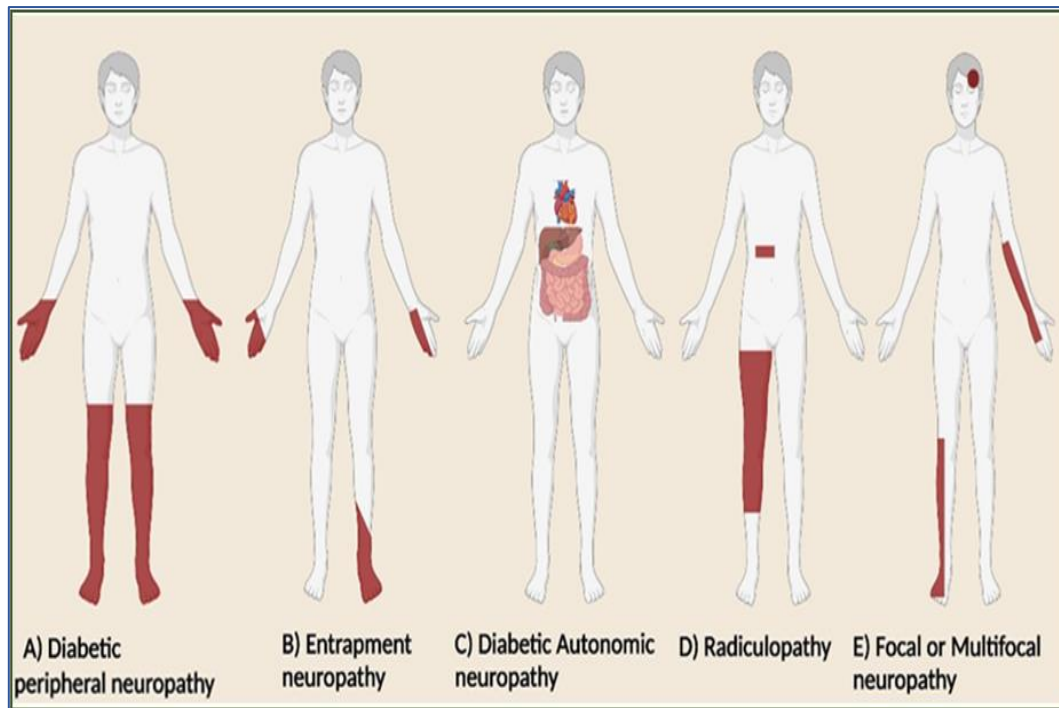
Figure 1.2 Types of Diabetic Neuropathy (DN)

(A) Diabetic peripheral neuropathy, the most common type affecting peripheral nerves in long axons. (B) Entrapment neuropathy affects the cranial, median, and peroneal nerves (C) Diabetic autonomic neuropathy affects the parasympathetic and sympathetic nerves (D) Radiculopathy affects the lumbar and sacral nerve (E) Multifocal neuropathy affects the brachial nerves. (Adopted from Kaur et al., 2023).

1.2.1 Diabetic Peripheral Neuropathy

Diabetic peripheral neuropathy (DPN) is the most common type of DN. It is defined as ''the presence of signs or/and symptoms of peripheral nerve dysfunction in the individual with diabetes after exclusion of other causes'' (Yu, 2021). DPN affect the long axons in the periphery. It begins distally in the lower limbs, particularly at the toe, and progresses proximally to affect the upper limbs, resulting in stocking and glove distribution (Peltier, Goutman and Callaghan, 2014). This anatomical pattern and the nerve damage consequent to T2DM highlight the distal-to-proximal symptomatology in DPN manifest (Eid *et al.*, 2023).

1.2.1.1 Epidemiology of DPN

Globally, DPN affects almost half of all individuals with diabetes (Iqbal *et al.*, 2018). In Europe, the prevalence of DPN is 20-60 % in patients who have been diagnosed with DM within 4-10 years (Abbott *et al.*, 2011; Burns and Mauermann, 2011). The prevalence of DPN between T1DM and T2DM varies across different studies; in T1DM, it ranges from 17.5% to 28.7%. DPN prevalence is higher in T2DM, ranging from 31.5% to 50.7%, with the highest reaching 73% (Cristian and Remus, 2018; Soundararajan *et al.*, 2021; Sun *et al.*, 2022). The incidence of DPN is also higher in T2DM (6,100 per 100,000 person-years) compared to T1DM (2,800 per 100,000 person-years) (Ang *et al.*, 2014; Martin, Albers and Pop-Busui, 2014).

1.2.1.2 Symptoms of DPN

The symptoms of DPN can involve both increased sensitivity (positive symptoms) and decreased sensitivity (negative symptoms) (Said, 2007). Approximately 13-22% of T2DM patients experience positive sensory symptoms, including tingling, pinpricks, burning, and stabbing-like pain (Spallone and Greco, 2013). These positive symptoms are accompanied by tactile allodynia (pain triggered by an ordinary non-painful stimulus) or thermal hyperalgesia (an increased pain response to a typically painful stimulus) (Feldman *et al.*, 2019). They may occur intermittently or persist from between a few months to several years. The positive symptoms of DPN can cause serious complications, including leg ulceration, gangrene, and an increased risk of amputation (Amin and Doupis, 2016). Patients often describe this pain as ''extreme pain which keeps individuals awake'' (Didangelos, Doupis and Veves, 2014). On the other hand, the negative symptoms of DPN are characterised by progressive sensory loss, which results in numbness (Divisova *et al.*, 2012). Numbness accounts for almost 50% of the total T2DM-DPN patients at risk of developing foot ulcers; of these, 25% are at risk of

amputation (Singh, Kishore and Kaur, 2014). T2DM accounts for almost half of foot amputations globally (Bruun *et al.*, 2013). Thus, no specific diagnostic approach is reliable due to this variability of T2DM-DPN symptoms.

DPN patients can be assessed for negative symptoms using the Neuropathy Disability Score (NDS), which is a scoring system for evaluating the risk of developing foot ulcers. While the Semmes-Weinstein 10-gram monofilament test is used to assess tactile impairment due to sensory cutaneous loss, the pinprick test is used to evaluate sensory deficits, and a 128 Hz tuning fork is used to identify impairment in vibration perception (Boulton, 2014). In addition, the Neuropathy Symptom Score (NSS) is used as a screening tool for pain sensation and severity (Zhu *et al.*, 2018).

1.3 The peripheral nerve constituent and function

The PNS comprises three divisions: the somatosensory, somatomotor, and autonomic divisions (Udit, Blake and Chiu, 2022). The somatosensory division contains afferent sensory neurons which relay sensory stimuli from the periphery to the CNS. The response signal is then transmitted through efferent neurons in the somatomotor components and expressed as movement. The autonomic nervous system contains the pre- and post-ganglionic neurons of the sympathetic nervous system, which innervate the muscles and glands (Jenkins and Lumpkin, 2017). The cell bodies of the somatomotor neurons are located in the ventral horn of the spinal cord. The pre-ganglionic sympathetic neurons reside in the intermediolateral cell column. The soma of the somatosensory neurons resides in the dorsal root ganglia (DRG).

The anatomy of the peripheral nerve is typically formed by a combination of large myelinated Aα-fibres, small-myelinated sensory Aβ- and Aδ-fibres, and unmyelinated C-fibres (Winston, 2023). These nerve fibres are covered by a layer of loose connective tissue (endoneurium) and form fascicles, surrounded by another layer of connective tissue (perineurium). These fascicles are grouped as bundles, covered by a further layer of connective tissue (containing collagen) called the 'epineurium'. This outer layer supports and protects the nerve against injury and compression. The peripheral nerves contain small blood vessels and arteries that extend into the epineurium and branch out to the perineurium to provide metabolic support (Figure 1.2) (Ilfeld, Preciado and Trescot, 2016; Winston *et al.*, 2023).
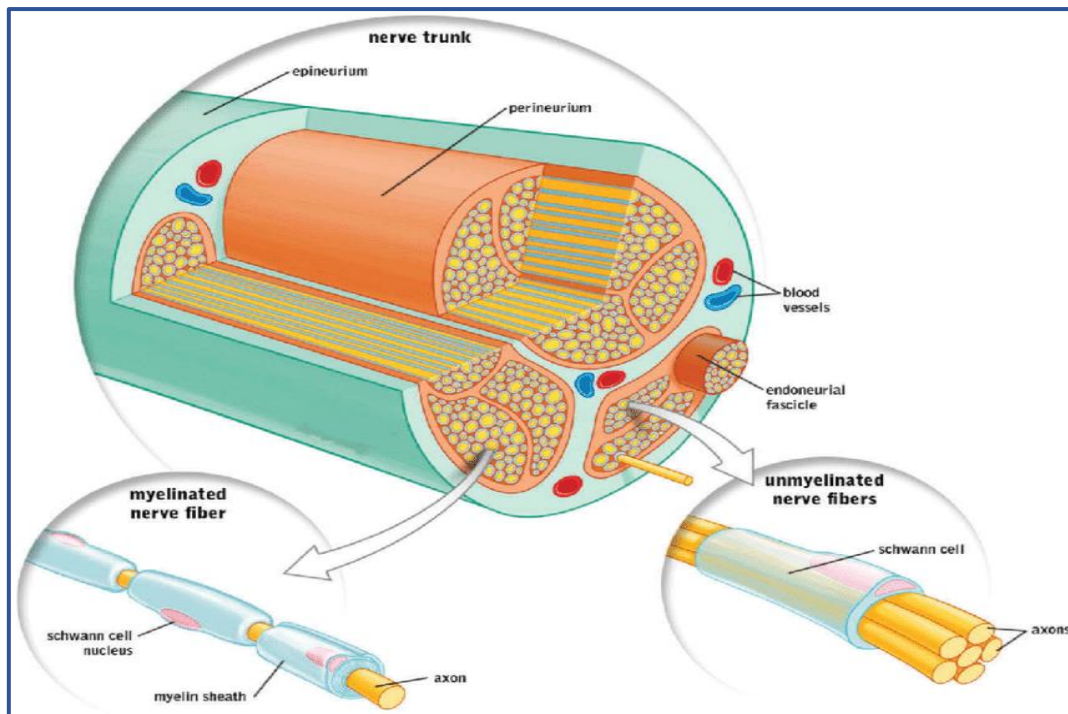
Figure 1.3 Anatomy of the Peripheral Nerve

A typical peripheral nerve is surrounded by three layers, arranged from the outer to the innermost layers. The innermost layer (the endoneurium) surrounds the individual nerve fibres within the nerve trunk. The bundle of nerve fibres is then covered by the middle layer (the perineurium) and forms fascicles, supplied by the blood vessels. The outermost layer (the epineurium) surrounds the peripheral nerve. Individual, large-myelinated fibres are covered by a myelin sheath, formed by Schwann cells, while the unmyelinated nerves are surrounded by non-myelinating Schwann cells. (Adopted from Winston, 2023).

1.3.1 Classification of the peripheral nerves

The peripheral nerve fibres are classified into three groups (A-fibres, B-fibres, and C-fibres), based on their myelination class, axon size, conducting velocity (CV), and function. **Type A-fibres** are myelinated and contain the largest group, with four subtypes (α, β, γ, and δ). Aα-fibres are thickly myelinated with large diameters (13-20 μm) and the fastest CV, ranging from 80-120m/sec. They innervate the muscle spindle and respond to muscle contraction. Aβ-fibres are myelinated, with diameters ranging from 6-22 μm and an intermediate CV (30-120m/sec). They represent low-threshold cutaneous mechanoreceptors, that are activated in response to light touch, vibration, and hair movement (Zochodne, 2008; Manzano et al., 2008; Purves et al., 2012). Aγ-fibres are thinly myelinated, with diameters ranging from 2-8 μm, and a slow CV (15-30m/sec). They innervate the muscle spindles and are activated in response to muscle lengthening. Aδ-fibres are thinly myelinated, with diameters ranging from 1-5 μm, and a slow CV (5-25m/sec). They process information on sharp pain, pressure, temperature (hot/cold) and crude touch (Gasser, 1941; Zochodne, Ramji and Toth, 2008). **Type B-fibres** are myelinated autonomic pre-ganglionic fibres. **Type C-fibres are** unmyelinated autonomic post-ganglionic, have a small diameter (0.4-1.2 μm), and have the slowest CV (0.4-2 m/s). Most Aδ- and C-fibres are nociceptive, primarily pain-sensory (slow, and long-lasting dull pain) (Basbaum *et al.*, 2009; Dubin and Patapoutian, 2010). These peripheral nerve fibre classifications are summarised in (Table 1.1).

Table 1.1 Classification of A-fibre peripheral nerve according to fibre class and size, myelination, conducting velocity (CV) and function

Fibre type	Fibre size	Fibre class	Conducting velocity (CV)	Function
Aa	13-20 μm	Myelinated	80-120m/sec	Muscle contractions
AB	6-22 μm	Myelinated	30-120m/sec	Touch, vibration, and pressure
Aγ	2-8 μm	Myelinated	15-30 m/sec	Muscle lengthening
Aδ	1-5 μm	Myelinated	5-25m/sec	Sharp pain, pressure, temperature

1.3.2 The Dorsal Root Ganglia

DRGs are structures found on both sides of the spinal cord, extending along the entire length of the spinal column. The cell bodies of the DRG do not connect with one another as they are separated by layers of satellite glial cells (SGCs) and Schwann cells (SCs) (Pannese, 2010). These sheaths facilitate the penetration of neurotransmitters and various molecules into the neuron, making the DRG somas vulnerable to inflammatory mediators and drugs (Esposito *et al.*, 2019). The pseudounipolar characteristics of DRG neurons cell bodies indicates that a single afferent fibre (axon) extends briefly from the soma before bifurcating into two branches. One branch projects centrally into the CNS via the spinal cord, while the other branch, which is longer, extends peripherally to innervate various tissue, ending in the skin, organs, tendons, bones and muscles (Figure 1.4) (Murtazina and Adameyko, 2023). The anatomy of the DRG is characterised by an inefficient neurovascular barrier and dense vascularisation, which make it vulnerable to structural damage by diabetes. DPN is attributed to damage that has been inflicted on the somatosensory neurons residing in the DRG (McHugh and McHugh, 2004).
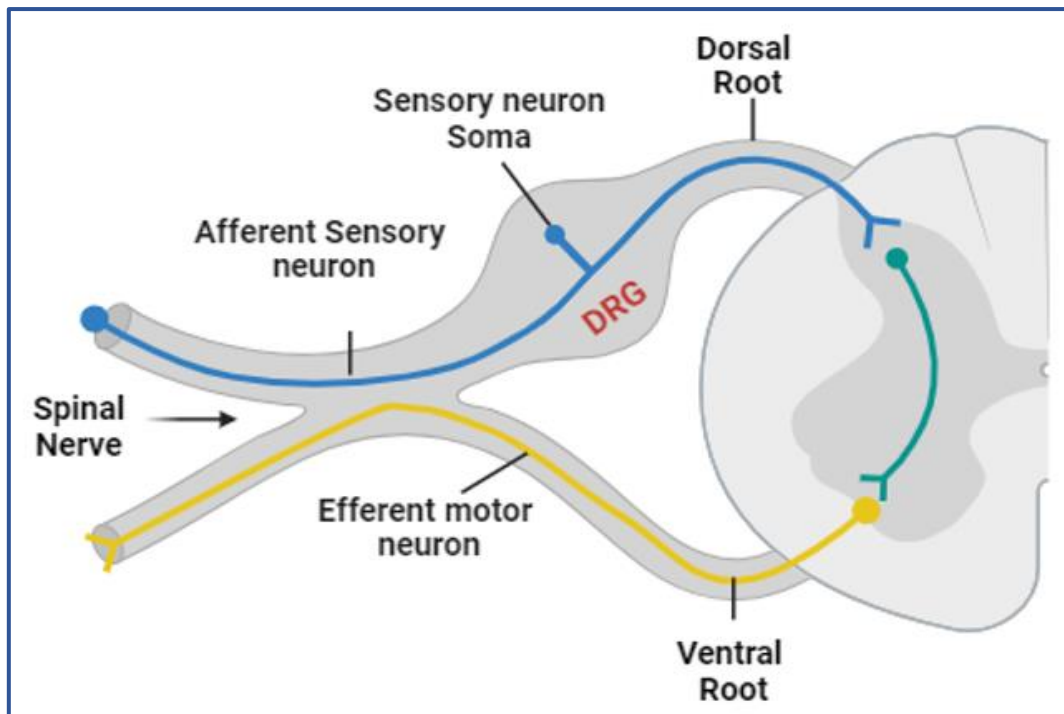
Figure 1.4 Anatomy and Location of the Dorsal Root Ganglia

The spinal nerve is formed by the dorsal root (Blue) and ventral root (Yellow) axons, which extend for a distance until bifurcating into the respective dorsal and ventral ramus. Dorsal root ganglia (DRG) contain the cell bodies (somata) of the sensory neurons. The ventral root axon somata are located either in the ventral horn (somatic motor neurons) or interomediolateral cell column (preganglionic sympathetic neurons) of the spinal cord. (Created by BioRender).

Sensory neurons detect various stimuli, including thermal, pressure, itching, and pain (Abraira and Ginty, 2013). Sensory neurons are referred to as "polymodal" allowing a single neuron to integrate various modalities, such as thermal and mechanical stimuli (Dubin and Patapoutian, 2010). The corresponding DRG neurons vary in terms of the soma's diameter and modality, where small diameters correspond to C-fibres (<30 µm), medium diameters to Aδ-fibres (30-40 µm), and large diameters to Aβ-fibres (>40 µm). Traditionally, DRG neurons were classified according to the relationship between their soma diameter and peripheral nerve axon size, myelination, and CV. The larger the soma's diameter, the higher the myelination and the faster the CV (Gasseh and Erlanger, 1929). Recently, DRG sensory neurons have been classified into various subtypes using transcriptomic techniques, including single-cell RNA-sequencing (scRNA-seq) (Usoskin *et al.*, 2015; Li *et al.*, 2018). Using scRNA-seq, 622 DRG were analysed by an *in-vivo* study, whereby around 3,900 genes per neuron were identified and classified accordingly into 11 distinct subtypes. A subsequent reanalysis of the previous data reduced the number of subtypes to nine classes of DRG neurons. More recently, a comprehensive scRNA-seq study, combined with molecular data using 1,580 DRG neurons, identified 18 distinct neuronal subtypes (Zeisel *et al.*, 2018). These transcriptomic classifications are summarised in (Table 1.2).

Table 1.2 Transcriptomic classification of sensory neurons in the DRG

Method	Number DRG neurons	DRG neurons subtypes	Reference
ScRNA-seq (in vivo)	622	11 classes	Usoskin etal., (2015)
In-depth RNA-seq1	197	9 classes	Li etal.,(2018)
ScRNA-se1	1580	18 classes	Zeisel etal., (2018)

Adopted from (Usoskin *et al.*, (2015) ; Li *et al.*, (2018) ; Zeisel et al., (2018)).

Immunohistochemically, sensory neurons in the DRG are classified based on their expression to specific neuronal markers. Large-diameter, myelinated neurons are characterised by the expression of neurofilament 200 (NF200) and encompass Aδ-fibres and Aβ-fibres, which are primarily involved in proprioception and the conducting of fast, non-painful mechanical stimuli. In contrast, small-diameter neurons express Peripherin and present C-fibre. These C-fibres are associated with transmitting innocuous mechanical cooling sensations (Gold and Gebhart, 2010; Ahimsadasan *et al.*, 2022). In mouse DRG, 40 % of the sensory neurons express only neurofilament 200 (NF200), 10 % co-express Peripherin (PRPH) and NF200, while 60 % express only peripherin (Figure 1.5) (Sleigh 2017). This classification highlights the diversity of DRG neurons, reflecting their specialised roles in sensory modalities and their varying susceptibility to neuropathic conditions.
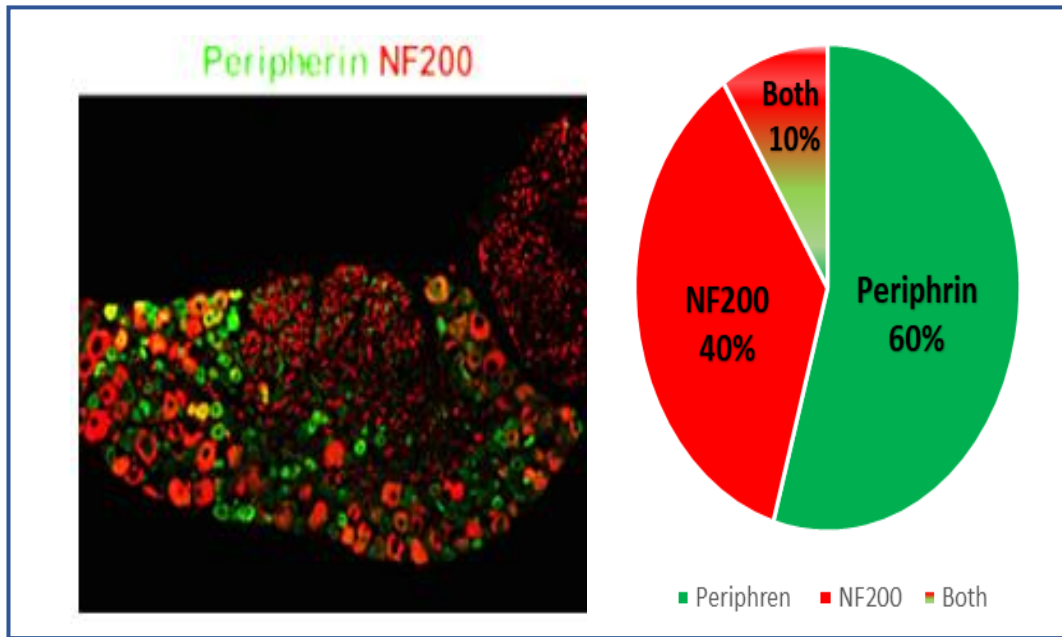
Figure 1.5 DRG sensory neurons express two distinct neuronal markers; Neurofilament 200 and Peripherin

A healthy mouse DRG demonstrates immunohistochemical classification of sensory neurons. Large-diameter neurons express neurofilament 200 (red) and account for 40%. Small-diameter neurons express peripherin (green) and account for 60%. Other neurons express both markers (yellow), accounting for 10%. (Adopted from Sleigh, 2017).

1.4 Pathogenesis of DPN

Several mechanisms have been proposed to explain the pathogenesis of DPN; however, the precise pathways remain unclear (Schreiber, 2015; Zang *et al.*, 2023).

1.4.1 Metabolic and cardiovascular factors

Hyperglycaemia, the hallmark of diabetes, results in a cascade of metabolic changes that affect the peripheral nerve in DPN (Liem *et al.*, 2015). These include polyol pathway hyperactivity (Tomlinson and Gardiner, 2008; Niimi et al., 2021), advanced glycation end products accumulation (AGEs) (Al-Saoudi et al., 2022), oxidative stress (Sandireddy et al., 2014), and Protein Kinase C activation (Geraldes and King, 2010) (Figure 1.6). Additionally, apart from excessive glucose, other cardiovascular complications increase the incidence of DPN, including high triglyceride levels, body-mass index (BMI), smoking and hypertension (Tesfaye *et al.*, 2005).

1.4.1.1 Polyol pathway

The theory of polyol pathway suggested that hyperglycemia causes the accumulation of intra-neuronal glucose levels. This will lead to the initiation of alternative catabolic pathway to convert excessive glucose to sorbitol which in final stage converted into fructose to balance these excess levels. This result of these oxidative reactions causes high stress levels which lead to metabolic damages to neurons therefore affecting peripheral nerve function (Oates, 2002; Tomlinson and Gardiner, 2008; Niimi *et al.*, 2021).

1.4.1.2 oxidative stress and formation of reactive oxygen species

This oxidative stress (OS) theory stated that, hyperglycemia cause the disruption of free radicals' production because of glucose oxidation and non-enzymatic protein glycation (AGEs), which generate reactive oxygen species (ROS). The accumulation of ROS can damage cells and trigger the apoptotic pathway, consequently leading to neuropathy (Obrosova *et al.*, 2005; Ibrahimpasic, 2013; Sandireddy *et al.*, 2014)

1.4.1.3 Advanced glycation end-products accumulation

The theory of advanced glycation end-products accumulation (AGEs) states that, high glucose level causes glucose to react with amino acid in proteins which lead to the formation of harmful products to the cells that is AGEs (Al-Saoudi *et al.*, 2022). An excessive accumulation of AGEs lead activation of various signalling cascades lead to neuronal dysfunction and loss of

nerve cells, reported in T2DM with DPN (Stitt *et al.*, 1997; Mišur *et al.*, 2004; Lukic *et al.*, 2008; Bellier *et al.*, 2019).
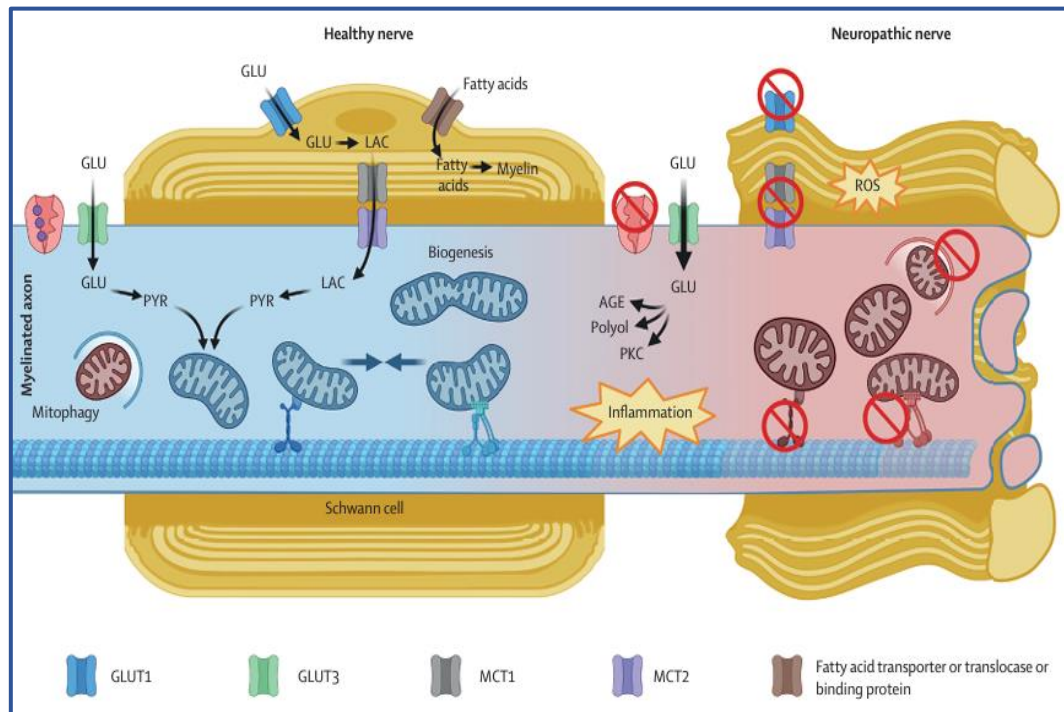
Figure 1.6 A summary of the metabolic mechanisms involved in the pathogenesis of DPN

Healthy condition (blue): nerve axons take up glucose (green). Schwann cells (Sc) take glucose (blue), convert it into pyruvate then lactate, which used for energy later. Mitochondria are transported to areas with high energy needs, creating ATP by maintaining a mitochondrial membrane potential, which powers the Na+/K+ ATPase channels (pink; the purple spheres represent cations). In a diabetic neuropathy condition (pink), the peripheral nerve takes up glucose; in the cytoplasm, excessive glucose activates other pathways, such as the polyol, AGEs, and PKC, which trigger inflammation, and so the activity of Na+/K+ ATPase channel activity is disrupted. Insulin resistance disrupts insulin-dependent uptake by SCs, thus impairing fuel transport to the axons and possibly affecting lipid metabolism and myelin production. Hyperglycaemia increases OS and apoptosis in SCs. GLUT=glucose transporter. LAC= lactate. MCT= monocarboxylate transporter. AGE = advanced glycation end products. PKC= protein kinase C. PYR=pyruvate. ROS=reactive oxygen species. (Adopted from Elafros et al., 2022).

1.4.2 Morphological changes to DRG reported in DN

The primary sensory neurons in the DRG are typically quiescent, exhibiting no spontaneous activity. However, following peripheral nerve damage caused by hyperglycaemia, DRG sensory neurons can become hyperactive, leading to sensory deficits such as hyper-sensation or a loss of sensation (Emery *et al.*, 2016). Several studies on diabetic animal models have found several morphological changes in the DRG, contributing to sensory dysfunction in DPN (Tesfaye and Kempler, 2005). These include thickening the perineural cell basement membrane, reduced DRG volume, and atrophy of the sensory neuron bodies (Johnson, 1983; Kobayashi *et al.*, 2017; Jende *et al.*, 2020). These changes indicate that diabetic neural complications, as in DPN, are not limited to the distal peripheral nerves. However, the primary target is the sensory neuron in the DRG. The following section will discuss the mechanism underlying the DRG's vulnerability and its contribution to the pathophysiology of DPN.

1.4.2.1 Changes in the number and soma size of the sensory neuronal population

Morphological studies have reported reduced neuronal counts and soma size among the DRG sensory neuronal population following diabetes (Sidenius and Jakobsen, 1980; Kishi *et al.*, 2002). This neuronal loss was attributed to sensory behaviour defects, including hyperalgesia and hyposensitivity (Shi *et al.*, 2013), and was observed in the T1DM animal model in both the early and late stages of diabetes at 4 and 24 weeks (Zochodne *et al.*, 2001). One study reported neuronal loss due to apoptosis, particularly in large-diameter neurons (Schmeichel, Schmelzer and Low, 2003). However, studies on T2DM models primarily focused on investigating the peripheral axons rather than central DRG for changes induced by DPN. It remains unclear if the loss occurs in the DRG in the T2DM animal models. This will be investigated in chapter 4.

1.4.2.2 Neuronal vacuolisation due to organelle dysfunction

Under cellular stress conditions, such as diabetes, DRG neurons might experience changes in their metabolic processes (Sango *et al.*, 2006). This results in the abnormal accumulation of lipids and waste products observed in the DRG neurons in the form of vacuole formation (Corral-Pujol *et al.*, 2023). The vacuolation in DRG neurons might alter the cellular structure, sensory signal transmission, and nerve dysfunction. In addition, vacuole formation in the DRGs has been associated with the development of DN in T1DM, due to a combination of metabolic dysfunction, inflammation, and OS (Eftekharpour and Fernyhough, 2022). These

vacuoles can develop early in life, even before the onset of DPN, suggesting that intrinsic alterations in the DRG neurons may trigger early neurodegenerative changes. These vacuoles have been linked to cellular organelles dysfunction, such as mitochondrial ballooning, Golgi apparatus fragmentation, and disruption in the autophagic and lysosomal pathways (Srinivasan, Stevens and Wiley, 2000; Kamiya *et al.*, 2006). This suggests that vacuole formation may be critical in accelerating neurodegenerative processes in diabetes, contributing to the selective vulnerability of sensory neurons in the DRG. However, the exact origin and mechanism of vacuole formation remain unclear in T2DM models. This will be investigated in chapter 5.

1.4.2.3 Changes to the non-neuronal cells surrounding the DRG neurons

Sensory neurons in the DRG are surrounded by supportive non-neuronal cells such as glial cells. In normal conditions, glial cells provide protection and support for the neurons. However, following peripheral injury, they release immune response cells, which cause a decrease in the inflammatory response at the DRG. This causes a process called peripheral sensitisation, which occurs in the primary nociceptors (C-fibres and Aδ-fibres). These fibres demonstrate low firing thresholds and increase spontaneous firing, causing hypersensitivity and hyperexcitability. During this process, the peripheral brunch at the injured site releases neuropeptide, which attracts leukocytes, which in turn activates macrophages, causing the activation of receptors located at the terminals/or cell bodies of the nociceptor, in turn leading to the removal and regeneration of damaged axons (Basbaum *et al.*, 2009). These processes collectively create a cascade of inflammation in the DRG, even after the peripheral nerve injury has abolished (Esposito *et al.*, 2019). T2DM patients with DN display higher levels of inflammatory mediators in their plasma than non-diabetic patients and T2DM patients without DN (Doupis *et al.*, 2009).

1.4.3 Morphological changes to DRG reported in neuropathic condition

1.4.3.1 Sympathetic-sensory connection

Several studies have highlighted the essential role of sympathetic activity in developing and maintaining pathological pain. The sympathetic-sensory abnormal connection aggregates various chronic pain conditions (Ji *et al.*, 2022). Of particular interest is the sympathetic sprouting of TH-immunoreactive fibres (TH-IR) into the DRG, that is observed in peripheral nerve injuries (Xie W etal 2011; Wu etal, 2017). Moreover, sympathetic TH-IR fibres have been

reported to form basket-like structures around sensory neurons in the DRG, particularly large-diameter neurons (Chien *et al.*, 2005), have been linked to increasing hypersensitivity and referred pain sensations (Zhu *et al.*, 2022). Meanwhile, localised sympathectomy effectively abolished fibre sprouting, which almost stopped pain behaviours, such as mechanical allodynia and reduced cold allodynia in neuropathic animals (Li *et al.*, 2018). This indicates that sympathetic innervation plays a role in the development and maintenance of sympathetically maintained pain (SMP) (Xie, Strong and Zhang, 2020). These findings suggest that sensory abnormalities in neuropathic disorders might be partially attributed to sympathetic TH-IR fibre sprouting into the DRG, thus providing new insights into the mechanism involved in chronic pain and somatic hyperalgesia. This will be investigated in chapter 3.

1.5 Management of DPN

Unfortunately, despite the understanding regarding the underlying mechanism involved in the pathophysiology of DN, no pharmacological treatment currently exists to cure the condition (Feldman *et al.*, 2019). The only existing therapy that is designed to alleviate the symptoms of DPN is glycaemic control through insulin supplements, which, when introduced sufficiently early, improve CV and prevent neuropathy. However, this is only effective with T1DM (Callaghan *et al.*, 2012), while T2DM shows no effect, even if the treatment period is extended up to five years. This indicates that hyperglycemia is not the single factor that triggers DN. Consequently, other therapeutic options, such as cholesterol management, body weight management, and surgical interventions (such as bariatric surgery), are being introduced to slow DPN's progression. With no pharmacological treatments available, the only practical approach to managing DPN symptoms is targeting the CNS. However, these treatments often cause side effects, particularly in older patients. A comprehensive approach that addresses multiple risk factors, including hyperglycemia, hypertension, and insulin resistance, is essential (Duehmke *et al.*, 2017). The recommended treatments include anticonvulsants and antidepressants, which are frequently used to reduce neuronal excitability and as a form of pain relief, while opioids and alpha-lipoic are less common treatments due to their risk of addiction and overdose (Wiffen *et al.*, 2017; Derry *et al.*, 2019). These treatments are summarised in (Table 1.3).

Table 1.3 FDA-approved treatments for DN, including anticonvulsants, antidepressants, tropical, opioid, and alpha-lipoic acid

Type of drug	Name	Target	Adverse effect	Reference
Anticonvulsant	Pregabalin & Gabapentin	Inhibit neurotransmitter release through VGCC	Dizziness, weight gain, dry mouth, edema, seizure (after rapid discontinuation)	(Wiffen *et al.*, 2017 ; Derry *et al.*, 2019)
Antidepressant	Amitriptyline & Duloxetine	Inhibit reuptake of noradrenaline and serotonin in presynaptic neurons	Hepatotoxicity, seizures, cardiac arthritis, serotonin syndrome	(Lunn, Hughes and Wiffen, 2014; Moore *et al.*, 2015)
Opioid	Tramadol	Inhibit reuptake of noradrenaline and serotonin in presynaptic neurons	Serotonin syndrome, seizures, hypertension, respiratory depression	(Duehmke *et al.*, 2017)
Tropical	Capsaicin	Removal of substance P from vanilloid nerve receptors	-	(Simpson *et al.*, 2017)
	Lidocaine	Prolong inactivation of VGSCs	-	(Derry *et al.*, 2014)
Alpha-lipoic acid	Thiotic acid	Antioxidant	Headache, heart burn, nausea, vomiting	(Ziegler *et al.*, 1999)

(Adapted from Jang and Oh, 2023).

1.6 Models for Studying DN

To confirm DN is established in diabetic rodent models, three parameters should be observed, and the animal model is recognised as proven. These include examining for any abnormal sensory symptoms, such as mechanical and thermal sensitivity, impairment in the CV, and decreases in the nerve structure, including myelinated fibre and/or intraepidermal nerve fibre densities (IENFDs). Two of these parameters must differ significantly from the control animals

for a neuropathic phenotype to be confirmed (Biessels *et al.*, 2014). Several diabetes-induced animal models have been reported in studies seeking to identify the underlying mechanisms for DN. These include chemically-modified, diet-induced, and genetically-modified models, which will be discussed below.

1.6.1 Chemically-induced Models

The most commonly used model is the Streptozotocin (STZ)-induced model, mimicking T1DM. STZ cause damage to pancreatic β-cells, leading to insulin defects and hyperglycaemia. STZ-induced models develop neuropathic alterations similar to those observed in diabetic humans, including slow CV, sensory implementation, and structural damage to the peripheral nerves. Nevertheless, these chemically induced models are useful for studying the onset and progression of DN in the context of T1DM. Although these models are low-cost, easy to handle and appropriate models for T1DN, they can be harmful to animals, causing severe distress and potential damage to the cells, which might impact the measurement of the sensory parameters (Usman *et al.*, 2015).

1.6.2 Diet-induced Models

High-fat diet (HFD)-induced models involve making various alterations to dietary intake. These alterations cause gradual obesity, followed by metabolic impairment, including hyperglycaemia and hyperinsulinemia, until T2DM is fully developed. HFD is characterised by motor and sensory abnormalities, along with peripheral nerve damage and neuropathy, as observed in diabetic humans HFD models are used to study prediabetes and obesity-associated neuropathy, which are early indicators of DN. Nevertheless, the diet method aspect of these models can prove time-consuming depending on various factors, such as the sex and age of the animal used, the diet period, the fat content and the source (Obrosova *et al.*, 2007).

1.6.3 Genetically-induce Models

1.6.3.1 The db/db model (Lepr^db/db)

Hummel and coworkers (1965) were the first to introduce the db/db mouse through a study that reported random mutations in mice associated with obesity and hunger (Hummel, Dickie and Coleman, 1966). The model was later refined by Robertson and Sima (1978), who observed the morphometric changes in db/db mice and reported that these models

effectively replicate the phases of DN progression in humans (Sima and Robertson, 1978). The db/db mouse is a robust, well-established model for studying T2DM and DN (Wua *et al.*, 2013; Guest and Rahmoune, 2019). It carries a homozygous mutation in the leptin receptor gene, which is fundamental for regulating the appetite via inhibiting hunger through leptin signalling to the hypothalamus (Chen *et al.*, 1996). The db/db mice are characterised by hyperphagia and obesity early in life. As early as two weeks of age, the db/db mice exhibited increased insulin levels and fasting blood glucose levels, progressing to obesity and insulin resistance by 3-4 weeks of age (Lee and Bressler, 1981). This metabolic impairment causes the development of T2DM and the onset of DN by eight weeks (De Gregorio *et al.*, 2018). The db/db mice closely mimic the progression of DN in human patients, particularly with regard to the gradual depletion of insulin-secreting pancreatic β-cells and an uncontrolled rise in blood glucose (Like *et al.*, 1972). In addition, the db/db model represents symptoms that mimic brain disorders, such as Alzheimer's disease (Jolivalt *et al.*, 2008). The relationship between metabolic and neurodegenerative disease has been strengthened by recent studies, which revealed that db/db mice acquire impairments in long-term potentiation and spatial memory (Li *et al.*, 2002).

Collectively, unlike chemically-induced models, such as the STZ model, which primarily mimics T1DM, or the ob/ob mouse (Lep^ob/ob), which has a similar mutation in the leptin gene as in db/db mice, these ob/ob mice exhibit the early stages of DN (Suriano *et al.*, 2021). The db/db mice develop DPN spontaneously in T2DM, thus closely resembling the metabolic and neuropathic progression observed in humans. These include peripheral nerve damage, sensory neuron deficits, and alteration in pain sensitivity, which align with the aims of this study (Guest and Rahmoune, 2019). The db/db model allows for a more natural and comprehensive investigation of DPN in the context of T2DM, making it a precious tool for studying changes in lumbar DRG sensory neurons. Given the focus of this study on investigating histological changes in sensory neurons associated with DPN in T2DM, the db/db mouse model was selected. Finally, to our knowledge, no previous studies have investigated the morphological changes in *db/db* mice DRG sensory neurons during DPN. From all of the above reasons and the proved strength of DN phenotype, the T2DM db/db mouse was selected as a model of DPN for this present study.

1.7 Gap in the Literature

Although several previous studies investigated the mechanism underlying the development of DPN symptoms, the exact mechanism remains only partially understood. This thesis examines the morphological changes in the sensory neurons in the DRG of db/db mice, which might contribute to understanding the altered sensations of touch and pain in DPN.

1.8 Rationale, Hypothesis and Aims

1.8.1 Rationale

DPN manifests through two key pathological features, which are hypersensitivity, including painful sensations like hyperalgesia and allodynia, and the loss of sensation like numbness and tingling. These opposing symptoms arise due to damage to the sensory neurons within the DRG.

1.8.2 Hypothesis

Morphological changes to the sensory neurons in the DRG might contribute to pain and loss of sensation in DPN.

1.8.3 Aims

1. To examine sympathetic fibre sprouting into the lumbar DRG of db/db mice, which might contribute to pain development in DPN (Chapter 3)
2. To examine the changes in the number and soma size of the lumbar DRG sensory neurons in db/db mice as a potential cause of the loss of sensation in DPN (Chapter 4)
3. To characterise vacuole formation in the sensory neurons in lumbar DRG of db/db mice for signs of stress and damage caused by DPN (Chapter 5)

Chapter 2: Materials and Methods

2.1 Materials

2.1.1 Animals

A total of 13 db/db male mice (BKS.Cg-+Leprdb/+Leprdb/OlaHsd) and a total of 12 lean (non-diabetic control) male mice (BKS.Cg-(lean)/OlaHsd) (Inotiv, The Netherlands) were used for this study. Female mice were not chosen to avoid hormonal alteration. The animals were sacrificed at 30-32 weeks, this represents the late neuronal phase which present the structural nerve damage. Then animals were kept in the Biological Services Unit at the University of Sheffield to allow a week for acclimatisation. The animals were housed in groups of 3-4, with free access to food and water, under controlled conditions related to temperature, humidity, and light-dark cycle. Every effort was made to minimise animal suffering and to reduce the number of mice used in the reported studies. All animal work was carried out in accordance with the UK Home Office Animals (Scientific Procedures) Act 1986.

2.1.2 Antibodies

2.1.2.1 Primary antibodies

Table 2.1 Primary antibodies used for all experiments in this study

Antibody name	Abbreviation	Raised in	Dilution	Supplier	Catalogue No
Tyrosine hydroxylase	TH	Rabbit	1:500	Millipore	AB152
Neurofilament 200	NF200	Rabbit	1:2000	Sigma Aldrich	N4142
Neurofilament 200	NF200	Mouse	1:2000	Sigma Aldrich	N0142
Peripherin	PRPH	Mouse	1:2000	Santa Cruz	SC-377093
Golgi matrix protein 130	GM130	Rabbit	1:200	Thermo Fisher	703794
ATP synthase-subunit alpha	ATP5A1	Rabbit	1:500	Thermo Fisher	PA5-27504
Calreticulin	Calr	Rabbit	1:200	Thermo Fisher	PA3-900
Autophagy-related 12	ATG12	Rabbit	1:500	Thermo Fisher	701684
Light chain 3B	LC3B	Rabbit	1:500	Thermo Fisher	PA1-46286
Synaptic vesicle glycoprotein 2A	SV2A	Rabbit	1:200	Thermo Fisher	PA5-52476
P53-binding protein 1	53BP1	Rabbit	1:200	Novus	NB-100-3

Hypoxia-inducible factor 1-alpha	HIF1A	Rabbit	1:200	Thermo Fisher	PA5-85494
Microtubule binding protein Tau	Tau	Rabbit	1:200	Thermo Fisher	44-752G

2.1.2.2 Secondary antibodies

Table 2.2 Secondary antibodies used for all experiments in this study

Antibody name	Raised in	Antigen	Dilution	Supplier	Catalogue No
Alexa Fluor™ 594	Goat	Mouse	1:2000	Thermo Fisher	A-11032
Alexa Fluor™ 488	Goat	Mouse	1:2000	Thermo Fisher	A-11029
Alexa Fluor™ 488	Goat	Rabbit	1:2000	Thermo Fisher	A-11070
Alexa Fluor™ 594	Goat	Rabbit	1;2000	Thermo Fisher	A-11037

2.1.3 Chemicals and Reagents

Table 2.3 Chemicals and reagents used for the IHC protocol

Name	Supplier	Catalogue No
Phosphate Buffered Saline x10 (PBS)	Fisher BioReagents	137797
4% Paraformaldehyde (PFA)	Thermo Scientific	J61899.AK
Triton x100	Sigma	107H0934
Prolong™ Diamond Antifade Mounting (DAPI)	Thermo Fisher	P36981
Blocking solution	Made in lab	N/A
Albumin Bovine Fraction V (BSA)	Melford	A1302
Gelatine from cold water fish skin	Sigma	G7765
Tween® 20	Sigma	9005-64-5
Optimal cutting Temperature (OCT)	Leica Biosystems	14020108926
Sodium Chloride	Fisher Scientific	S/3160/65

2.1.4 Solution and recipes

Name	Quantity	Final concentration
BSA	8 g	2%
Fish skin gelatine	8 ml	2%
Twwn-20	0.4 ml	0.1%
10Xpbs	40 ml	1x
Sodium Azide	0.2 g	0.5%
Normal Goat Serum	8 ml	2%
Reagents added to 400 ml of water. Solution was used as is. Also, used to dilute primary and secondary antibodies that are not conjugated. Stored at -20°C.		

2.2 Methods

2.2.1 Preparation of DRG samples

2.2.1.1 Isolation of Lumbar DRGs

Following euthanasia with isoflurane and cervical dislocation, the spinal column was extracted and immediately placed into ice-cold PBS. Then, using a dissection microscope, the spinal column was divided into two halves along its mid-sagittal plane, and the spinal cord was excised to expose the dorsal root ganglia (DRG) within the intervertebral foramina. Then, the vertebral column was counted to locate the DRGs at the end of thoracic level T13 and the start of lumbar level L1. Then, the DRGs at L1-L5 were dissected out of their foramina, trimmed of connective tissue and nerve roots, and placed immediately into a 35mm dish containing cold PBS. Once all of the DRGs had been isolated, each lumbar DRG was fixed in an OCT (Optimal Cutting Temperature) embedding medium and stored at -80°C (Figure 2.1).
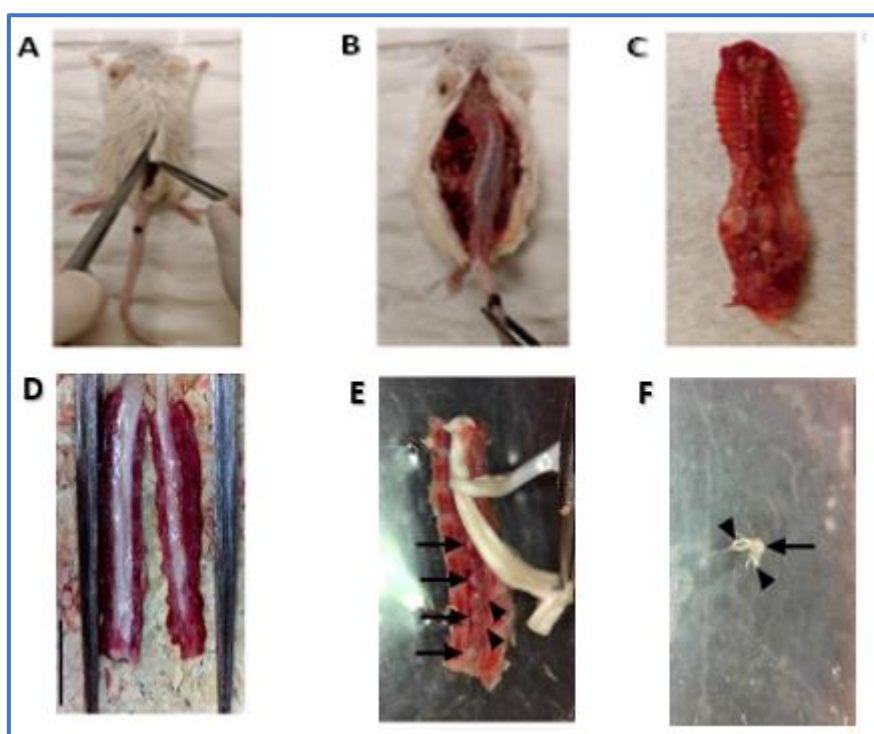
Figure 2.1 Method for spinal cord dissection and lumbar DRG extraction

(A) animal dissection via a small incision in the dorsal skin (B) The incision from the abdominal wall muscles laterally to the spinal column in both directions (C) The removed Spinal cord (D) The spinal column halved along the mid-sagittal plane (E) The peeled spinal column, with the DRGs' locations exposed; the arrow indicates the position of the DRGs within the intervertebral foramina (F) Isolated DRGs from lumbar regions L1-L5.

The lumbar L1-L5 DRGs were frozen sectioned at 15 µm thickness using a cryostat (the thickness was selected according to other histological studies who used to section DRG at range between 12-15 µm). This resulted in 15 SuperFrost™ microscopic slides per DRG, each slide contained two DRG sections, although these were not consecutive. Instead, the sections were arranged sequentially across the slides, so that slide number 1 contained DRG sections 1 and 16, slide number 2 contained DRG sections 2 and 17, and so on, until slide 15, which contained DRG sections 15 and 30. This arrangement made it possible to visualise the entire DRG but with an effective sampling interval of 30 µm (Figure 2.2). A total of 3,750 slides were prepared, labelled, and dated and then stored at -80°C.
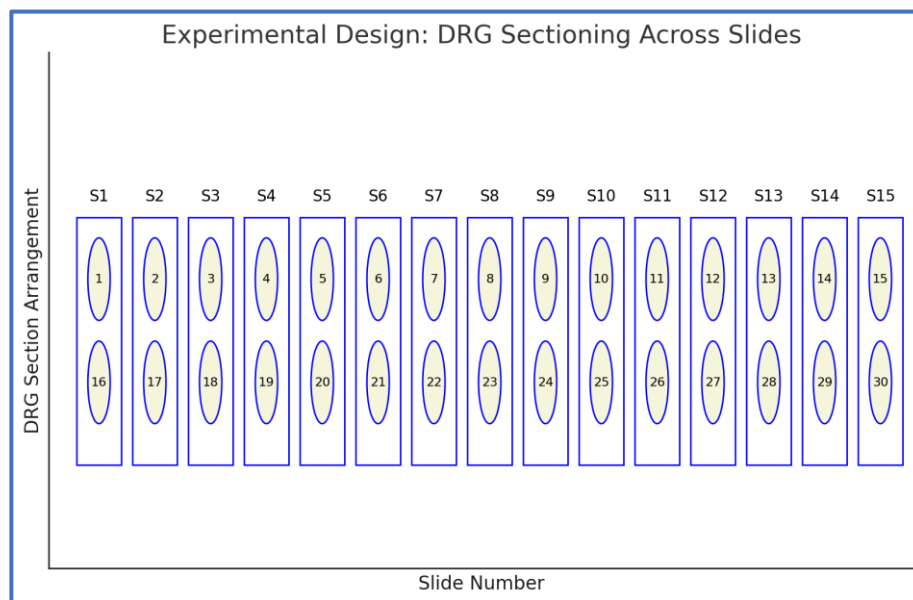
Figure 2.2 DRG serial sectioning and slide preparation

The lumbar L1-L5 DRGs were sectioned at 15um across 15 microscopic slides. Each slide contained two non-consecutive DRG sections arranged sequentially. This setup provided a 30 µm sampling interval across the entire DRG.

2.2.2 Immunohistochemistry (IHC) protocol

All of the sections were dried at Room Temperature (RT) for ten minutes. The slides were washed in ice cold 1X Phosphate Buffered Saline (1XPBS) for five minutes, then fixed in 4% PFA for ten minutes, followed by washing in 1XPBS for five minutes. After that, the slides were permeabilised in 0.1% Triton-X100 for ten minutes, then washed with 1XPBS, followed by Ammonium Chloride (NH4CL) for five minutes each. After that, the slides were incubated in a

blocking solution (Table 2.1.4) for two hours at RT, followed by incubation in a primary antibody (Table of antibodies, section 2.1.2.1) diluted in blocking solution and left overnight at 4°C. Then, the slides were washed three times with 1XPBS for five minutes. After that, the slides were incubated in a secondary antibody (Table of antibodies, section 2.1.2.2) diluted in blocking solution for two hours at RT and kept in the dark. Finally, the slides were coated with mounting solution (ProLong™ Diamond Antifade Mountant with DAPI, ThermoFisher) and covered for later examination under a fluorescent microscope. For each experiment, negative (secondary) controls were subjected to the same IHC protocol, except for the fact that the slides were only incubated with a secondary antibody, with no primary antibody to validate the staining integrity.

2.2.3 Images analysis

The images were visualised using a Leica DMi8 fluorescent microscope at x20, x40, and x63 (oil objectives), with a 100-millisecond exposure time. The fluorophores were excited at 488 nm (ALexaflour-488), 594 nm (Alexaflour-594), and 350 nm (DAPI). The images were analysed using Fiji-ImageJ software (Version 1.54f for Windows), by first converting them into an 8-bit format, after which an automatic algorithm, with the initial threshold based on 'minimum error', was used to generate the binary images. After that, a comparison between the threshold of the binary image histogram allowed the raw image to be manually adjusted in order to ensure that the areas of interest (AOI) were differentiated from the background. These images were exported in TIFF format, and the final image editing and labelling were processed using Image J and PowerPoint software.

2.2.4 Data processing and statistical analysis

The data were presented as a mean ± standard Error (SEM), and the sample numbers were represented by ''N''. A Student t-test was used to calculate the significant difference between the two groups. An ANOVA test was used to calculate the significant difference in the mean value between more than two groups. The statistical test used for the analysis and the sample size for each experiment are listed under the figure legend.

2.2.4.1 Quantification of sensory neurones and non-neuronal cells

After performing thresholding (as detailed above in section 2.2.3) for each neuronal marker used in the exact experiment, a plug-in function tool, "Analyse Particles", was used to identify and neuron count within the DRG sections. Specific parameters for the minimum and

maximum particle size (in pixels) were set to exclude non-neuronal structures or artefacts. In addition, manual verification was applied following the automatic particle count by manually reviewing each image to ensure the accurate identification of neurons. Neuronal somas that had been incorrectly identified by the software or overlooked were manually deleted for precise quantification. Examples of neuronal and non-neuronal cell counting are provided below (Figure 2.3).
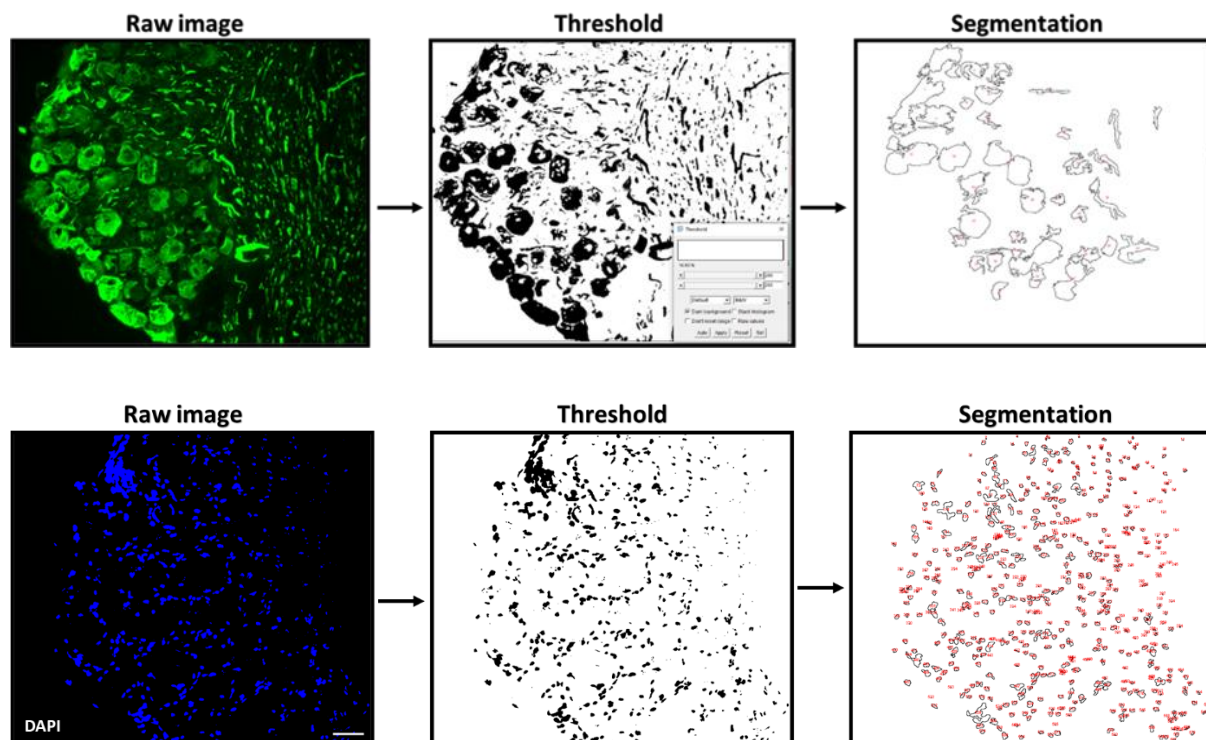
Figure 2.3 Representative image of the counting method used for neuronal and non-neuronal cell in the DRG section

(Upper panels) Representative images of a DRG section showing NF200-positive neurons counting method. Raw image of NF200-positive neurons (left). Thresholding distinguishes the object of interest from the background (middle). Image segmentation for counting using the ''analyse particles'' plug-in (right). (Lower panels) Representative images of a DRG section showing the non-neuronal cells counting method. Raw image of non-neuronal cells stained with DAPI (left). Representative image thresholding distinguishing the object of interest from the background (middle). Image segmentation for counting using the ''analyse particles '' plug-in (right). Scale bar = 20 μm (applied to all images).

2.2.4.2 Quantification of vacuolated neurons

The vacuolated neurons were manually quantified using the "Point Tool" in ImageJ software. For each vacuolated neuron, a dot was placed over the neuron, and the total count was

recorded for each section. The percentage of vacuolated neurons relative to the total number of neurons was calculated for each section. Manual verification ensured that the vacuolated neurons were correctly identified.

2.2.4.3 Quantification of fibre in the peripheral nerve

The number of immunoreactive fibres was manually calculated in the peripheral nerve under an immunofluorescent microscope (at a magnification of x20). Only one count was made per section, and at least seven sections were sampled from each nerve.

2.2.4.4 Measurement of the soma size of sensory neurons

After performing the thresholding (as detailed above in section 2.2.3) for each neuronal marker used in the exact experiment, the neuronal circumference was calculated automatically using the "Outline" tool to detect and circle individual neurons based on a specific threshold. After that, the function tool "Measure" (analyse > Measure) was used to quantify the area of each neuronal soma. The in-built software formula then calculated the cell area. The generated cell area was then used to calculate the cell diameter (μm^2), following the formula:

$$Diameter\ (d) = 2\ \sqrt{\frac{area}{\pi}}$$

2.2.4.5 Measurement of DRG neurons and fibre labelling intensity

After performing thresholding (as detailed above in section 2.2.3) for each neuronal marker used in the exact experiment, the identified areas were measured automatically using a plugin '' Intensity'', and the neuron intensity was calculated.

Chapter 3: Examining Sympathetic Fibre Sprouting in the Lumbar DRG of db/db Mice

3.1 Introduction

Normally, sensory neurons in the DRG undergo no direct innervation by the sympathetic nervous system. Inside the DRG, the sympathetic fibres are restricted to the blood vessels (Xie, Strong and Zhang, 2010). However, following peripheral nerve injury, these fibres invade the DRG, where they abnormally form a network around sensory neurons in the DRG (Figure 3.1). The sympathetic-sensory connection leads to the development of sympathetically-mentained pain (SMP), which is characterised by spontaneous burning pain combined with hyperalgesia and allodynia (Lee *et al.*, 1998; Ramer, Thompson and McMahon, 1999; Zhang, 2017). Sympathetic sprouting is characterised by either the regrowth of noradrenergic fibres (immunoreactive to tyrosine hydroxylase, TH) in the form of ''basket'' or ''ring''-like structures around the sensory neurons or/and increasing fibre density at the cellular site of the DRG (Djouhri *et al.*, 2006). Sympathetic fibres either sprout from those fibres which are already innervating the blood vessels in the DRG or newly growing collateral fibres from the distal sympathetic regions (Ma and Bisby, 1999).
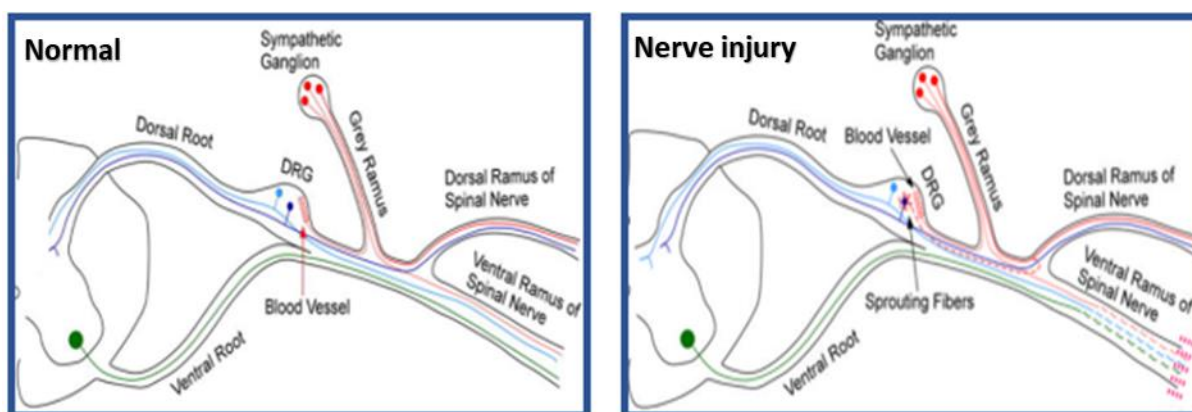
Figure 3.1 The anatomy and location of the DRG and sympathetic fibres in healthy and lesioned DRG

(A) Healthy DRG showing sympathetic fibres travelling beside the blood vessels. (B) Lesioned DRG showing the course and invasion of sympathetic fibres into the DRG (the dotted red lines). The sensory neurons are shown in blue, and the motor neurons are in green. The SNL cut is shown as blue, green, and red (the dashed lines). (Adopted from Xi, Strong and Zhang, 2010).

Sympathetic sprouting was first reported by McLachlan *et al.* (1993) as invading the lumbar DRG in axotomised nerves such as the sciatic nerve ligation (SNL) model. The density of TH-IR sympathetic fibres increased post operation (PO), forming 132-199 sympathetic rings around thr axotomised sensory neurons at seven weeks PO, which further doubled to 326 rings by

ten weeks PO, particularly encircling large-diameter neurons. Axotomised large-diameter neurons, which were wrapped by TH-IR fibres, were reported to release chemotactic substances that trigger sympathetic fibres, contributing to sympathetically mediated pain (McLachlan *et al.*, 1993). Additionally, sympathetic sprouting was also reported by Lee and Yoon, (1998), in the lumbar L3-L6 DRGs of two different models of nerve injuries, including segmental spinal ligation (SSI) and partial nerve ligation (PNI). The researchers documented the presence of few dopaminergic TH-labelled neurons in the DRG of the SNL model (Figure 3.2) (Lee *et al.*, 1998).
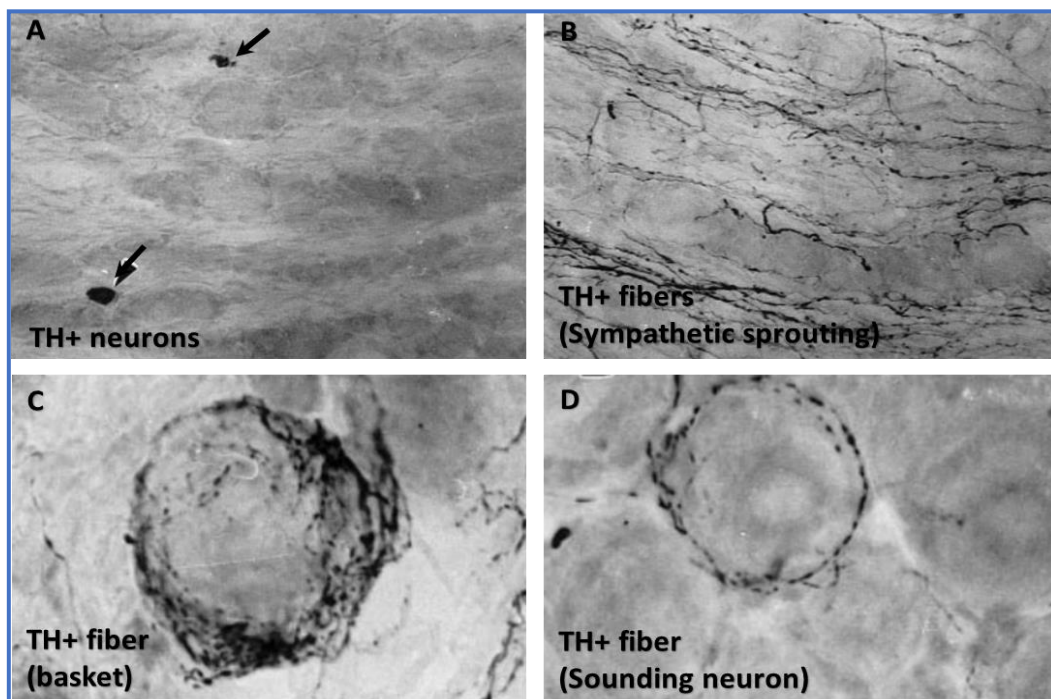
Figure 3.2 Sympathetic sprouting and basket formation in the axotomised DRG of SNL model

(A) TH labelled neurons observed in the lumbar DRG (arrows) (B) Sympathetic sprouting of TH labelled fibres in the SNL model (C-D) TH labelled fibres forming a network (basket-like structure) around DRG neurons of SNL model. (Adopted from Lee and Yon (1998).

In addition to the axotomised nerve, sympathetic sprouting is reported in non-axotomised nerves if the DRG is ligated or compressed (Lee *et al.*, 1998; Chien *et al.*, 2005). In chronic compressed DRG (CCD), sympathetic fibre is distributed throughout the whole DRG in the fibre tract and cellular region and is more extensive in the fibre site. The density of sympathetic fibres increased bilaterally in the DRGs, with higher density on the lesion side (Figure 3.3) (Chung and Chung, 2001).
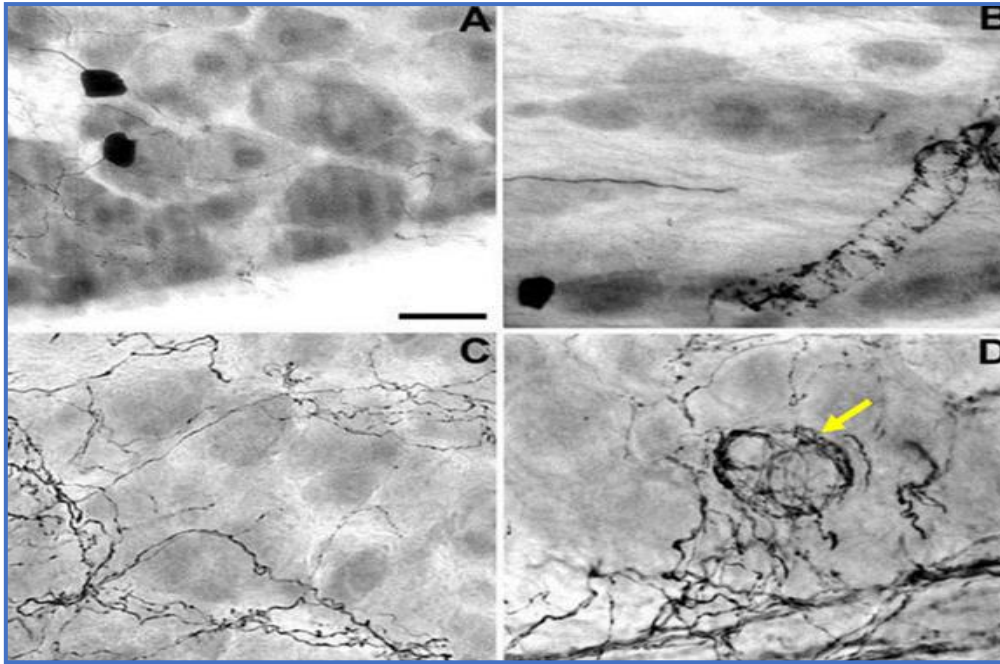
Figure 3.3 Sympathetic Sprouting in the non-axotomised DRG of the CCD model

(A) Healthy rat DRG showing no signs of sympathetic sprouting (B) Sympathetic fibres form varicose plexuses around the vascular processes. (C) Sympathetic fibres sprouting into the lumbar DRG of a CCD rat. (D) Sympathetic fibres are arranged in basket-like structures around DRG neurons (arrow). (Adopted from Chung and Chung (2001).

Sympathetic fibres were reported to decrease in peripheral nerves when sympathectomy was performed, which reduced pain behaviours, including mechanical allodynia and thermal hyperalgesia, by nearly half in neuropathic models (Figure 3.4) (Xie, Strong, and Zhang, 2020). This suggested that the sympathetic nervous system in the injured DRG controls at least part of pain development and maintenance (Chung *et al.*, 1996).
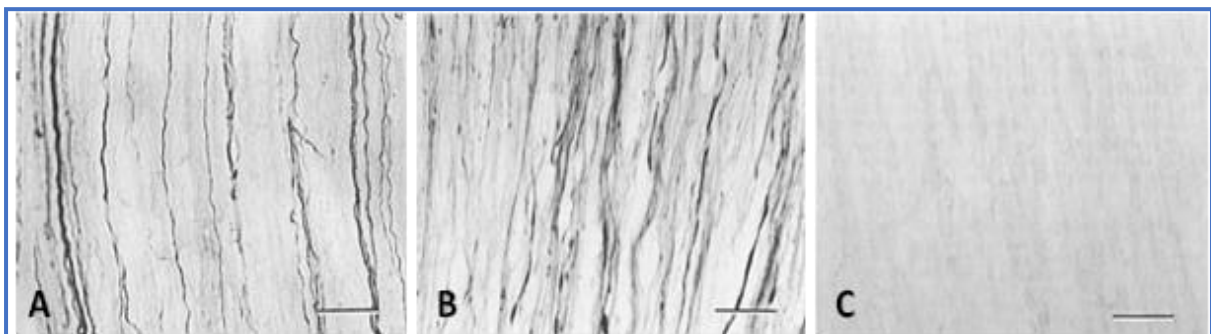
Figure 3.4 Sympathectomy abolished sympathetic fibre in the SNL model

(A) Healthy spinal nerve (B) SNL spinal nerve (C) Sympathectomy in the SNL spinal nerve showed the complete disappearance of TH-IR fibres. (Adopted from Chung et al., (1996).

The sympathetic fibre sprouting rate was found to change depending on the location of the nerve injury from the DRG. The rate of sympathetic sprouting increased in the SSI model where the injury is in the L5 and L6 spinal nerves compared to most distal injury locations, such as CCI and PNI models, in the mid-thigh and upper-thigh levels of the sciatic nerve, respectively (Lee *et al.*, 1998). The behaviour-related signs also differ in these models (Table 3.1). Although the density of sympathetic fibres increased in the CCI model (20 weeks PO), the numbers of TH-positive neurons remained unchanged, whereas, in the SSI model, both the TH-positive neurons and TH-positive fibres increased (20 weeks PO). Others reported a tendency towards a decline in the number of TH-positive neurons seven days after axotomy (Brumovsky, Villar, and Hökfelt, 2006). The reasons for these reported discrepancies in the number of TH-positive neurons in DRG remain unknown. These findings confirm that sympathetic sprouting in DRG is a phenomenon that emerges following nerve damage.

Table 3.1 Summary of various models of peripheral nerve injury showing different sympathetic sprouting rates and various behaviour signs in the lumbar L4-L5 DRG

Type of injury/model	Evoked pain	Cold allodynia	Time of sympathetic sprouting (PO) in Lumbar L5	Time of sympathetic sprouting (PO) in Lumbar L4
CCI			20 weeks	20 weeks
PSI			20 weeks	20 weeks
SSI			1 weeks	20 weeks

(Adopted from Lee and Yoon (1998).

The studies reviewed above demonstrate that nerve injury-induced sympathetic sprouting, which consequently contributed to the development of neuropathic pain. This phenomenon is well-documented among various animal models of nerve damage, suggesting that a consistent relationship exists between sympathetic fibre sprouting and extensive pain symptoms. Considering the known link between nerve damage and pain manifestations in diabetes, particularly DPN, it is essential to consider the potential implications of sympathetic sprouting in this context. While the previous research documented sympathetic sprouting in

non-diabetic models of neuropathic pain, there remains a gap in the literature regarding its occurrence and impact in diabetic models.

3.2 Hypothesis

Diabetes triggers the formation of basket-like structures, indicative of sympathetic sprouting around the lumbar DRG neurons, which may contribute to pain in DPN.

3.3 Aims

- To investigate whether diabetes leads to sympathetic sprouting in the lumbar DRG of db/db mice.
- To count the number and intensity of TH-positive fibres in the nerve axon of db/db mice
- To count the number and intensity of TH-positive neurons in the lumbar DRG of db/db mice

3.4 Results

3.4.1 Diabetes does not cause sympathetic sprouting or the formation of basket-like structures in the lumbar DRG of db/db mice

TH labelling was examined to detect the incidence of sympathetic sprouting in the lumbar DRG of db/db mice. We examined 112 DRG sections from db/db mice and found a single case of sympathetic sprouting of TH-positive fibres, observed in a single DRG section from one db/db mouse surrounding a large-diameter neuron (Figure 3.5). This result suggests that diabetes does not trigger sympathetic sprouting into the lumbar DRG of the db/db mice model at 32 weeks of diabetes.
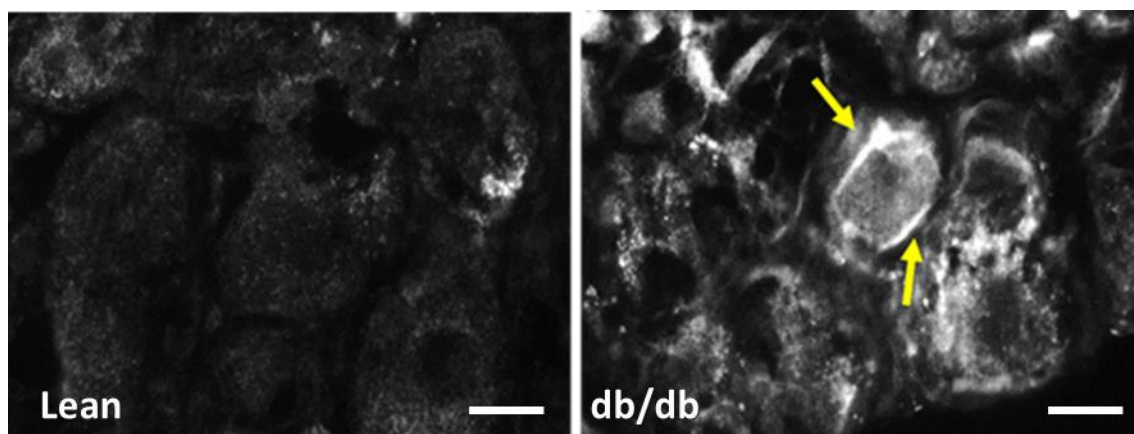
Figure 3.5 A single sympathetic sprouting of a TH-positive fibre in the lumbar DRG of a db/db mouse

(A) DRG from a lean mouse shows no sympathetic sprouting of TH-positive fibre. (B) DRG from a db/db mouse shows a single TH-positive sympathetic fibre surrounding one large-diameter neuron (arrows). n=8, Scale bar= 40 μm.

3.4.2 Characterisation of TH-positive fibres in the peripheral nerve of db/db mice

We measured the number and intensity of TH-positive fibres at the peripheral nerve site (yellow arrow) (Figure 3.6A). The number of TH-positive fibres varied between the lean and db/db mice, ranging from 3-7 fibres per section (Figure 3.6B (Lower panels)). Note that some of the TH-positive fibres were distributed randomly around the nerve; although the majority, were located at the edges of the section.

The average number of TH-positive fibres in lean mice was (8 ±1.37, n=4) and in db/db mice was (11.25±3.25, n=4). This indicated a slight (3.25%) increase in diabetic mice, although this was not significantly different (P= 0.0563) (Figure 3.6C).

The intensity of the TH-positive fibres labelling was slightly higher in the db/db mice (4520±679.8, n=4) compared to the lean mice (3890±335.1, n=4); however, no significant difference was found between the two groups (*P*= 0.635) (Figure 3.6D).
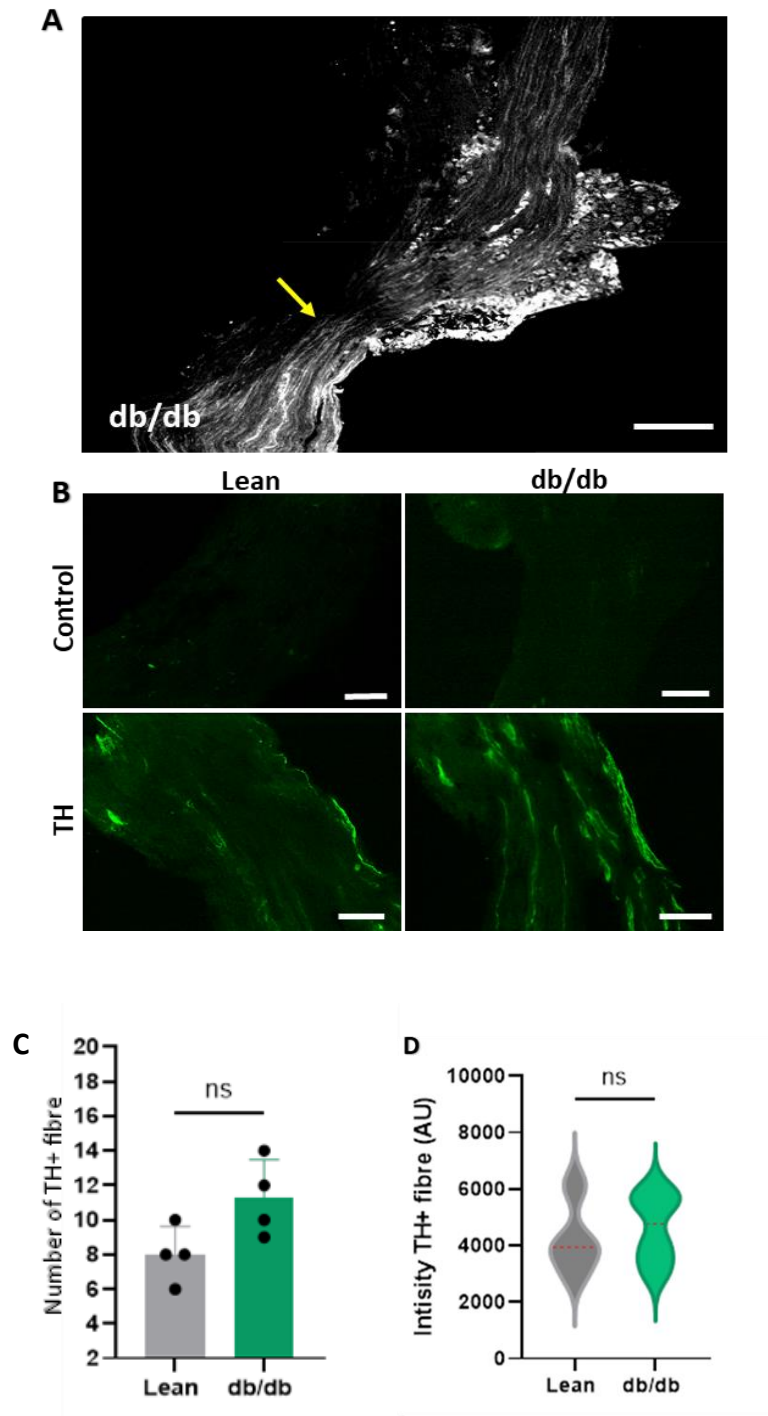
Figure 3.6 Characterisation of TH-positive fibres in the peripheral nerves in the lean and db/db mice

(A) A representative image showing TH-positive fibres extending into the DRG (yellow arrow). (B) Negative controls (upper panels), TH-positive fibres in the peripheral nerves of the lean and db/db mice (lower panels) (C) The average number of TH-positive fibres in lean (8 ±1.37) and db/db (11.25±3.25) show no significant differences, P=0.0563. (D) The Intensity of TH-positive fibres in the lean (3890±335.1) and db/db mice (4520±679.8) with no significant differences, p=0.635. N=4. Scale bar: 20 μm (applied to all images). Two-tailed paired Student's t-test, data shown as mean ± SEM. Grey= lean, green=db/db.

3.4.3 Characterisation of TH-positive neurons in the lumbar DRG of db/db mice

Three parameters were investigated: the number, soma size, and intensity of TH-positive neurons. TH-positive neurons were examined from 16 mice (8 lean and 8 db/db). A total of 2000 neurons from lean mice and 2400 neurons from db/db mice were calculated.

TH-positive neurons were noted in the majority of the DRG sections. The number of TH-positive neurons was consistent between the sections and varied from 5-15 (Figure 3.7A (Lower panels)). No specific pattern was observed in the distribution of the TH-positive neurons within the DRG section.

In lumbar L4, the percentage of TH-positive neurons in the lean mice was (22.36%±3.69, n=8) and in the db/db mice was (26.05%±3.68, n=8), which represented a 3.69% increase in the diabetic mice; however, this was not statistically significant (P=0.655) (Figure 3.2B). Similarly, in lumbar L5, the percentage of TH-positive neurons in the lean mice was (18.21%±3.50, n=8) and in the db/db mice was (22.63%±4.43, n=8), which represented a 4.42% increase in the diabetic mice, however, it was not statistically significant (P=0.846) (Figure 3.7B).

Next, the intensity of the TH-positive neurons was measured. The intensity of TH-positive neurons in lean mice was (39030±654.3, n=8), which was similar to the intensity of TH-positive neurons in the db/db (392269±238.4, n=8) (p= 0.7156) (Figure 3.7C).

Furthermore, the soma size distribution of TH-positive neurons was measured. The soma size distribution showed that TH-positive neurons were mostly of small diameter (range 6-20 μm) (Figure 3.7D). In the lean mice, the median diameter was (13.07μm, 2,739 neurons), while in the db/db the median diameter was (12.97μm, 2,550 neurons), with no significant difference between both groups.
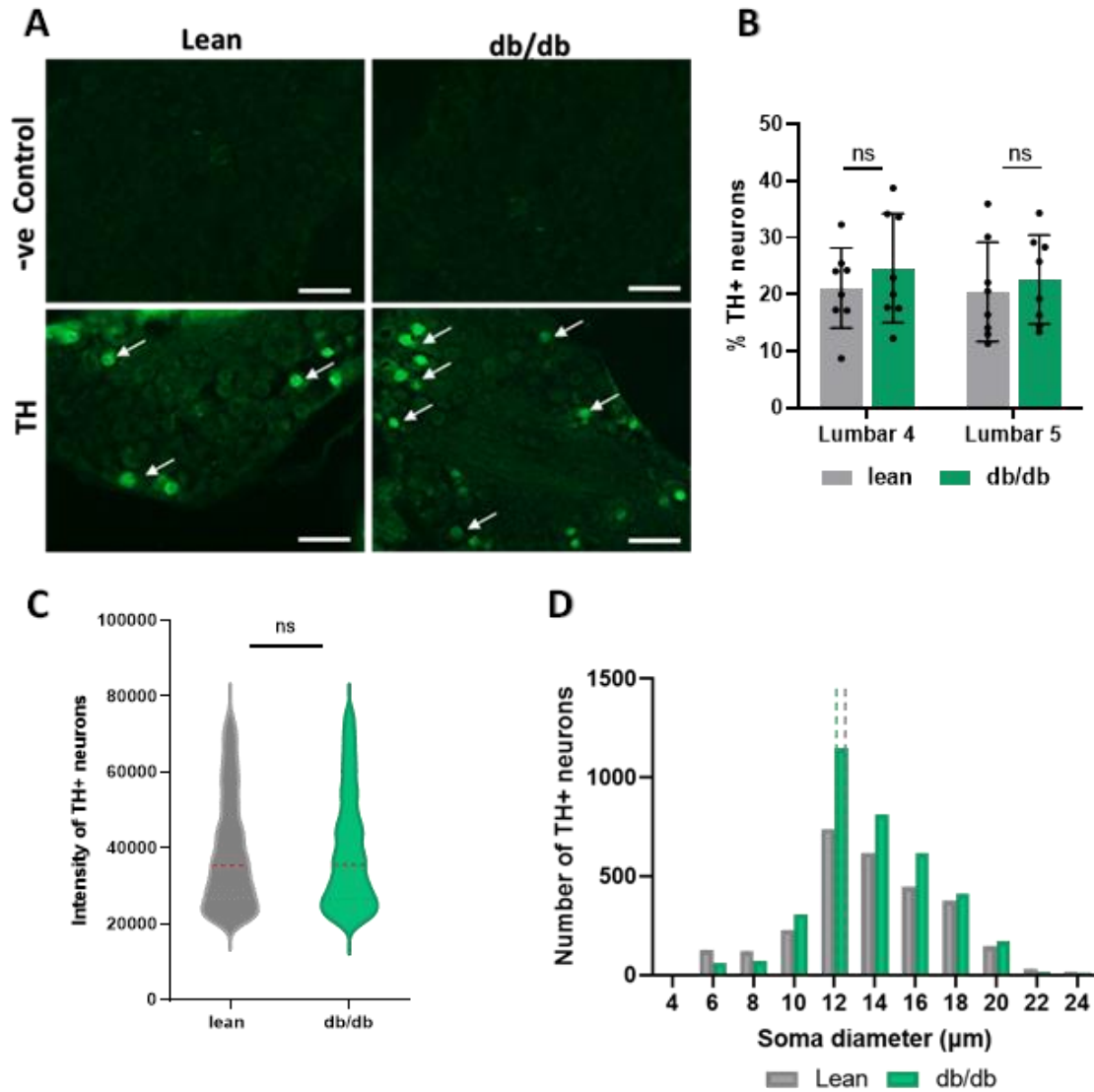
Figure 3.7 Characterisation of TH-positive neurons in the lumbar DRG of lean and db/db mice

(A) Representative images showing the expression of TH in the lumbar DRG of lean and db/db mice. Negative controls (upper panel), TH-positive neurons in lean mice and db/db mice (arrows) (lower panel) (B) Percentage of TH-positive neurons in L4 and L5 DRGs in lean and db/db mice. In L4, TH-positive neurons in lean mice (22.36%±3.69) and db/db mice (26.05%±3.68) represented a 3.69% increase, with no significant difference (P=0.655). In L5, the TH-positive neurons in lean mice (18.21%±3.50) and bd/db mice (22.63%±4.43) represented a 4.42% increase, with no significant difference (p=0.846). (C) The intensity of TH-positive neurons was similar in lean (39030±654.3) and db/db mice (392269±238.4) with no significant differences, p=0.7156. (D) Soma size of TH-positive neurons shows that the median for lean mice was (13.07µm,2,739 neurons) and db/db mice (12.97µm, 3,550 neurons) with a predominance of small diameter neurons. Scale bar: 20 µm (applied to all images). Two-tailed paired Student's t-test; data are shown as mean ± SEM. Symbols (black circles) represent the sample size, N=8. Grey= lean, green=db/db. The dotted lines represent the median soma size for each group.

3.5 Discussion

3.5.1 Main findings

This chapter examined evidence of sympathetic sprouting after diabetes as a contribution to diabetic pain in DPN. We observed that diabetes causes no sympathetic sprouting into the lumbar DRG of the db/db mice. We found that the number of TH-positive fibres was 4% higher in db/db mice and a trend of increase in their intensity. However, these were not significant. We found that TH-positive neurons expressed in lumbar DRG with robust staining. The number of TH-positive neurons was ~4% higher in db/db mice, but this was insignificant. In addition, we measured the size and intensity of TH-positive neurons; there were no changes in either parameter. The lack of sprouting in our model could be attributed to several factors: the differences in injury type, the rate of development, the frequency of occurrence, the proximity of the lesion and species differences.

3.5.2 Sympathetic sprouting is absent from the lumbar DRG of db/db mice at 32 weeks of diabetes

We found no sympathetic TH-fibre sprouting into the lumbar DRG of db/db mice at 32 weeks (Figure 3.5). Studies that performed axotomy, such as spinal nerve ligation (SNL) and sciatic nerve ligation (SNL) found an increased occurrence of sympathetic sprouting (McLachlan *et al.*, 1993; Chung *et al.*, 1996; Lee *et al.*, 1998). However, studies which only applied compression/construction to the peripheral nerves, such as chronic compressed DRG (CCD) and chronic construction injury (CCI), found the sympathetic sprouting to be less extensive (Ramer and Bisby, 1997; Chien *et al.*, 2005). This might explain why we found a lack of sympathetic sprouting. First, the type of injury in our model does not involve a direct cut to the peripheral nerve, which is different from nerve models where nerve damage is caused physically, in which sympathetic sprouting was detectable. Second, the nerve properties in our model are altered by the hyperglycaemic condition in the form of diabetic neuropathy, which might affect the peripheral nerve rather than the DRG where we anticipate observing the sympathetic sprouting.

The distance between the nerve injury and the DRG, on the other hand, and the rapidity of the sprouting on the other hand, were found to be interrelated. The closer the damage to the

peripheral nerve to the DRG, the more extensive the sprouting (Kim *et al.*, 1996). For example, sprouting was observed two days PO after spinal nerve ligation, which is considered the closest injury model to the DRG site (Figure 5.9A) (Chung and Chung, 2001). In contrast, sympathetic sprouting was observed three weeks PO in sciatic nerve ligation, where the injury was considered further away from the DRG compared to SNL (Figure 5.9B). In our db/db model, the peripheral nerve damage was considered the furthest away from the DRG (Figure 5.9C), as we are examining lumbar DRG extending to long axons in the foot. This is similar to sympathetic sprouting observed in the distal injuries, which were more persistent and slower than the rapid sprouting observed following proximal injury (Ramer and Bisby, 1997; Chen and Zhang, 2015).
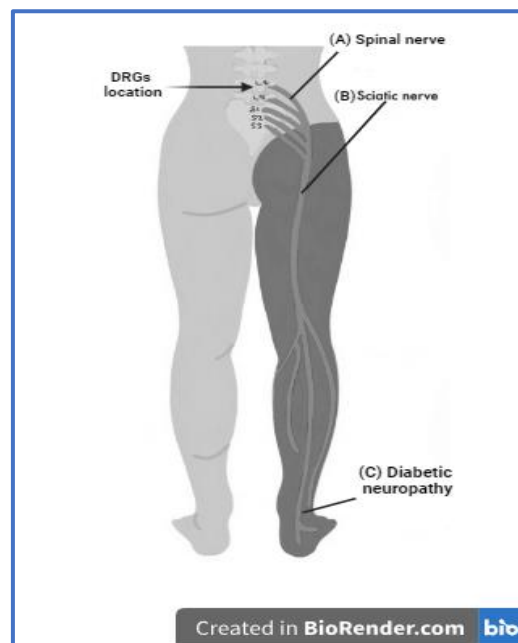
Figure 3.8 Different sites of peripheral nerve injury in relation to DRG

(A) Spinal nerve injury closest to DRG. (B) Sciatic nerve injury is further away from DRG than (A). (C) Diabetic neuropathy is furthest from DRG than (A) and (B).

In addition, sprouting was reported to be more rapid in the case of a chronic compressed injury compared to complete nerve transection at the same distance. Following CCI, but not complete transection, intact axons commingle with damaged axons distal to the injury site, where Wallerian degeneration, inclusive of macrophage infiltration, occurs (Ramer and Bisby, 1998). The production of inflammatory mediators distally might retrograde and travel back

to the DRG. This was also confirmed in transgenic mice, where sympathetic sprouting was not observed in CCI, which are deficient in Wallerian degeneration, although it does occur following SNL (Ramer and Bisby, 1997).

3.5.3 Characterisation of TH-positive fibres in the peripheral nerve remained unchanged in db/db mice

The average number of TH-positive fibres in lean mice was 8 ±1.37 and in db/db mice was 11.25±3.25, with no significant difference (P= 0.0563) (Figure 3.6C). TH-positive fibres were observed near the edge of the nerves, which might mean that the nerve possible indicating that the nerve is surrounded by connective tissue that has a blood supply, so these TH-positive fibres might be those innervating the blood vessels rather than the regrowth fibres. The minimal fibre counts further support our conclusion that sympathetic sprouting is probably absent from the db/db mice, suggesting that the phenomena may not manifest in DPN. Lee and Yoon (1998), observed an increase in TH-positive fibres in the spinal nerve proximal to the nerve ligation one week PO. After that period, these fibres maintained a level (close to normal), suggesting a regenerative process from the proximal part of the injured sympathetic fibres (Lee *et al.*, 1998). In contrast, McLachlan etal (1993) observed a decrease in TH-positive fibre leading to degeneration (McLachlan *et al.*, 1993). These findings might indicate the regenerative characteristics of these TH-positive fibres, which might restore sympathetic innervation following nerve damage.

3.5.3 Characterisation of the TH-positive neurons showed no significant changes in the lumbar DRG of db/db mice

Our findings show that a 3.69% and 4.42% increase occurred in the TH-positive neurons in L4 and L5 DRGs of diabetic mice, respectively (Figure 3.7). Despite this, the analysis did not show significant differences. TH-positive neurons in the DRG increased in rats following CCD (Chien *et al.*, 2005), which aligns with our observations of an increase in the number of TH-positive neurons in db/db mice. However, contrary to our findings, the number of TH-positive neurons decreased in rats after SNI on ipsilateral DRG by 3.7%, seven days PO (Brumovsky, Villar and Hökfelt, 2006). In addition, the number of TH-positive neurons declined by 7% in pelvic and pudendal nerve axotomy (McCarthy *et al.*, 2016). Furthermore, the TH mRNA content was decreased in the DRGs of CCI rats (Herradon *et al.*, 2008). Our findings of a slight increase in

TH-positive neurons in the db/db mice show a different pattern with other models of nerve injuries, indicating a different role for these neurons in mediating sensory dysfunction or compensatory mechanisms in response to DN. However, the nature of the insult—whether metabolic, mechanical, or traumatic might trigger the TH-positive neurons in various ways. The slight increase in TH-positive neurons observed in db/db mice might indicate a shift in the sensory neurons' population in the DRG. As TH-positive neurons are recognised as C-LTMRs (C-fibre low threshold mechanoreceptors), which are involved in the plausible touch and mechanical hypersensitivity, the increase may indicate an adaptive or maladaptive response to an altered sensory environment in DPN (Le Pichon and Chesler, 2014).

Next, we measured the intensity of TH-positive neurons and observed no significant changes in the TH expression in the db/db mice compared to the lean mice (Figure 4.7C). The only study we found that examined changes in the TH gene expression in the lumbar L4 and L5 DRG of STZ diabetic rats (representing T1DM) found no difference after four weeks of diabetes induction. (Athie *et al.*, 2018). This further supports our observation that TH expression in the db/db neurons is not directly involved in the pain mechanism in DN.

Next, we measured the TH-positive neuron's soma size and found that the TH-positive neurons in the db/db DRG fell mainly within a small diameter (Figure 3.6 D). We are the first to investigate the soma size distribution of TH-positive neurons in the DRG of db/db mice. These findings indicate that TH-positive neurons are not structurally affected by diabetes.

3.6 Conclusion

This chapter examined evidence of sympathetic sprouting after diabetes as a possible contribution to painful DPN. We also examined changes to TH-positive neurons and fibres in DRG and peripheral nerves after diabetes. Our findings indicate that diabetes causes no sympathetic sprouting or basket formation, as seen in pain injury models. The most likely reason for this outcome is the type of damage caused by hyperglycaemic conditions in our model, which might not be sufficient to harm the nerve similarly to those seen in other injury models.

Chapter 4: Examining the Number and Soma Size of Sensory Neurons in the Lumbar DRG of db/db Mice

4.1 Introduction

4.1.1 Classification of DRG sensory neurons

Sensory neurons in the DRG represent a heterogenous population of specialised neurons which transmit various stimuli such as touch, temperature, pain, and itching from peripheral axons to the CNS (Wang *et al.*, 2023). DRG sensory neurons are classified according to their morphologically into two categories: large-diameter neurons and small -diameter neurons (Price, 1985; Ruscheweyh *et al.*, 2007; Herweijer *et al.*, 2014). Alternatively, DRG neurons can be classified based on their expression in various intermediate filament proteins. These intermediate filaments are specifically expressed within DRG sensory neurons, including neurofilament (NF200) for large-diameter and peripherin for small-diameter neurons (Fornaro *et al.*, 2008; Le Pichon and Chesler, 2014). Soma size of DRG neurons correlates to different sensory stimulation; large-diameter neurons are involved in touch and pressure, while small-diameter neurons are involved in pain and heat sensation (Harper and Lawson, 1985; Ohtori *et al.*, 2007).

Changes to the number of sensory DRG neurons have been observed in cultured DRG from the db/db model. A significant reduction by 22% in large-dimeter cells and a matched increase by 38% in small-diameter cells were found in diabetic mice compared to control mice (unpublished data from Dr. Nassar's lab). A similar reduction by 40% was observed in large-diameter neurons in other diabetic models such as STZ-rats (40 weeks) with 18% reduction in the same model at a younger age (four weeks) (Sidenius and Jakobsen, 1980; Kishi *et al.*, 2002).

In addition, changes to the number of DRG sensory neurons were observed under neuropathic conditions. Bondok and Sansone (1984), found a significant reduction in large-diameter neurons (>40 μm) in rats after sciatic nerve crush in L4 and L5 DRG, which were 69% and 79%, respectively, with 44-54% decrease in small neurons (Bondok and Sansone, 1984). A significant reduction has also been found affecting all types of lumbar DRG neurons following sciatic nerve transection and amputation in various mammalian (Tandrup, Woolf and Coggeshall, 2000). These studies are summarised in (Table 4.1) below.

Table 4.1 Summary of the studies of neuronal loss in the lumbar DRG of various species following nerve injuries

Study	Animal	Nerve injury	DRG level	Neuronal loss
(Devor *et al.*, 1985)	Rat	Sciatic	L4-L5	8%
(Rich, Disch and Eichler, 1989)		Sciatic	L4-L5	12%
(Himes and Tessler, 1989)		Sciatic	L5	50%
(Vestergaard, Tandrup and Jakobsen, 1997)		Sciatic	L5	35%
(Rich *et al.*, 1987)		Sciatic	L4-L6	17%
(Lekan *et al.*, 1997)		Sciatic	L5-L6	50%
(Feringa *et al.*, 1985)		amputation	L5	30%
(Johnson and Yip, 1985)	Pig	Sciatic	L6	20%
(Risling *et al.*, 1983)	Cat	Sciatic	L7	30%

(Adopted from Tandrup, Woolf and Coggeshall, 2000).

4.1.2 Non-neuronal cells in the DRG

Non-neuronal cells surround the DRG sensory neurons and provide support and modulate the overall properties of the sensory neurons. Several forms of neuronal to non-neuronal crosstalk have been found under neuropathy and inflammation (Ciglieri *et al.*, 2020). In the DRG of CCD rats, the activation of satellite glial cells (SGCs), was found to contribute to neuronal excitability, leading to pain (Warwick and Hanani, 2013). Under these conditions, non-neuronal cells are found to release various mediators such as interleukin 1B (IL-1B), nerve growth factor (NGF), and tumour necrosis factor-α (TNF-α). These mediators stimulate the nociceptive terminals in the peripheral axons leading to increasing pain sensation (Suter *et al.*, 2007; Song *et al.*, 2014; Ji, Chamessian and Zhang, 2016). In addition, changes in the number of non-neuronal cells were observed between different classes of DRG neurons, although these were not affected by diabetes in diabetic STZ rats. Non-neuronal cells, specifically SGC, exhibited a 5% higher number surrounding small-diameter neurons compared to those surrounding large-diameter neurons in both control and STZ rats (Ciglieri *et al.*, 2020).

These studies show that changes in the number and soma size of the DRG sensory neurons and non-neuronal cells have been observed after neuropathic conditions and other diabetic models (in vitro). To our knowledge, no studies have explored changes in the number and soma size distribution of sensory neurons in the lumbar DRG of db/db mice (*in vivo*) or changes in the number of non-neuronal cells.

4.2 Hypothesis

Diabetes causes a reduction in the number of large-diameter neurons labelled NF200 in db/db mice.

4.3 Aims

- To assess the number and soma size distribution of large-diameter neurons labelled NF200 and small-diameter neurons labelled PRPH in the lumbar DRG of db/db mice.
- To assess the number of non-neuronal cells in lumbar DRG of db/db mice.

4.4 Results

4.4.1 Characterisation of NF200-Positive Neurons and PRPH-Positive Neurons in Lumbar DRG of db/db mice

The negative controls show a clear, low background for the anti-rabbit secondary (Figure 4.1A), but the background was higher for the anti-mouse secondary (Figure 4.1B). The labelling of NF200 was robust and consistent across all DRG sections in both lean and db/db mice. As expected, NF200 labelled large-diameter neurons (Figure 4.1C and D). The labelling of PRPH was robust and consistent in all DRG sections, and as expected, PRPH labelled small diameter neurons (Figure 4.1E and F). Several neurons expressed NF200 and PRPH in lean and db/db DRG sections (Figure 4.2G and H).

Vacuolisation was observed in the cytoplasm of a few NF200-positive neurons in both lean and db/db mice (Figure 4.2). However, no vacuoles were observed in PRPH-positive neurons. Vacuolisation appeared to have a higher occurrence in diabetic mice compared to lean mice. This will be investigated in chapter 5.
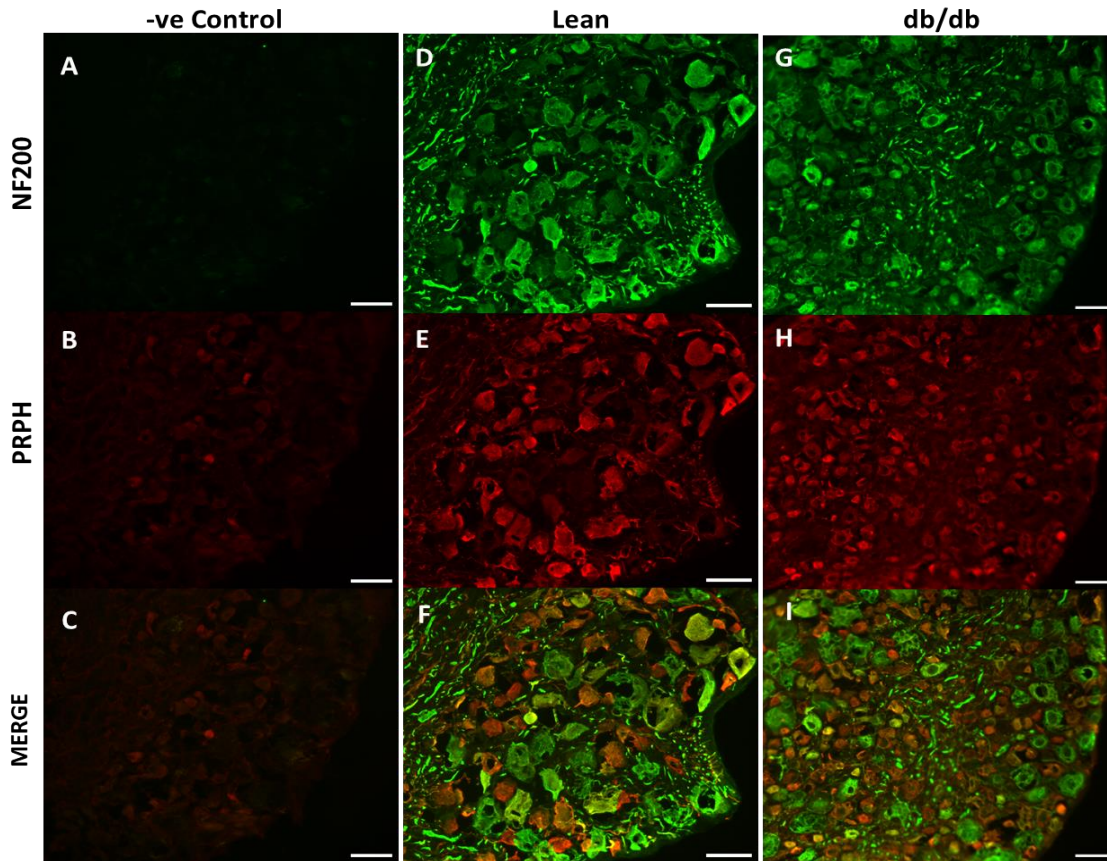
Figure 4.1 NF200-positive and PRPH-positive sensory neurons labelling in lumbar DRG of lean and db/db mice

*Representative images showing the expression NF200 (green) and PRPH (red) and merged channels in DRG sections from lean **(D, E, F)** and db/db **(G, H, I)** mice. Negative controls **(A, B, C).** NF200 show robust staining of the large-diameter neurons in DRG of lean mice **(D)** and db/db mice **(G)**. The PRPH show robust staining of small-diameter neurons in lean mice **(E)** and db/db mice **(H)**. Merged images show a few DRG neurons labelled NF200 and PRPH in lean mice **(F)** and db/db mice (**I**). Scale bars= 20 µm (applied to all images).*
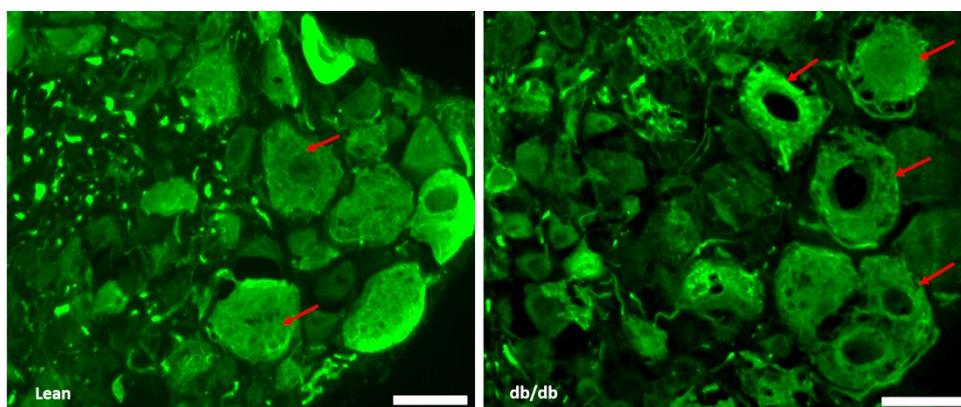
Figure 4.2 Vacuoles-like structure in a few NF200-positive neurons in DRG of lean and db/db mice

*Representative images showing a few neurons labelled NF200 containing vacuoles-like structures (red arrows) in lean mice **(A)** and db/db mice **(B)** DRGs. Scale bars: 40 µm.*

4.4.2 Diabetes results in a significant reduction in NF200-positive neurons in the lumbar DRG of db/db mice

The total percentage of NF200-positive neurons in lean mice was (41.27±3.495), compared to (28.81±12.46) in db/db mice, reflecting a 12.46% reduction in diabetic mice (Figure 4.3A, n=16, 32 DRGs, P=0.0031).

In lumbar L4 DRG, the percentage of NF200-positive neurons decreased from 45.55±4.86 in lean mice to 30.25±15.30 in db/db mice, representing a 15.3% reduction (Figure 4.3B, n=16, 16 DRGs, P=0.0072). Similarly, in lumbar L5 DRG, NF200-positive neurons decreased from 39.01±3.86 in lean mice to 27.73±11.34 in db/db mice, representing 11.28% reduction (Figure 4.3C, n=16, 16DRGs, P=0.0109).

Overall, these findings confirm that diabetic peripheral neuropathy leads to a significant decrease in the percentage of NF200-positive neurons in both lumbar L4 and L5 DRG.
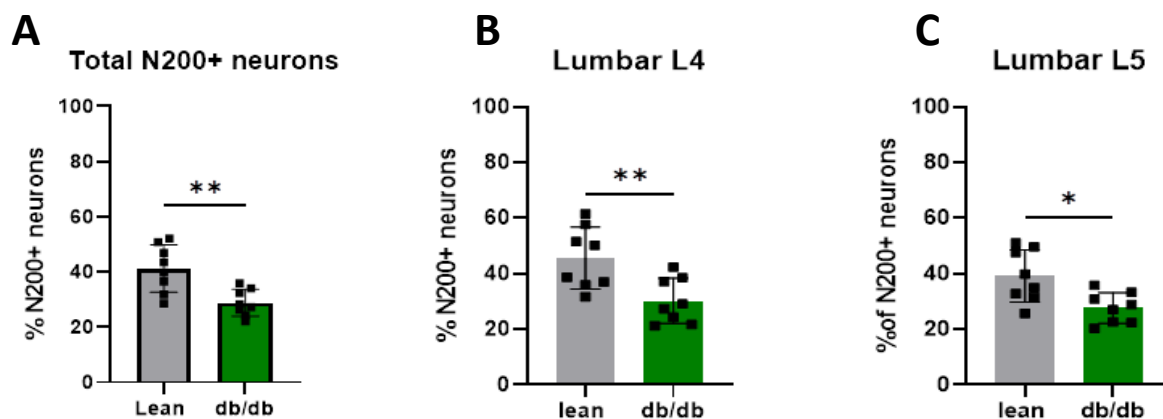
Figure 4.3 Percentages of NF200-positive neurons in total, L4 , and L5 DRGs in lean and db/db mice

(A) The total percentage of NF200-positive neurons in lean mice (41.27±3.495) and in db/db mice (28.81±12.46), reflecting a 12.46% significant decrease in diabetic mice, p=0.0031 (B) In lumbar L4 DRG, the percentage of NF200-positive neurons in lean mice (45.55±4.865) and in db/db mice (30.25% ±15.30), reflecting 15.3% significant reduction, p=0.0072 (C) In lumbar L5 DRG, the percentage of NF200-positive neurons in lean mice (39.01±3.863) and in db/db mice (27.73±11.34), reflecting a 11.28% significant reduction, p= P=0.0109. N=16. Two-tailed unpaired Student's t-test, data represented as mean±SEM. Grey= lean, green=db/db.

4.4.3 Shift in the soma size distribution of NF200-positive neurons toward smaller diameter in lumbar DRG of db/db mice

The soma size distribution of NF200-positive neurons in the lumbar DRG of db/db mice exhibited a significant reduction, particularly in the lumbar L4 DRG. The decrease was observed across all neuron sizes and was not limited to a specific diameter.

In lumbar L4 DRG, the median soma diameter in lean mice was 36 μm (1,197 neurons), while in db/db mice, it was significantly reduced to 27 μm (572 neurons). The difference was statistically significant (Figure 4.4A and B, n=16, 16 DRGs, P<0.0001). The histogram showed that the reduction in soma size was most pronounced in neurons with a diameter of around 33 μm.

In contrast, the lumbar L5 DRG did not show a statistically significant difference between the two groups. The median soma diameter was 36 μm for both lean (792 neurons) and db/db (505 neurons), with no significant shift in the overall distribution (Figure 4.4C and D n=16, 16 DRGs, ns).

Collectively, these findings show that diabetic peripheral neuropathy causes the soma diameter of NF200-positive neurons to shift toward smaller sizes.
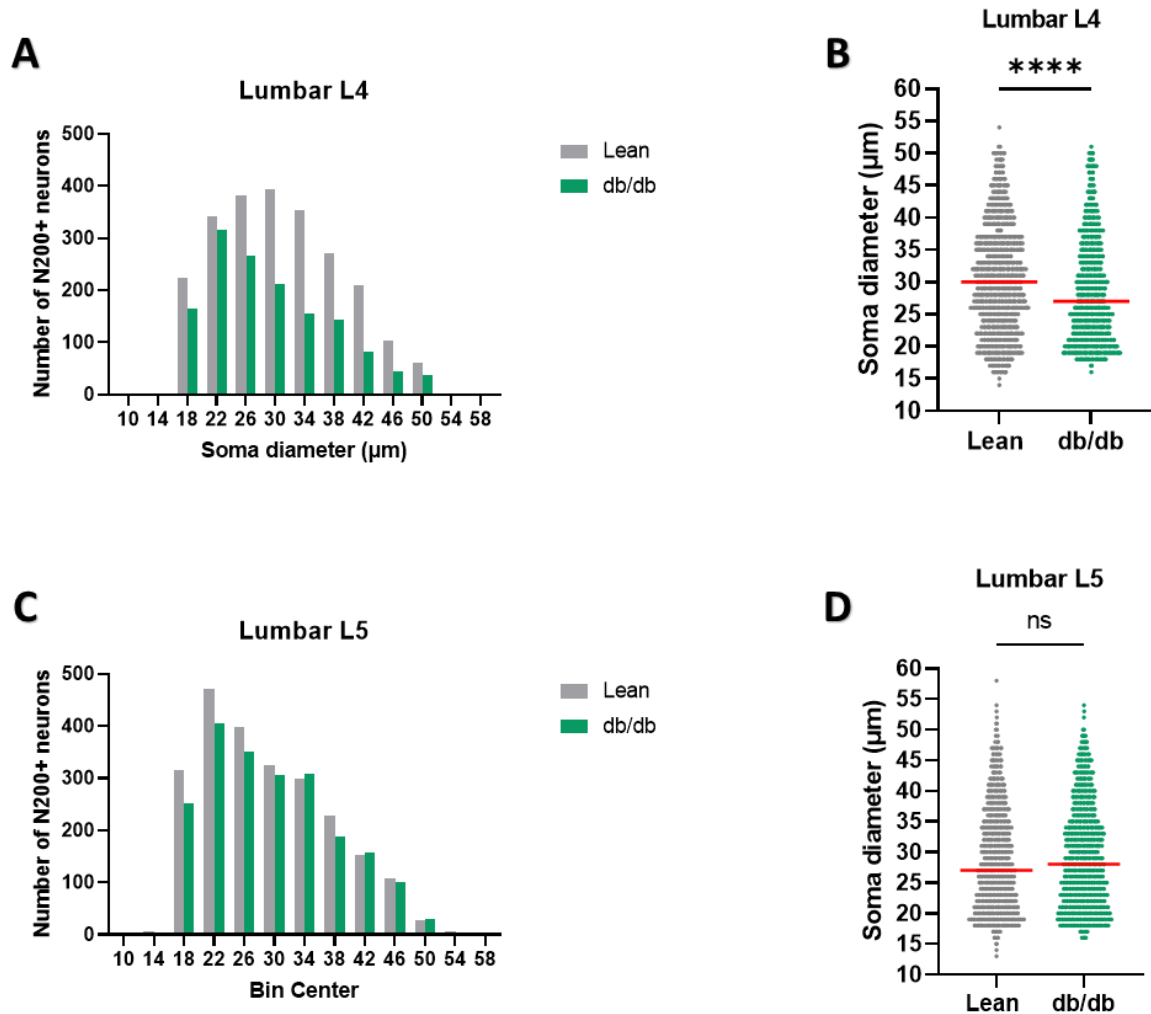
Figure 4.4 Frequency distribution of NF200-positive neurons in L4 and L5 DRGs of lean and db/db mice

The soma size of NF200-positive neurons shifted toward smaller sizes, with size 33 µm being more affected ≥26 µm. (A) Lumbar L4, the soma size distribution of NF200-positive neurons in db/db shows a shift toward smaller diameter compared to lean mice, with the most pronounced reduction observed around the 33 range µm. The median diameter: lean= 36 µm (1197) neurons; db/db= 36 µm (572 neurons). (B) Individual data points for NF200-positive soma diameter in lumbar L4 show the median diameter (indicated by red lines) in db/db mice is significantly smaller than in lean mice (P<0.0001). (C) Lumbar L5, the soma distribution shows no significant differences between lean and db/db mice. The median soma diameter was 36 µm in both groups; Lean=36 µm (792 neurons); db/db=36 µm (505) neurons. (D) Individual data points for NF200-positive soma diameter in lumbar L5 show the median diameter (indicated by red lines) in db/db mice similar to lean mice. N=16. Soma size plotted as number of neurons observed in each 4 µm bin of diameter. Two-tailed unpaired Student's t-test, data represented as mean±SEM. P<0.0001, ns= non-significant. Grey= lean, green=db/db.

4.4.4 PRPH-positive Neurons showed no changes in their number in Lumbar DRG of db/db mice

The total percentage of PRPH-positive neurons in lean mice was (57.09±3.06), and in db/db mice was (71.50±14.42). This represented a 14.41% increase in diabetic mice (Figure 4.5A n=16, 32 DRGs, P=0.0003).

In the lumbar L4 DRG, the percentage of PRPH-positive neurons in lean mice was (54.45±4.733) and in db/db mice was (69.01±14.55) (Figure 4.5B n=16, 16DRGs, P=0.0082). Similarly, in the lumbar L5 DRG, the percentage of PRPH-positive neurons in lean mice was (61.37±4.136) and in db/db mice was (72.33±10.97) (Figure 4.5C n=16, 16DRGs, P=0.0190).

Overall, these findings confirm that diabetic peripheral neuropathy does not change the number of PRPH-positive neurons in the lumbar L4 and L5 DRG.
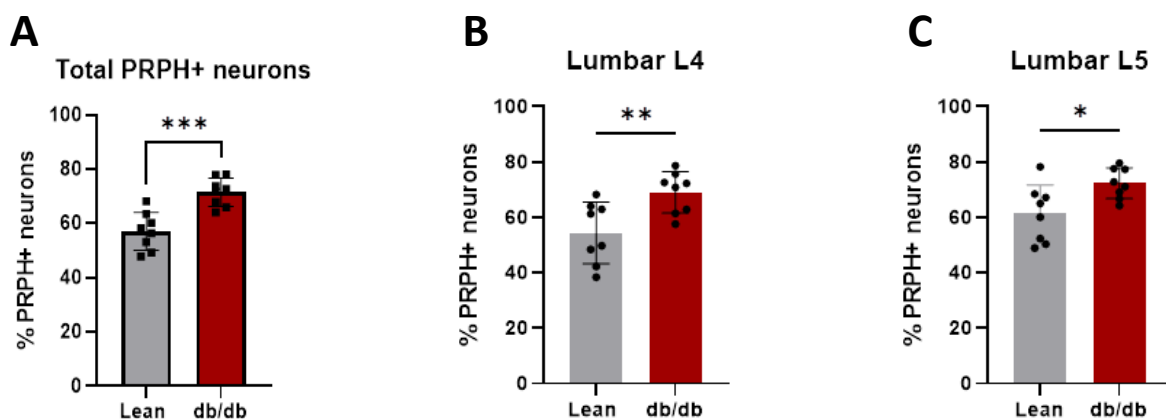
Figure 4.5 Percentages of PRPH-positive neurons in total, L4, and L5 DRGs in Lean and db/db Mice

(A) The total percentage of PRPH-positive neurons in lean mice (57.09±3.06) and in db/db mice (71.50±14.42), reflecting 14.41% increase in diabetic mice, p=0.0003 (B) In lumbar L4 DRG, the percentage of PRPH-positive neurons in lean mice (54.45±4.733) and in db/db mice (69.01±14.55), p= P=0.0082 (C) In lumbar L5 DRG, the percentage of PRPH-positive neurons in lean mice (61.37±4.136) and in db/db mice (72.33±10.97), p= P=0.0190. N=16. Two-tailed unpaired Student's t-test, data represented as mean±SEM. Grey= lean, green=db/db.

4.4.5 Soma diameter of PRPH-positive neurons showed no changes in lumbar L4 and L5 DRG of db/db mice.

The soma size distribution of PRPH-positive neurons in lean and db/db mice did not significantly change.

In the lumbar L4 DRG, the median soma diameter of PRPH-positive neurons in db/db mice were 12 µm (3312 neurons) compared to 11 µm in lean mice (3080) neurons. Despite a slight shift in the distribution toward larger diameters in db/db mice, this difference was not statistically significant (Figure 4.6A n=16, 16 DRGs, P<0.0001). The overall distribution pattern in lumbar L4 remained similar between the two groups.

In the lumbar L5 DRG, the median soma diameter was identical at 12 µm for both db/db and lean mice (lean=2,907 neurons; db/db= 3499 neurons). There were no significant differences in the distribution or median diameter between the groups (Figure 5.6C and D n=16, 16 DRGs, P<0.0001).

These findings show that diabetic peripheral neuropathy does not cause changes in the soma diameter distribution of PRPH-positive neurons in either lumbar L4 or lumbar L5 DRG of db/db mice.
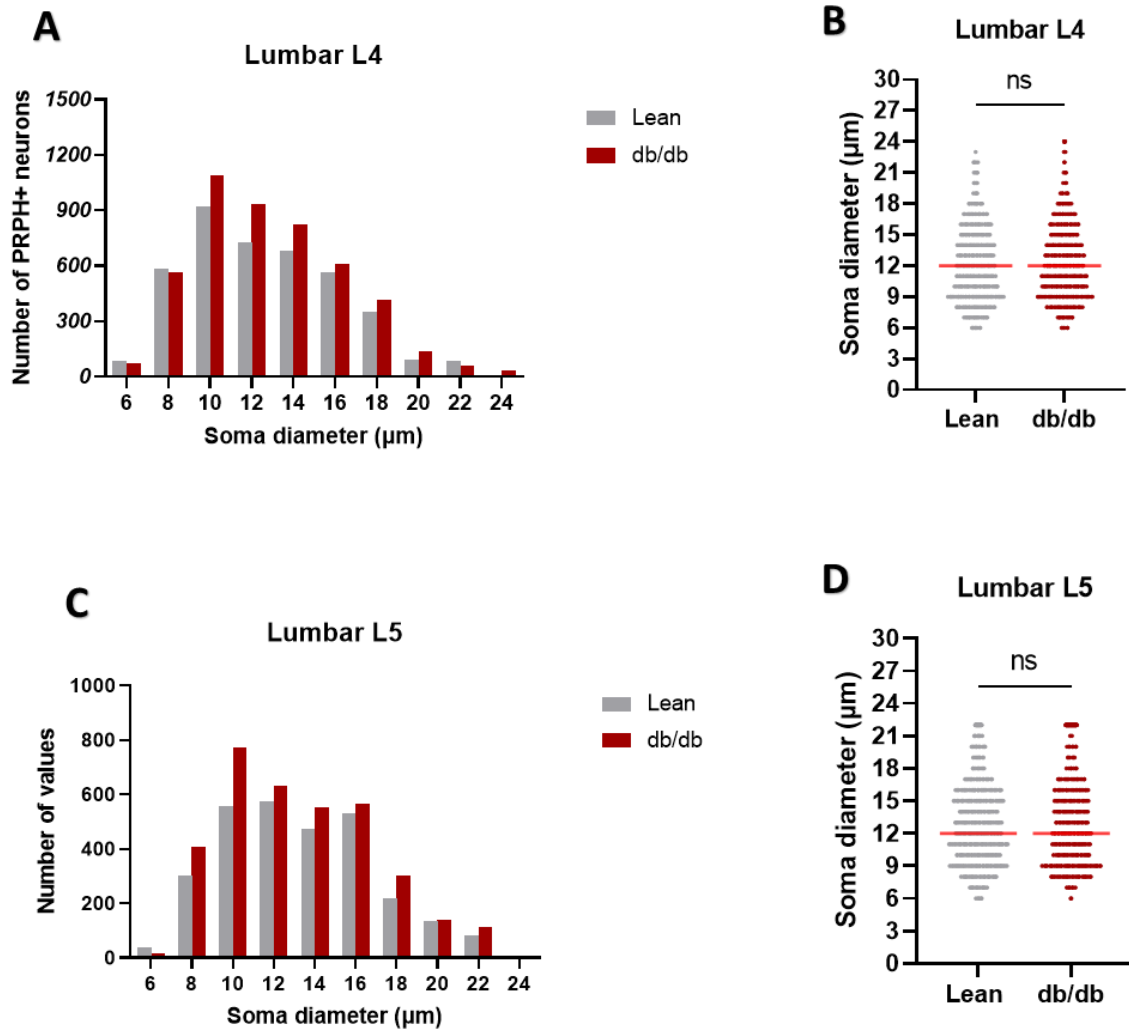
Figure 4.6 Frequency distribution of PRPH-positive neurons in L4 and L5 DRGs of lean and db/db mice

(A) The soma size distribution of PRPH-positive neurons in lumbar L4 DRG shows a similar distribution pattern between lean and db/db mice. db/db mice shows a slight shift toward larger diameters compared to lean mice, with median diameter for lean= 11 μm (3080 neurons) and db/db= 12 μm, (3312 neurons). (B) Individual data points for PRPH-positive soma diameter in lumbar L4 show the median diameter (indicated by red lines) in db/db mice is slightly higher than lean mice, however not significant. (C) The soma size distribution of PRPH-positive neurons in lumbar L5 DRG shows no significant differences between lean and db/db mice. The median soma diameter is identical at 12 μm for both; db/db= 3,499 neurons and lean= 2,907 neurons. (D) Individual data points for PRPH-positive soma diameter in lumbar L5 show the median diameter (indicated by red lines) in db/db mice is similar to lean mice. N=16. Soma size plotted as number of neurons observed in each 2 μm bin of diameter. Two-tailed unpaired Student's t-test, data represented as mean±SEM. ns= non-significant. Grey= lean, red=db/db.

4.4.5 The number of non-neuronal cells in lumbar DRG showed no change in db/db mice

There was no change in the percentage of non-neuronal cells in db/db mice compared to lean mice.

In the lumbar L4, the percentages of non-neuronal cells show a slight increase in db/db mice (46.25±8.062) compared to lean mice (38.19±6.573), however, this was not statistically significant (Figure 4.7A, n=16, 16 DRGs, ns). Similarly, in the lumbar L5, non-neuronal cells showed no difference between lean (35.64%8.371) compared to db/db (22±8.577) (Figure 4.7B, n=16, 16 DRGs, ns).

Overall, these findings showed that the number of non-neuronal cells was not affected by diabetic peripheral neuropathy.
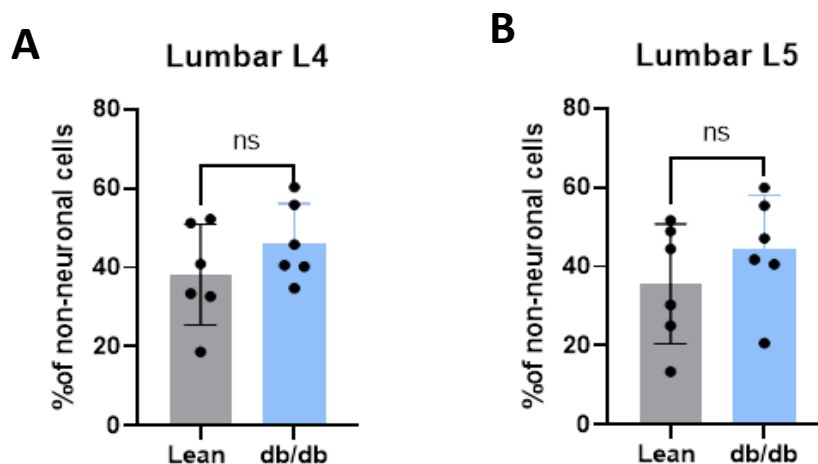
Figure 4.7 Percentage of non-neuronal cells in L4 and L5 DRGs of lean and db/db mice

The percentage of non-neuronal cells shows no significant difference between db/db and lean DRG. (A) In lumbar L4, the percentage of non-neuronal cells in lean mice (38.19±6.573) and in db/db mice (46.25±8.062), showed no significant differences. (B) In lumbar L5, the percentage of non-neuronal cells in lean mice (35.64±8.371) and in db/db mice (44.22±8.577), showed no significant differences. N=16. Two-tailed unpaired Student's t-test, data represented as mean±SEM. ns= non-significant. Grey= lean, blue=db/db.

Taken together, these findings confirm that DPN leads to changes in the number and soma size distribution of NF200-positive neurons. However, no significant changes were observed in either PRPH-positive neurons or non-neuronal cells in db/db mice.

4.5 Discussion

4.5.1 Main findings

This chapter examined the changes in the percentage and soma size distribution of NF200-positive neurons and PRPH-positive neurons in the lumbar L4 and L5 DRGs of db/db mice. The total percentage of NF200-positive neurons was significantly reduced by 11.57% in the lumbar DRG of db/db mice compared to lean mice (Figure 4.3). The soma size distribution of NF200-positive neurons showed a significant reduction across all neuron sizes in lumbar DRG of db/db mice, particularly in lumbar L4 DRG (Figure 4.4). In addition, there were no changes in the number or soma size of PRPH-positive neurons in diabetic mice (Figure 4.5 and 4.6). The percentage of non-neuronal cells after diabetes was not affected (Figure 4.7). An interesting finding was the presence of vacuole-like structures in the cytoplasm of NF200-positive neurons in both lean and db/db mice, with a higher incidence in diabetic mice (Figure 5.3) (Investigated in Chapter 5).

4.5.2 The percentage of NF200-positive neurons was reduced in the lumbar DRG of db/db mice

We found a significant reduction in the percentage of NF200-positive neurons (large-diameter neurons) of 11.57% in db/db mice compared to lean mice (Figure 4.4A). This aligns with the significant reduction in the number of large-diameter cells obtained from cultured DRG of the same model db/db, which was 22% lower in diabetic mice compared to control mice (unpublished data from Nasar's lab). Additionally, the reduction in large-diameter neurons was observed in other (in vitro) diabetic models. Kishi etal. (2002), found a 40% reduction in large-diameter neurons (≥ 50 µm according to their size group) in L5 DRG of STZ rats at 42 weeks (Kishi *et al.*, 2002). Sidenius and Jakobson (1980) also found an 18% reduction in the number of large-diameter neurons in the DRG of STZ rats at a younger age of 4 weeks (Sidenius and Jakobson, 1980). Similarly, Shi etal. (2013) observed a 33% loss in medium to large-diameter neurons (20 µm -40 µm, according to their size group) in L5 DRG of db/db mice at 32-33 weeks, although this loss was not present at 5-6 weeks, suggesting a progressive impact of diabetes over time (Shi *et al.*, 2013). These studies align with our finding of a decrease in the number of large-diameter neurons (labelled NF200) at the older age of 32 weeks and the reduction reported by other studies that employed *in-vitro* diabetic models.

Additionally, large-diameter neurons labelled NF200 were found to be decreased in neuropathic models. A significant reduction of 26.1% in NF200-positive neurons in L4 and L5 DRGs following sciatic nerve transection (90 days PO) (Chelyshev and Raginov, 2002). In the chronic nerve compression (CNC) model, a marked decrease in the number of NF200-positive neurons from L4 and L5 DRGs was observed 2 weeks and 1-month following injury (Chao *et al.*, 2008). In contrast, in spinal nerve ligation (SNL), the total number of NF200-positive neurons was not reduced, although a significant reduction of 30% was observed in neurons with the largest diameter (44-58 µm according to their group sizes) (Hammond *et al.*, 2004).

Large-diameter neurons are myelinated A-fibre neurons, which convey proprioception and mechanical stimuli (touch and pressure) (Scroggs and Fox, 1992; Le Pichon and Chesler, 2014). A reduction in their number indicates an accompanying decrease in the number of myelinated sensory neurons, which leads to sensory deficits (Boulton, 2010). This reduction in diabetic conditions contributed to hyposensitivity and hypoalgesia, according to behaviour studies (Shi *et al.*, 2013). Their loss could also provide a mechanistic explanation for the decreased tactile sensitivity reported by patients with T2DM (Sosenko *et al.*, 1993; Rinkel *et al.*, 2018).

4.5.3 Soma size distribution of NF200-positive neurons shifted toward smaller sizes in the lumbar DRG of db/db mice.

Our findings found the soma size distribution of NF200-positive neurons in the lumbar DRG of db/db mice to be reduced. This aligns with the significant reduction in soma size of large-diameter neurons (>30 µm) in lumbar L5 DRG of STZ rats, accounting from 38.3 µm in control rats to 32.6 µm in diabetic rats (P<0.05) (Zochodne *et al.*, 2001). This reduction shifted the soma size toward the left at 48 weeks but not at eight weeks of diabetes, which indicated the development of atrophy (Zochodne *et al.*, 2001). Similarly, Sidenius and Jakobsen (1980), observed a reduction in the perikaryal volume (soma size) of A-cells (large-diameter) in lumbar L5 DRG in STZ rats (4 weeks), from 35.6 µm in control rats to 32.4 µm in diabetic rats (Sidenius and Jakobsen, 1980). However, Rees and Alcolado (2005) observed no changes in the soma size distribution in DRG neurons of STZ rats at 4 weeks of diabetes (Rees and Alcolado, 2005) (Rees and Alcolado, 2005). There are several reported morphological changes in the soma size of large-diameter neurons due to inclusions and demyelination (Sasaki *et al.*, 1997). In addition, large-diameter neurons were reported to undergo apoptosis associated

with oxidative damage and caspase-3 expression (Russell *et al.*, 1999; Srinivasan, Stevens and Wiley, 2000).

In addition, in our finding, the soma diameter of Lumbar L4 DRG neurons was significantly reduced from 36 μm in lean mice to 27 μm in db/db (P<0.0001) compared to lumbar L5, which reduced too, however, was not significant (Figure 4.5A-D). Our finding generally aligns with others indicating that diabetes can lead to morphological changes in DRG neurons, although the specific regional differences between L4 and L5 have not been extensively documented. To our knowledge, we are the only study that measured the soma size distribution for lumbar L4 and lumbar L5 separately. There is one study that differentiated L4 Vs L5 DRG in humans in terms of cell body count. They found the cell body counts were slightly higher by 14% in L4 DRG compared to L5 DRG with no significant differences (p=0.0492) (Sperry *et al.*, 2020).

4.5.4 Characterisation of peripherin-positive neurons in the lumbar DRG of db/db mice

Our finding observed that accompany the reduction in N200-positive neurons in db/db DRG, the percentage of small-diameter neurons labelled PRPH increased by 25.23% in lumbar DRG of db/db mice compared to lean mice (Figure 4.6 A). Note that the increase in percentage is only due to the loss of N200, which leads to the change in the total number of neurons in a DRG. However, other studies reported changes to the number of small-diameter neurons after diabetes. In STZ rats, a slight increase of 7% in B-type neurons (representing small-diameter neurons) was observed at 48 weeks but not at four weeks of diabetes (Sidenius and Jakobsen, 1980; Kishi *et al.*, 2002). On the other hand, a significant reduction of 40% was observed in small-diameter neurons labelled SP (Substance P, marker for small-diameter neurons) in the lumbar DRG of BB/Wor rats (40 weeks) (Kamiya *et al.*, 2006). In addition, we found no significant changes in the soma size distributions of PRPH-positive neurons between db/db and lean mice in either L4 or L5 DRGs (Figure 4.6). To our knowledge, only one study compared the soma distribution of PRPH-positive neurons between rat and marmoset models, which reported the distribution pattern was similar in both species, which aligns with our findings (Kudo *et al.*, 2021). Small-diameter neurons are known to be involved in pain perception. It is reported that half a percentage of diabetic patients suffer from pain sensations (Ko *et al.*, 2013; Lima *et al.*, 2017). However, in our db/db model, we could not conclude that pain in DPN is attributed to PRPH-positive neurons.

4.5.5 The percentage of non-neuronal cells was not affected in lumbar DRG of db/db mice

Our findings showed no significant changes in the percentage of non-neuronal cells in the lumbar DRG of db/db mice compared to lean mice (Figure 4.8). Note that we counted the non-neuronal cells using DAPI staining as a general marker rather than specific markers for specific types of non-neuronal cells. To our knowledge, no available studies examined the changes in the number of non-neuronal cells after diabetes. However, the available information about changes to the proportion of non-neuronal cells has been observed after nerve injury. In the CCD model, non-neuronal cells (specifically endothelial cells) were activated in the form of angiogenesis, i.e., an increased number of capillaries in the DRG (LaMotte and Ma, 2008). In addition, activation of SGCs was observed in CCD rats, which contributed to neuronal excitability, leading to pain (Warwick and Hanani, 2013). These responses are typically associated with neuroinflammation, mediator release, and an attempt to support neuronal survival and repair.

4.6 Conclusion

This chapter explored changes in the number and soma size of large-diameter neurons NF200-positive and small-diameter neurons PRPH-positive in the lumbar L4 and L5 DRG of db/db mice at 32 weeks. It also examined changes in the number of non-neuronal cells in db/db mice. Our findings indicated that diabetes significantly reduces the number and soma size of NF200-positive neurons. These large-diameter neurons are proprioceptive, which might explain the loss of touch sensation reported by T2DM. However, no change in the peripherin-positive neurons nor the non-neuronal cells was detected.

Chapter 5: Characterising Cytoplasmic Vacuoles in the Lumbar DRG of db/db Mice

5.1 Introduction

In Chapter 4, we observed cytoplasmic vacuoles in NF200-positive neurons in the lumbar DRG. Our preliminary observations showed that vacuoles appeared in both lean and db/db DRGs. This chapter will characterise cytoplasmic vacuoles in NF200-positive neurons in the lumbar DRG of db/db mice. Cytoplasmic vacuoles in the DRG sensory neurons have been reported in various models of T1DM. As early as four weeks after the onset of diabetes, vacuoles were observed in STZ-induced diabetic rats (Sasaki *et al.*, 1997; Russell *et al.*, 1999). Later stages of diabetes also show vacuole formation in BB/Wor rats at 40 weeks and Non-Obese Diabetic (NOD) mice at 32 weeks (Kamiya, Zhang and Sima, 2006; Corral-Pujol *et al.*, 2023). These findings suggest that the observation of vacuoles in both early and late stages of diabetes might reflect ongoing cellular stress and damage throughout the course of the diabetes. This progression underscores the possibility that vacuoles are not merely a consequence of advanced diabetes but could be an early indicator of neurodegeneration, persisting as the condition worsens. While vacuoles are found in both control and diabetic DRGs, diabetic models exhibited a significantly 1.7-fold higher percentage of vacuolated neurons (VN) (Sasaki *et al.*, 1997). This implies that vacuolation in the DRG might occur because of the underlying mechanisms of hyperglycemia, such as oxidative stress, metabolic dysfunction, and impaired cellular repair, which might accelerate their formation. The vacuoles observed in DRG neurons vary in appearance, ranging from multiple small vacuoles to a single large vacuole within the cytoplasm of both small- and large-diameter neurons (Figure 5.1) (Sasaki *et al.*, 1997; Kamiya, Zhang and Sima, 2006; Corral-Pujol *et al.*, 2023).
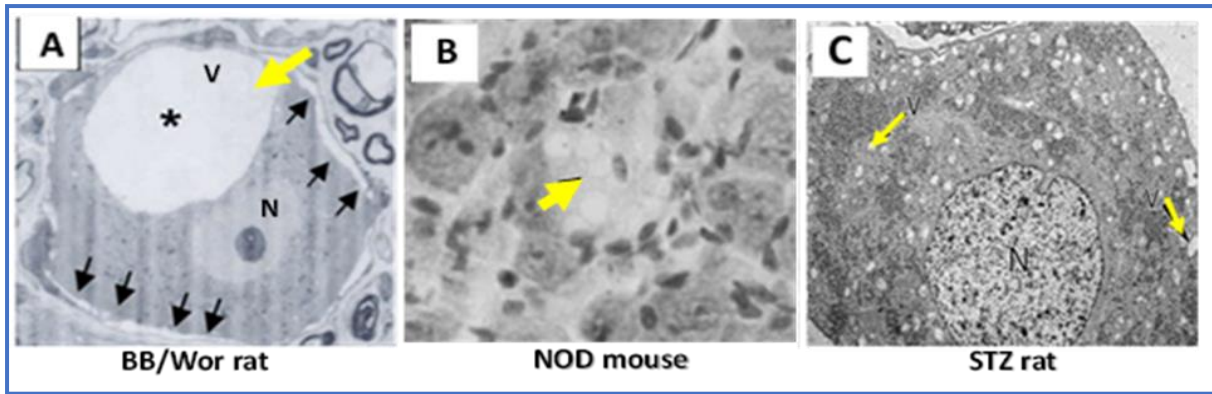
Figure 5.1 Cytoplasmic Vacuoles in DRG of T1DM models

(A) DRG of BB/Wor rat shows a single large vacuole (V) (yellow arrow) which occupied most of the cytoplasmic region compared to the nucleus (N), and subplasmalemmal small vacuoles (black arrows). (B) DRG of NOD mice show many vacuoles (arrow) in the cytoplasm of neurons DRG neuron of STZ rats. (C) DRG of STZ-rat shows many small-size vacuoles (arrow) distributed evenly in the cytoplasm. (Adopted from Kamiya, Zang and Sima, (2006), Corral-Pujol etal., (2023), Sasaki (1997)).

In addition to diabetic models, vacuole formation has been reported in neuropathic models, such as those exposed to neurotoxic agents like organophosphates (Rogers-Cotrone *et al.*, 2010). In these cases, vacuoles are predominantly located in large-diameter neurons and characterised by a single membrane within the neuronal periphery (Figure 5.2). Moreover, similar vacuole formation has been detected in models of nerve injury, including sciatic nerve transection (Groves *et al.*, 1997) and compression (Tang *et al.*, 2009). This broad distribution of vacuoles across diabetic, neuropathic, and neurodegenerative models demonstrates their involvement in various forms of neuronal damage. However, the exact origin and mechanism of vacuole formation remain subjects of ongoing debate.
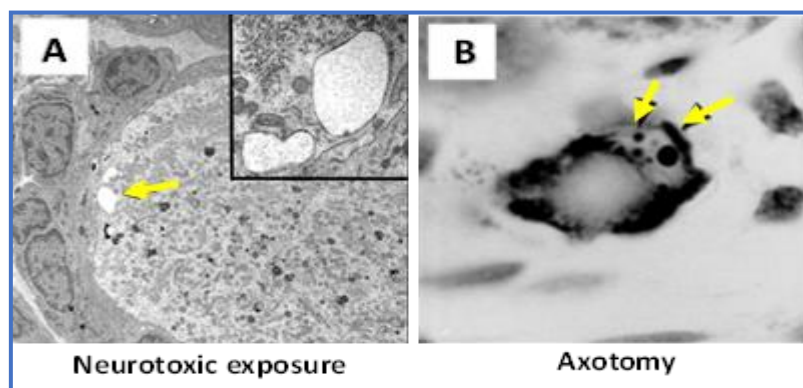
Figure 5.2 Cytoplasmic Vacuoles in DRG of nerve injury models

(A) DRG of neuropathic rats showing large vacuoles at the periphery of large-diameter neurons (arrow) after exposure to a neurotoxin (inset magnification of vacuole). (B) DRG of axotomised rats showing various vacuoles in the cytoplasm of neurons. (Adopted from Rogers-Cotrone etal, (2010) and Groves etal., (1997)).

Cytoplasmic vacuoles in the DRG sensory neurons are reported to originate due to organelle dysfunction (Pop-Busui, Sima and Stevens, 2006; Rogers-Cotrone *et al.*, 2010). For example, in BB/Wor diabetic rats, vacuoles have been linked to the Golgi apparatus (GA) fragmentation within DRG sensory neurons (Kamiya *et al.*, 2006). In STZ-diabetic rats, vacuoles are occurred because of mitochondrial swelling or "ballooning" (Russell *et al.*, 1999; Cavaletti *et al.*, 2007). Moreover, dysfunction in the autophagic pathway, a key feature of neurodegenerative diseases (NDD) such as Alzheimer's disease (AD), leads to the accumulation of autophagic vacuoles that fail to mature and degrade their contents (Nixon and Yang, 2011). While vacuoles were found to originate from cellular dysfunction, others reported an artificial and spontaneous origin (Butt, 2010) or were observed during normal ageing (Sulzer *et al.*, 2008). These organelle dysfunctions are not a separate phenomenon but are closely linked to cellular stress and damage. In diabetic conditions, DRG neurons experience many stress conditions, including oxidative stress, hypoxia, and inflammation, which damage cellular components like DNA, proteins, and lipids (Piras *et al.*, 2016; Tay *et al.*, 2019). These stressors contribute to organelles dysfunction, which might eventually lead to vacuole formation. While vacuoles have been well-documented in T1DM and neuropathic models, this study is the first to characterise their presence in T2DM (db/db) mice at 32 weeks. The connection between vacuole formation, cellular stress, and organelle dysfunction highlights a possible link between vacuoles and the progression of DN in T2DM, which could serve as a marker of neuronal damage and stress.

5.2 Hypothesis

Cytoplasmic vacuoles in the lumbar DRG of db/db mice originate from the dysfunction of cellular organelles and may indicate cellular stress induced by diabetes.

5.3 Aims

- To characterise vacuolated neurons labelled NF200 in lumbar DRG of db/db mice (building on observations from the previous chapter where vacuoles were identified in NF200-positive neurons)
- To investigate the origin of cytoplasmic vacuoles with general cellular and secretory vesicle markers
- To explore signs of stress in vacuolated neurons with cellular stress and damage markers

5.4 Results

5.4.1 Characterisation of cytoplasmic vacuoles in NF200-positive neurons in lumbar DRG of db/db mice

NF200 staining was robust and distinguishable from the background in db/db and lean DRGs (Figure 5.3A (upper panel)). NF200 labelled both vacuolated neurons (VNs) and non-vacuolated neurons (non-VNs) in lean and db/db mice (Figure 5.3A (lower panels)). In lean mice, VNs were relatively few in number, while a more significant proportion of VNs were observed in db/db mice.

The quantification of NF200-positive VNs revealed a significant increase in their percentage in db/db mice compared to lean mice. Specifically, the percentage of NF200-positive VNs in lumbar DRG was 7.78±1.95 in lean mice and 19.05±2.03 in db/db mice, representing an 11.27% increase in diabetic mice (P=0.0002) (Figure 5.3B).

The soma size distribution of NF200-positive VNs displayed variability between lean and db/db mice (Figure 5.3C). In lean mice, the soma diameters of VNs ranged between 28 and 44 µm, with a peak frequency of around 32-36 µm. In contrast, db/db mice exhibited a broader range of soma diameters, from 24 to 52 µm, with a higher frequency of larger VNs, particularly in the 36-44 µm range (Figure 5.3C). Despite the variability of the soma size, the median between the two groups showed no significant differences (lean=36.77±5.58 µm, db/db= 37.18±5.77 µm).

The number of vacuoles per NF200-positive VNs was significantly higher in db/db mice compared to lean mice (Figure 5.3D and E). In lean mice, most NF200-positive VNs contained 3–4 vacuoles per neuron (13.67%). However, in db/db mice, NF200-positive VNs more frequently presented with higher vacuole counts, with 5–6 vacuoles per neuron being the most common (19.08%) and a subset of neurons exhibiting as many as 7–8 vacuoles per neuron (7.41%) (Figure 5.3E).

A

Lean   db/db

Control

NF200

VN   Non-VN

B

***

% NF200+ VN

Lean   db/db

C

Number of NF200+ VN

Soma diameter (μm)

Lean   db/db
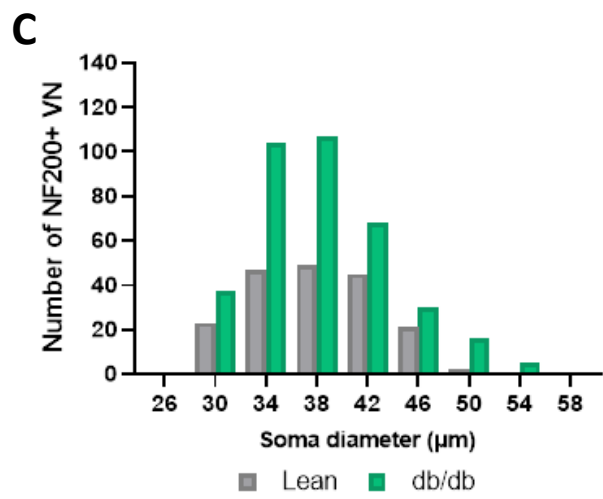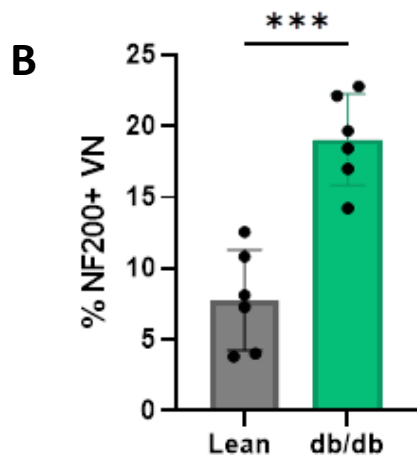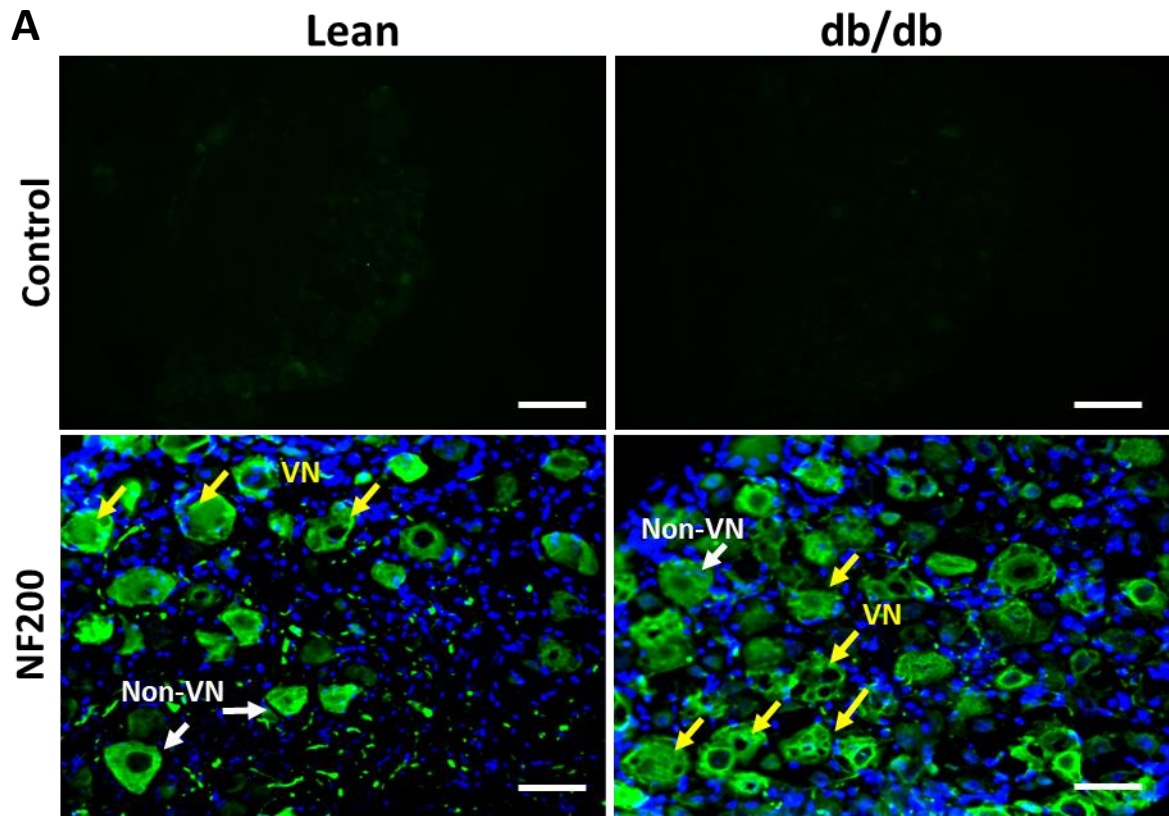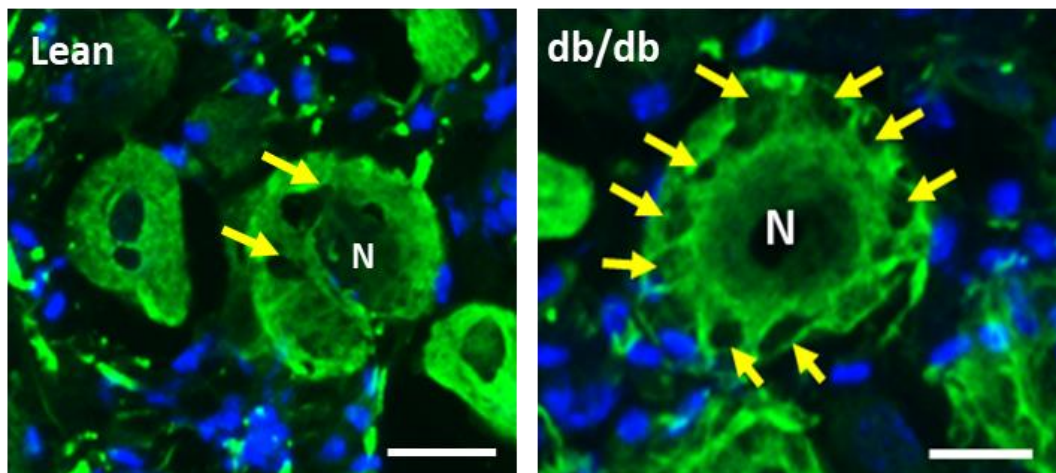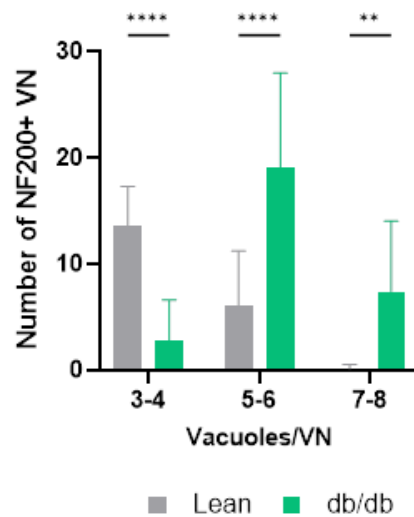
Figure 5.3 Characterisation of cytoplasmic vacuoles in NF200-positive neurons in lumbar DRG of lean and db/db mice

(A) Representative images show NF200-positive neurons in the DRG of lean (left) and db/db (right) mice. NF200 staining identified both vacuolated neurons (VNs: yellow arrows) and non-vacuolated neurons (non-VNs: white arrows) in both groups. Scale bars = 20 μm. (B) Quantification of NF200-positive VNs revealed a 2.2-fold increase in db/db mice (19.05 ± 2.03%) compared to lean mice (7.78 ± 1.95%) (***P < 0.0001). (C) Soma diameter distribution of NF200-positive VNs in lean and db/db mice. The median soma diameter was similar in both groups (Lean = 33.64 μm, db/db = 33.75 μm), with no significant differences. The distribution is plotted in 4 μm bins, showing the number of NF200-positive neurons measured (Lean: 200 neurons; db/db: 389 neurons). (D) Representative images showing varying numbers of cytoplasmic vacuoles (arrows) per single NF200-positive VNS in lean (left) and db/db (right) DRG. (E) The number of vacuoles per NF200-positive VNs was generally higher in db/db mice compared to lean mice. In lean mice, NF200-positive VNs predominantly contained 3-4 vacuoles per neuron (13.67%), while in db/db mice, most NF200-positive VNs contained 5-6 vacuoles per neuron (19.08%) or 7-8 vacuoles per neuron (7.4%). N = 12 for each group. P < 0.0001; Two-tailed unpaired Student's t-test; data presented as mean ± SEM. One-way ANOVA was used for vacuole comparison, and results are shown as mean ± SEM.

5.4.2 Characterising of the origin of cytoplasmic vacuoles with cellular markers

To characterise the origin of cytoplasmic vacuoles, we co-labelled NF200-positive neurons with cellular markers; these are discussed in the following sections.

5.4.2.1 Golgi apparatus did not contribute to vacuoles formation in db/db mice

The Golgi matrix protein 130 (GM130) is a Golgi-shaping protein located in the cis-surface of the Golgi apparatus (Huang, Li and Zhu, 2021). GM130 expression was analysed in db/db mice to investigate its potential role in vacuole formation.

GM130 colocalised NF200-positive neurons in lean mice (Figure 5.4A, upper panels), and db/db mice (Figure 5.4A, lower panels). Some VNs in lean and db/db mice showed GM130 staining within vacuoles (arrows). The confocal image further confirmed the absence of GM130 around the rims of vacuoles (arrows) in VNs in db/db mice (Figure 5.4B).

This finding confirms that the Golgi apparatus does not contribute to the formation of vacuoles in db/db lumbar DRG neurons.
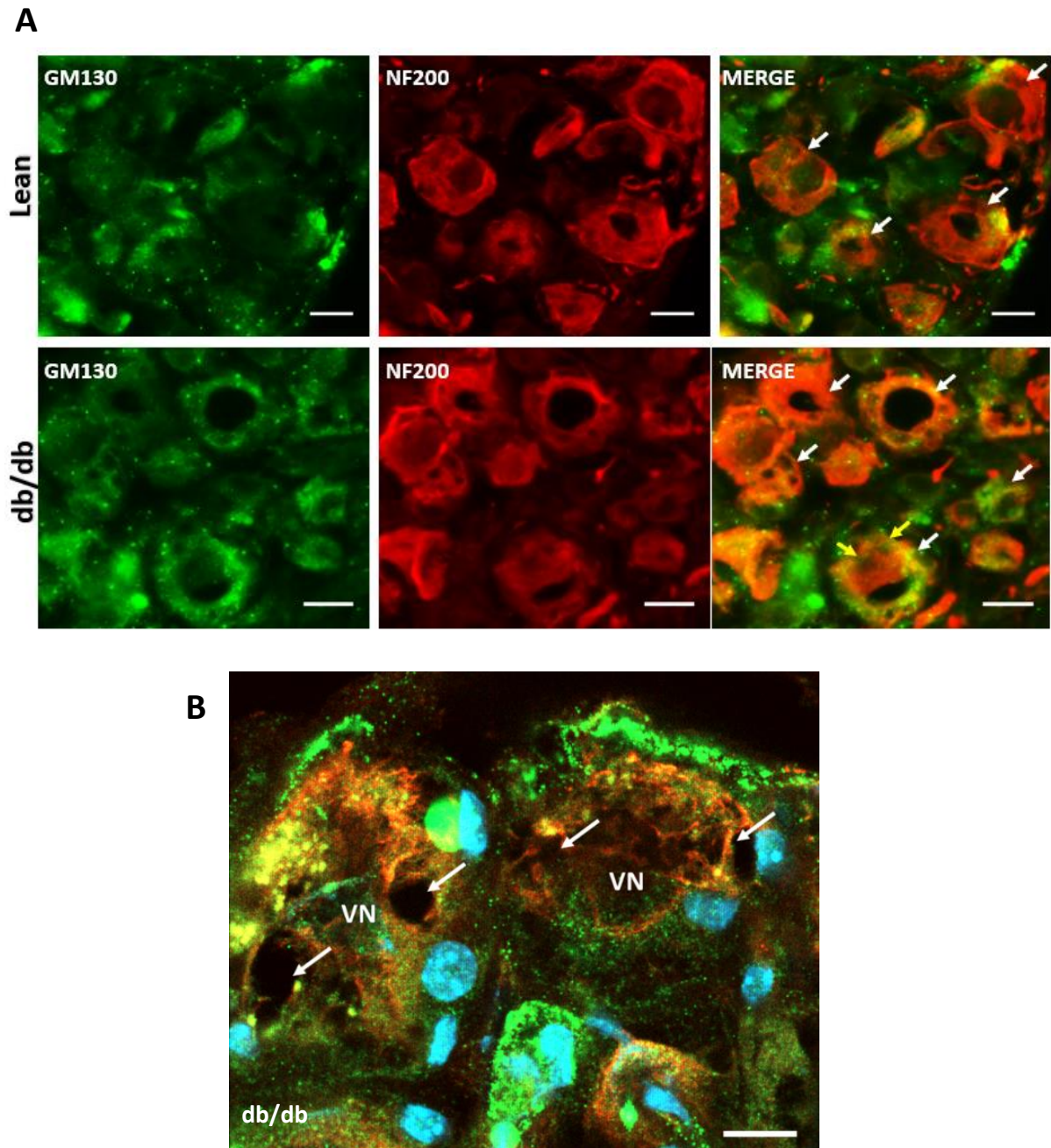
Figure 5.4 GM130 colocalisation with NF200-positive neurons in lumbar DRG of lean and db/db mice

(A) Representative images shows co-localisation of GM130 (green) with NF200 (red) in DRG neurons of lean (upper panels) and db/db mice (lower panels). No significant difference in the expression of GM130 was observed between groups. Vacuolated neurons labelled NF200 (arrows) show vacuoles stained with GM130 (arrowheads) in db/db DRG. Scale bars = 40 µm (applied to all images). (B) A confocal image of NF200-positive VN in the DRG of db/db shows the absence of GM130 around vacuole rims (arrows). Scale bar= 63 µm.

5.4.2.2 Mitochondria did not contribute to vacuoles formation in db/db mice

ATP-synthase subunit alpha (ATP5A) is a component of ATP synthase, an essential enzyme in the mitochondrial inner membrane involved in ATP production (Franco-Iborra *et al.*, 2018). ATP5A expression was analysed in db/db mice to investigate its potential role in vacuole formation.

ATP5A colocalised with NF200-positive neurons in lean mice (Figure 5.5A, upper panels), and db/db mice (Figure 5.5A, lower panels). Some VNs in lean and db/db mice showed ATP5A staining within vacuoles (arrows). The confocal image further confirmed the absence of ATP5A around the rims of vacuoles (arrows) in VNs in db/db mice (Figure 5.5B).

This finding confirms that the mitochondria do not contribute to the formation of vacuoles in db/db lumbar DRG neurons.
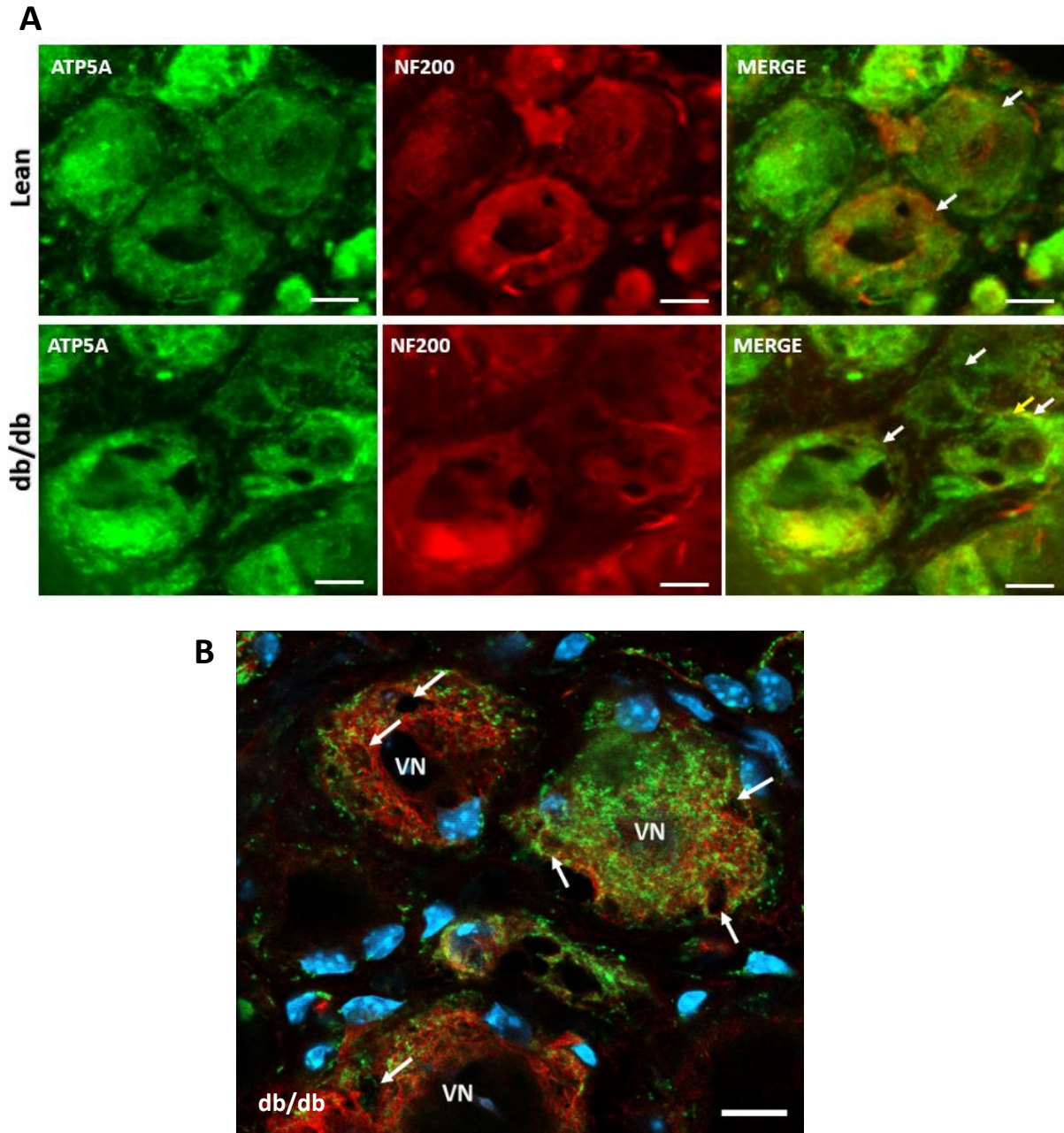
Figure 5.5 ATP5A colocalisation with NF200-positive neurons in lumbar DRG of lean and db/db mice

(A) *Representative images shows co-localisation of ATP5A (green) with NF200 (red) in DRG neurons of lean (upper panels) and db/db mice (lower panels). No significant difference in the expression of ATP5A was observed between groups. Vacuolated neurons labelled NF200 (arrows) show some vacuoles stained with Calr (arrowheads) in db/db DRG. Scale bars = 40 μm (applied to all images).* ***(B)*** *A confocal image of NF200-positive VN in the DRG of db/db shows the absence of ATP5A around vacuole rims (arrows). Scale bar= 63 μm.*

5.4.2.3 Endoplasmic reticulum did not contribute to vacuoles formation in db/db mice

Calreticulin (Calr) is a calcium-binding chaperone protein that resides in the endoplasmic reticulum lumen and plays an essential role in regulating cellular homoeostasis and the ER's capacity for protein folding (Michalak *et al.*, 2009). Calreticulin expression was analysed in db/db mice to investigate its potential role in vacuole formation.

Calr colocalised with NF200-positive neurons in lean mice (Figure 5.6, upper panels), and db/db mice (Figure 5.6A, lower panels). Some VNs in lean and db/db mice showed Calr staining within vacuoles (arrows). The confocal image further confirmed the absence of Calr around the rims of vacuoles (arrows) in VNs in db/db mice (Figure 5.6B).

This finding confirms that the ER does not contribute to the formation of vacuoles in db/db lumbar DRG neurons.

A

Lean
Calr | NF200 | MERGE

db/db
Calr | NF200 | MERGE

B

VN
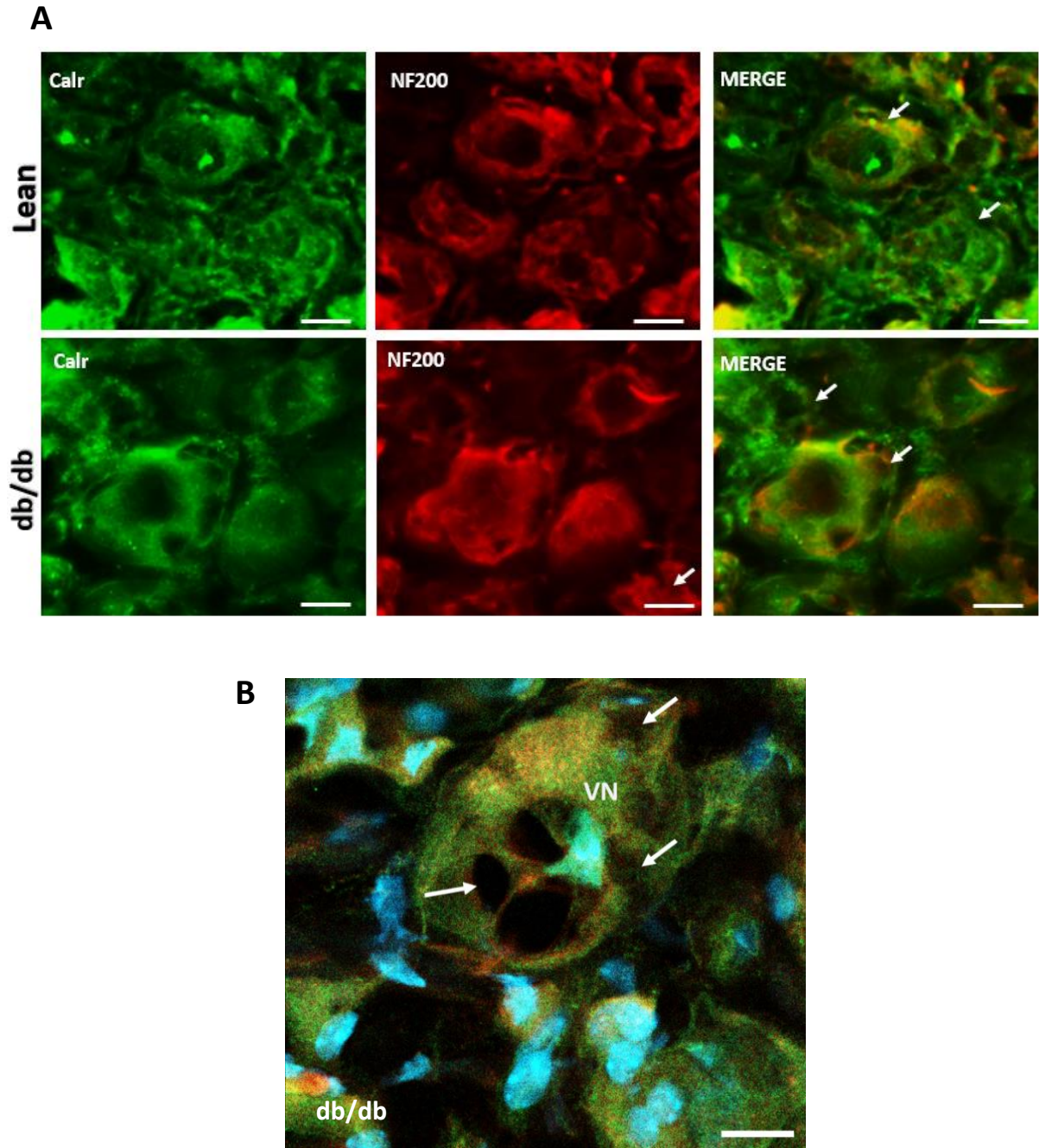
db/db

Figure 5.6 Calreticulin colocalisation with NF200-positive neurons in lumbar DRG of lean and db/db mice

(A) *Representative images shows co-localisation of Calr (green) with NF200 (red) in DRG neurons of lean (upper panels) and db/db mice (lower panels). No significant difference in the expression of Calr was observed between groups. Vacuolated neurons labelled NF200 (arrows) show some vacuoles stained with Calr (arrowheads) in db/db DRG. Scale bars = 40 µm (applied to all images).* ***(B)*** *A confocal image of NF200-positive VN in the DRG of db/db shows the absence of Calr around vacuole rims (arrows). Scale bar= 63 µm.*

5.4.2.4 Autophagosomes did not contribute to vacuoles formation in db/db mice

Autophagy-Related 12 (ATG12) and light chain 3B (LC3B) are essential in regulating the autophagy process, forming a complex on the membrane of developing autophagosome (Mai *et al.*, 2012). ATG12 and LC3B expression were analysed in db/db mice to investigate their potential role in vacuole formation.

ATG12 colocalised with NF200-positive neurons in lean mice (Figure 5.7A, upper panels) and db/db mice (Figure 5.7A, lower panels). In addition, VNs in lean and db/db mice showed no staining of ATG12 within vacuoles (arrows).

Similarly, LC3B colocalised with NF200-positive neurons in both lean (Figure 5.7B, upper panels) and db/db DRGs (Figure 5.7B, lower panels). In addition, VNs in lean and db/db mice showed no staining of LC3B within vacuoles (arrows). Thus, further investigation with confocal images was rulled out.

This finding confirms that the autophagosomes does not contribute to the formation of vacuoles in db/db lumbar DRG neurons.
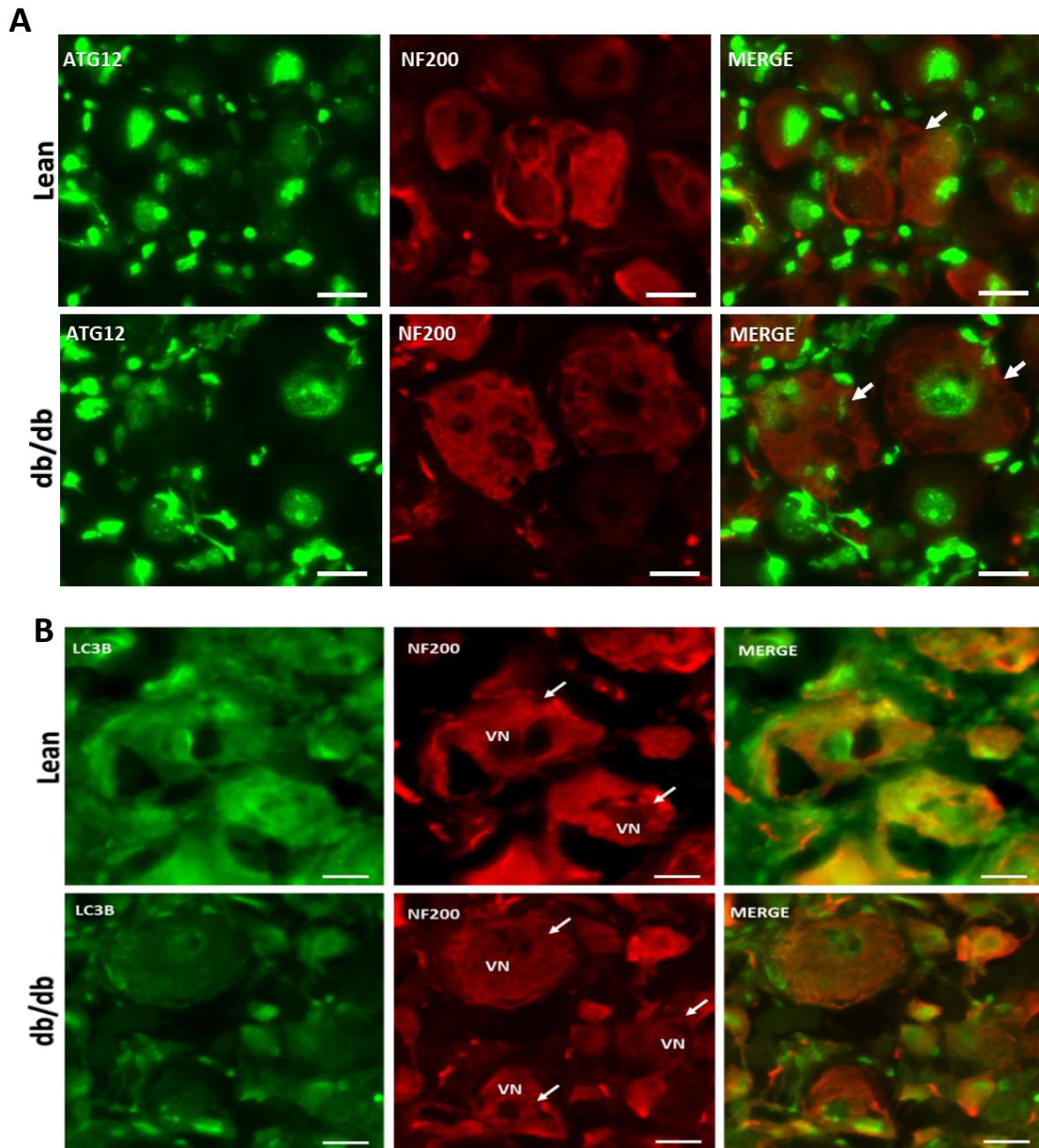
Figure 5.7 ATG12 and LC3B, colocalisation with NF200-positive neurons in lumbar DRG of lean and db/db mice

(A) *Representative images show co-localisation of ATG12 (green) with NF200 (red) in DRG neurons of lean (upper panels) and db/db mice (lower panels). No significant difference in the expression of ATG12 was observed between groups. Vacuolated neurons labelled NF200 (arrows) show the absence of ATG12 within vacuoles in lean and db/db DRG.* *(B)* *Representative images show co-localisation of LC3B (green) with NF200 (red) in DRG neurons of lean (upper panels) and db/db mice (lower panels). No significant difference in the expression of LC3B was observed between groups. Vacuolated neurons labelled NF200 (arrows) show the absence of LC3B within vacuoles in lean and db/db DRG. Scale bars = 40 µm (applied to all images).*

5.4.3 Characterising the origin of cytoplasmic vacuoles with secretory vesicle marker

5.4.3.1 Secretory vesicles did not contribute to vacuoles formation in db/db mice

Glycoprotein 2-alpha (SV2A) is a membrane glycoprotein essential in regulating vesicle exocytosis and neurotransmitter release. It also serves as a marker of synaptic vesicles and is involved in protecting neurons from cellular stress and damage (Rossi *et al.*, 2022). SV2A expression was analysed in db/db mice to investigate its potential role in vacuole formation.

SV2A colocalised with NF200-positive neurons in lean mice (Figure 5.8, upper panels) and db/db mice (Figure 5.8, lower panels). VNs in lean and db/db mice showed no staining of SV2A within vacuoles (arrows). Thus, further investigation with confocal images was rulled out.

This finding confirms the vacuoles in db/db lumbar DRG neurons do not contribute to secretory vesicles.
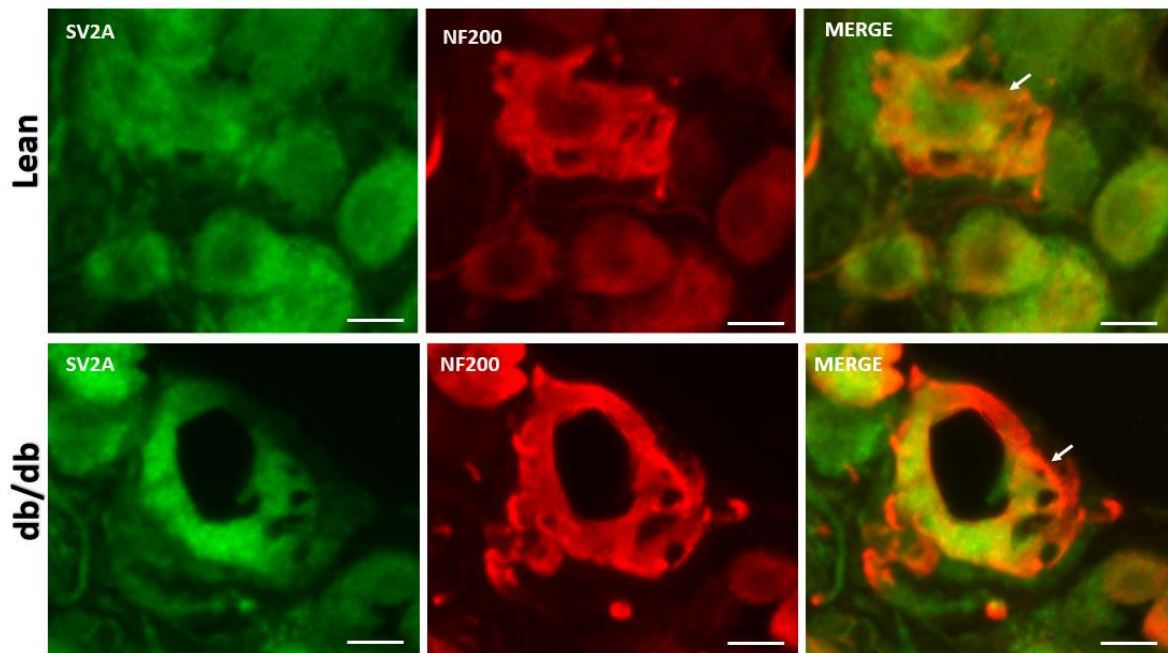
Figure 5.8 SV2A colocalisation with NF200-positive neurons in lumbar DRG of lean and db/db mice

(Upper panels) Representative images show co-localisation of SV2A (green) in large-diameter neurons labelled NF200 (red) in DRG in lean mice. (Lower panels) Representative images show co-localisation of SV2A (green) in large-diameter neurons labelled NF200 (red) in DRG in db/db mice (lower panels). No significant difference in the expression of SV2A was observed between groups. Vacuolated neurons labelled NF200 (arrows) show no staining of SV2A within vacuoles in lean and db/db DRG sections. Scale bars= 40 μm (applied to all images).

5.4.4 Investigating signs of stress and damage in vacuolated neurons in db/db mice

5.4.4.1 53BP1 distribution pattern changed in DRG neurons of db/db mice

DRG neurons are susceptible to undergo DNA damage due to increased OS (Ward *et al.*, 2003). P53-binding protein1 (53BP1), facilitates the repair of double-strand breaks and a key mediator of DNA damage response (DDR). 53BP1 ensuring proper cell cycle regulation at sites of DNA damage, which showed elevated levels in damaged neurons after cellular stress (Tay *et al.*, 2019). We examined the distribution pattern of 53BP1 in DRG neurons of db/db mice, for signs of DNA damage in vacuolated neurons.

53BP1 staining was distinguishable from the background in lean and db/db DRG (Figure 5.9A, upper panels). 53BP1 distribution pattern changed in db/db mice compared to lean mice (Figure 5.9, lower panels). In lean mice, 53BP1 was expressed primarily as diffused staining localised within the nucleus (Figure 5.9A; lower left), while in db/db mice, 53BP1 appeared to as nuclear foci (Figure 5.9A; lower right).

The percentage of 53BP1-positive neurons showing foci in lean mice was (11.33±0.60) and in db/db mice was (16.18±4.85), which represented a 4.85% increase in diabetic mice (P=0.0013) (Figure 5.9B).

VNs in db/db mice showed no difference in the distribution pattern of 53BP1 staining compared to non-VNs (Figure 5.9C).

These findings showed that the distribution pattern of 53BP1 changes in db/db neurons compared to lean, indicating signs of DNA damage.
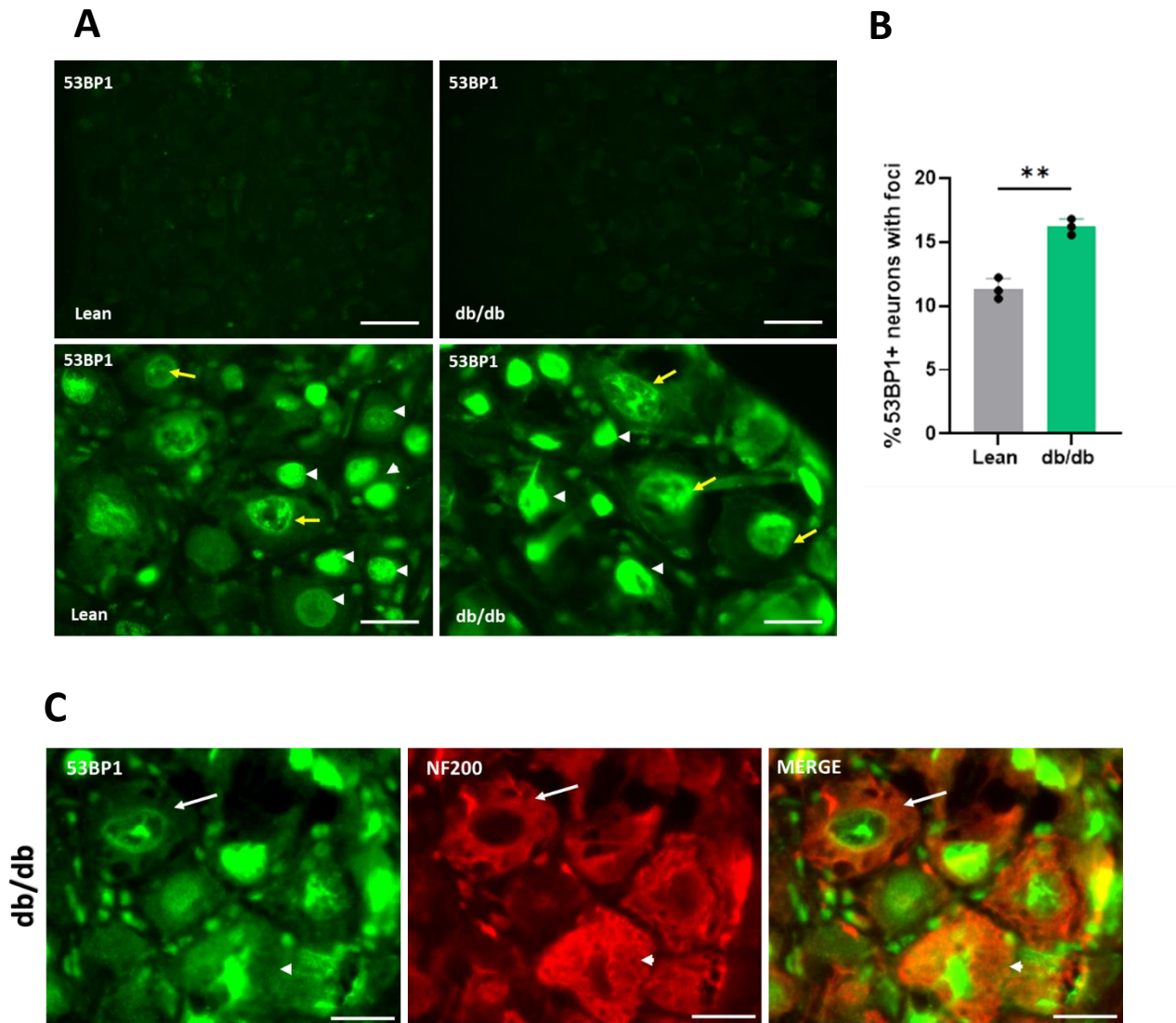
Figure 5.9 53BP1 expression in lumbar DRG neurons of lean and db/db mice

(A) 53BP1 distribution pattern in lean and db/db DRGs. 53BP1 changed their distribution from dense staining in the nucleus (arrowheads) to foci distribution (arrows) in lean and db/db (arrows) (B) Quantification of 53BP1+ neurons with foci in lean and db/db DRG. A significant increase in the percentage of neurons with 53BP1+ foci, in lean (11.33±0.60) and db/db (16.18±4.85) (P=0.0013) (C) NF200-positive VNs show either dense (arrowhead) or foci (arrow) expression of 53BP1+. N=3.Two-tailed unpaired Student's t-test, data shown as mean ± SEM. Grey bar= lean; green bar= db/db.

5.4.4.2 HIF1a expression was not changed in vacuolated neurons in db/db mice

Hyperglycaemia is known to cause hypoxia as a form of cellular stress (Kishi et al., 2002). Hypoxia-inducible factor 1-alpha (HIF1a) is a transcriptional mediator of cellular response to hypoxia, which is found to accumulates within the nucleus of neurons under stress (Bruick, 2003). We examined signs of hypoxia in DRG neurons of db/db mice.

HIF1a staining was robust and distinguishable from the background in lean and db/db DRG (Figure 5.10A, upper panels). HIF1a staining was comparable in lean and db/db mice (Figure 5.10A, lower panels). The percentage of HIF1a+ neurons in lean mice was (16.97±2.23) and in db/db mice was (20.27±3.29), which showed no significant differences between both groups (Figure 5.10B).

VNs in db/db mice showed no difference in the distribution pattern of HIF1a staining compared to non-VNs (arrows) (Figure 5.10C)

These findings show that DRG neurons in db/db mice show no signs of hypoxia.
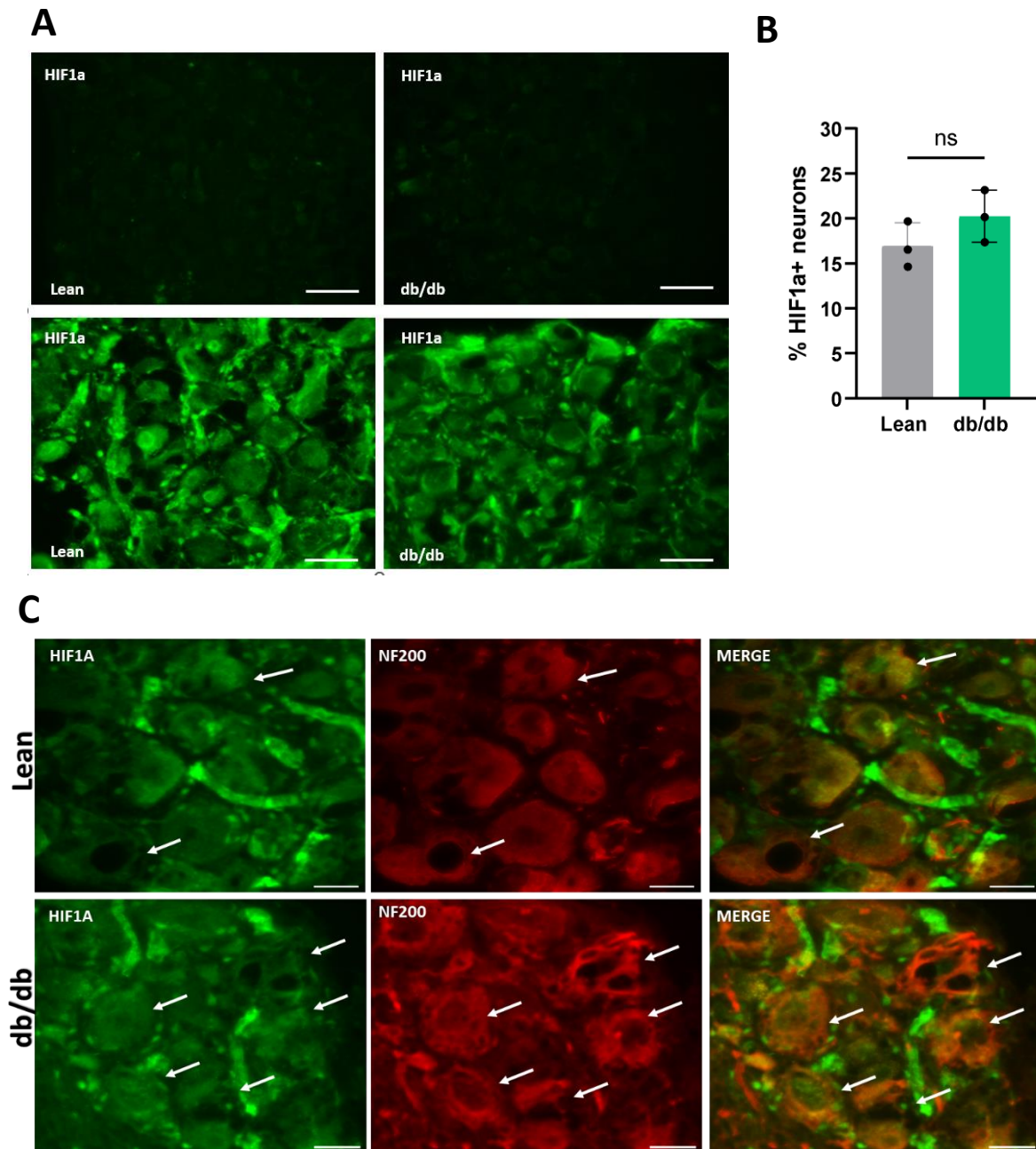
Figure 5.10 HIF1a expression in lumbar DRG neurons of lean and db/db mice

(A) Representative images showing the expression of HIF1a in lean and db/db DRG. The expression of HIF1a was robust and distinguishable from the background (upper panels), with no difference in expression pattern between lean and db/db (lower panels) (B) The percentage of HIF1a-positive neurons in lean mice (16.97±2.23) and in db/db mice (20.27±3.29) showing no significant difference (C) The co-localising of HIF1a (green) with NF200 (red) in lean and db/db DRGs shows no change in the expression in NF200 VN in lean (upper panels) and db/db (lower panels) (arrows). N=3. Two-tailed unpaired Student's t-test, data are shown as mean ± SEM.

5.4.4.3 Tau expression was not changed in vacuolated neurons in db/db mice

Microtubule binding protein Tau (Tau) is a protein found to increase due to cellular damage and dysfunction (Bras and Singleton, 2009). We examined the distribution pattern of Tau in DRG neurons of db/db mice.

Tau staining was robust and distinguishable from the background in lean and db/db DRG (Figure 5.11A, upper panels). Tau staining showed a slight change in their distribution pattern between lean and db/db mice (Figure 5.11A, lower panels). In lean, Tau showed smooth defuses puncta (Figure 5.11A, lower left) compared to db/db mice, which showed aggregated puncta (arrows) (Figure 5.11A, lower right). However, this was only observed in one db/db mouse.

The percentage of Tau positive neurons in lean was (5.7±0.60) and db/db was (7.16±1.39), which showed no significant differences between both groups.

VNs in db/db mice showed no difference in the distribution pattern of Tau staining compared to non-VNs (arrows) (Figure 5.11C).

These findings show that Tau was not affected in in db/db mice, neither in vacuolated neurons.
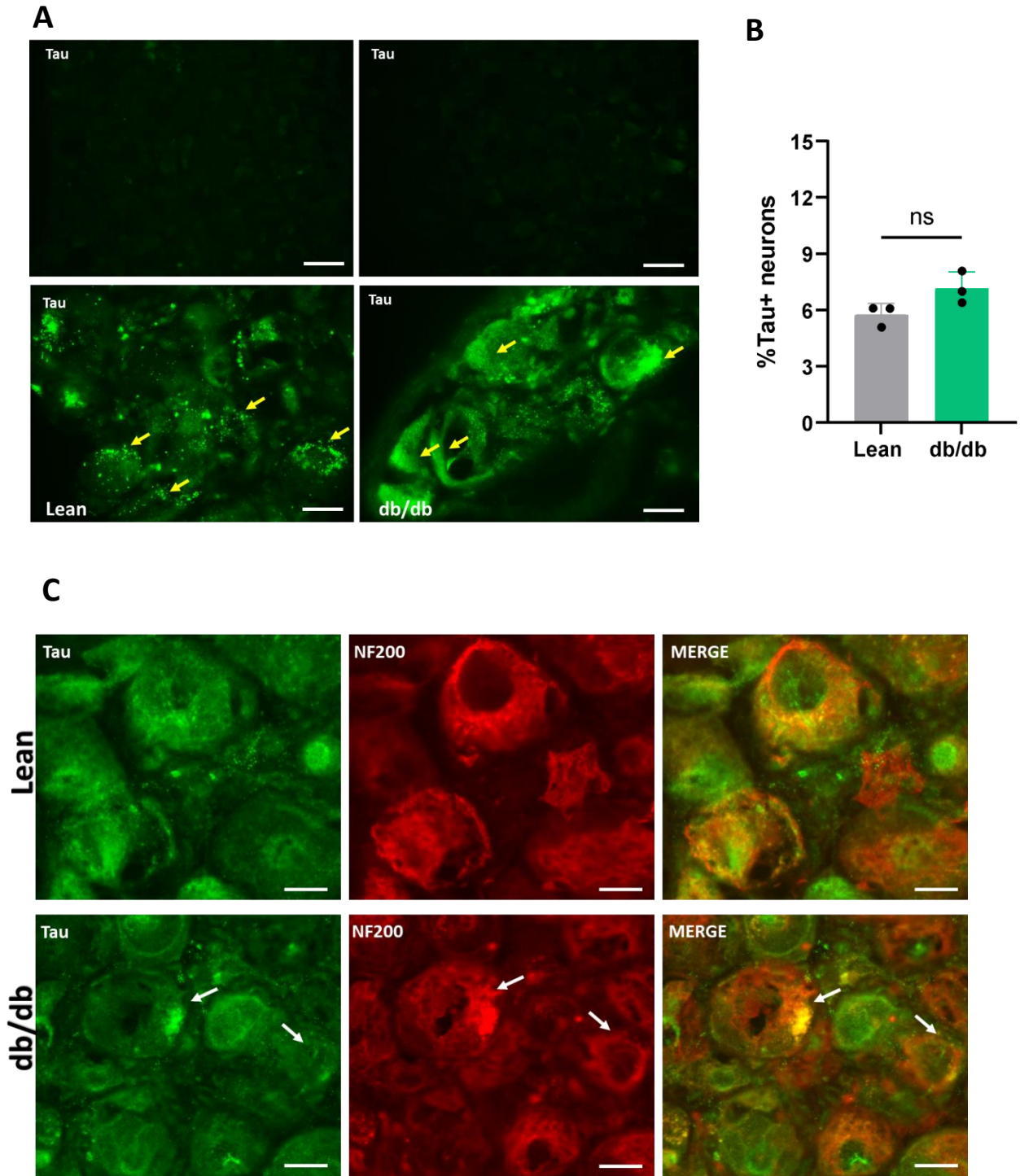
Figure 5.11 Tau expression in lumbar DRG neurons in lean and db/db

(A) Representative images showing the expression of Tau in lean and db/db DRG. The expression of Tau was robust and distinguishable from the background (upper panels); however, in lean, it showed small smooth puncta while aggregating in db/db mice (lower panels) (B) The percentage of Tau-positive neurons in lean mice (5.7±0.60) and db/db (7.16±1.39) showing no significant difference (C) The co-localising of Tau (green) with NF200 (red) in lean and db/db DRGs shows no change in the expression in NF200 VN in lean (upper panels) and db/db (lower panels). N=3. Two-tailed unpaired Student's t-test, data are shown as mean ± SEM.

5.5 Discussion

5.5.1 Main findings

In this chapter, we investigated the origin of cytoplasmic vacuoles in NF200 labelled neurons in lumbar DRG of db/db mice (32 weeks). To our knowledge, we are the first to confirm the existence of cytoplasmic vacuoles in lumbar DRG neurons labelled NF200 in db/db mice. The percentage of vacuolated neurons was 11.27% higher in db/db mice. The number of vacuoles per neuron was also higher in db/db mice. The origin of these vacuoles was not related to organelles dysfunction. However, a sign of stress in the form of DNA damage was observed in the lumbar DRG of db/db mice.

Several studies have observed the occurrence of cytoplasmic vacuoles in the sensory neurons within the DRG in various T1DM animal models, such as BB/Wor rats (40 weeks) and STZ rats (24 and 48 weeks). The percentage of vacuolated neurons was 4.6-fold higher in BB/Wor diabetic than in lean rats (Kamiya *et al.*, 2006) and 1.19-fold higher in STZ rats compared to lean rats in both cases (Sasaki *et al.*, 1997; Kishi *et al.*, 2002). Our observation of a 1.2-fold increase in the db/db model aligns with other studies that employed different diabetic animal models, which suggest that cytoplasmic vacuoles in NF200-labelled neurons are a common pathological feature that is accelerated by diabetes.

In addition, cytoplasmic vacuoles were observed in different neuropathic conditions. These include models of nerve injuries such as peripheral nerve transection (Groves *et al.*, 1997) and compression (Tang *et al.*, 2009). Sensory neurons have been found to form many small vacuoles due to NAD/NADP-dependent pathway inhibition and decreased Na/K-ATPase activity. The vacuoles observed in these studies were of small sizes, which differs from our findings of large-size vacuoles. Large vacuoles were observed in control animals but had a very low incidence (Groves *et al.*, 1997). Moreover, cytoplasmic vacuoles have been reported in neurodegenerative diseases (NDDs). During the early stages of amyotrophic lateral sclerosis (ALS), vacuoles observed in motor neurons of superoxide dismutase (SOD) transgenic mice, which carry a human mutant gene that mimics ALS-like cytoskeletal pathology (Mourelatos *et al.*, 1996). Similarly, vacuoles were reported in the human brain of Alzheimer's disease (AD)(Nixon and Yang, 2011; Piras *et al.*, 2016).

Our finding shows that cytoplasmic vacuoles appeared in NF200-positive large-diameter neurons (Figure 5.3C). However, other studies observed the presence of cytoplasmic vacuoles in small-diameter neurons in BB/Wor rats and STZ rats (Sasaki *et al.*, 1997; Kamiya *et al.*, 2006). NF200-positive VNs were observed in the DRG of both lean and db/db mice, with significantly more vacuolated NF200 labelled neurons in diabetic mice, which contained many vacuoles in a single neuron ranging between 3-8 (Figure 5.3E).

Next, we investigated if cytoplasmic vacuoles originated from cellular organelles; however, no evidence was obtained to link with many markers. Additionally, we investigated if vacuolated NF200 neurons were related to neuronal damage or stress. Our findings showed that the expression of Tau protein increased slightly in db/db DRG compared to lean, with no statistical significance (Figure 5.13). Tau showed a change in the distribution pattern from large, clustered puncta in lean to fine fused puncta in db/db mice (arrows) (Figure 5.13B). In addition, the DNA nuclear expression 53BP1 changed in db/db mice compared to lean (Figure 5.14). However, examining hypoxia with HIF1a revealed no changes between both groups (Figure 5.15). The experiments of this chapter confirmed that diabetes accelerated vacuole formation in large-diameter neurons labelled NF200 in db/db; however, we could not specify the origin of vacuoles.

Our observations ruled out cellular organelles as the source of cytoplasmic vacuoles in the DRG of db/db mice, as no cellular markers were identified within or around the vacuoles' rim. This aligns with a study by Corral-Pujol (2023), which demonstrated that ultrastructural analysis in NOD diabetic rats revealed vacuoles with a single membrane, ruling out an autophagic origin since autophagosomes typically exhibit a double-membrane (Corral-Pujol *et al.*, 2023). This finding also mirrors early work by Jones and Cavanagh (1984), who suggested that a single membrane indicates that vacuoles are fluid-filled and may originate from cellular organelles. However, several studies in diabetic and neuropathic models proposed different origins of cytoplasmic vacuoles arise from swollen intracellular organelles, including mitochondria (Cavaletti *et al.*, 2007), the endoplasmic reticulum (Groves *et al.*, 2003), and the Golgi apparatus (Kamiya *et al.*, 2006). In addition, research in NDD has shown that Golgi fragmentation contributes to cellular dysfunction and vacuole formation, suggesting activation of the endosomal-lysosomal pathway (Cataldo *et al.*, 1996; Joshi *et al.*,

2014; Mohan *et al.*, 2023). Autophagic vacuoles have been found to accumulate in AD (Hamano *et al.*, 2021) and PD (Lu, Wu and Yue, 2020).

Next, we examined signs of stress or damage in VNs in the lumbar DRG in db/db mice, using stress markers. We found that a slight increase in the number of 53BP1-positive neurons in diabetic mice (Figure 5.9). While this suggests that diabetic conditions induce DNA damage in neurons, no direct link to vacuoles was observed, indicating that DNA damage in diabetic neurons might occur independently of vacuolation. These results are consistent with elevated OS and DNA damage reported in STZ rats (Shadfar *et al.*, 2023). Abnormalities in DNA damage repair mechanisms have been linked to neurological disorders such as those in AD (Welch and Tsai, 2022).

5.6 Conclusion

This chapter characterised cytoplasmic vacuoles in lumbar DRG neurons of the db/db mice. Our findings confirmed that diabetes increases the formation of vacuoles in lumbar DRG of db/db mice, particularly in large-diameter neurons.

Chapter 6: General Discussion and Future Works

6.1 Discussion

Diabetic Peripheral neuropathy (DPN) is a severe complication of diabetes that affects the quality of life. The specific mechanisms underlying complex sensory disturbances in DPN, including painful and non-painful symptoms, remain unknown. While up to 50 % of DPN patients experience numbness and loss of sensation, 25% of these develop foot ulcers, gangrene and amputation. These sensory defects of DPN continue to cause a significant therapeutic challenge globally. To date, no effective treatments can heal or reverse DPN symptoms; the only currently available approaches are glycaemic control, diet modification, and lifestyle changes. The presently approved medications target the central nervous system (CNS), however, these treatments are often associated with significant side effects. Several research has focused on targeting the peripheral nervous system instead to understand the mechanism underlying the development of DPN symptoms. Several promising targets have been identified, the most popular being the dorsal root ganglia, particularly targeting the sensory neurons responsible for detecting various sensory stimuli. The present study aimed to characterise histological changes in the lumbar DRG sensory neurons in db/db mice, an established model for T2DM.

In Chapter 3, we investigated whether diabetes leads to the formation of sympathetic sprouting and basket-like structures of TH-positive fibres around lumbar DRG neurons, which may contribute to the development of pain in DPN. Here, sympathetic sprouting was investigated using IHC, where the omission of the primary antibody served as a negative control. However, future studies could employ blocking peptides to further confirm antibody specificity by pre-incubating the antibody with its target antigen, ensuring that observed staining reflects the specific localization of sympathetic markers. Our finding demonstrated that from 512 lumbar DRG sections obtained from 8 db/db mice, we only observed a single TH-positive fibre which surrounded a large-diameter neuron in one DRG section from one db/db mouse (Figure 3.5). This finding indicated that diabetes does not trigger sympathetic fibres sprouting in the lumbar DRG of db/db mice. Sympathetic sprouting into DRG has been well-documented in various models of nerve injury models. In sciatic nerve ligation or transection, significant sympathetic fibre sprouting into the DRG has been observed which contribute to neuropathic pain by forming abnormal connections between sympathetic and sensory neurons, amplifying pain signals. Studies by McLachlan et al. (1993) and Ramer et al.

(1999) demonstrated robust sympathetic sprouting following nerve injury, suggesting a potential role in chronic pain development.

Lee etal (1998) reported the presence of few dopaminergic TH-positive neurons in the lumbar DRG of the nerve injury models (Lee *et al.*, 1998). The number of TH-positive neurons increases in the SSI model, whereas, in the CCI model, the TH-positive proportion was not affected 20-weeks PO. In contrast, Brumovesky, Villar and Hökfelt (2006) reported a reduction in the number of TH-positive neurons one week after axotomy (Brumovsky, Villar and Hökfelt, 2006). However, the cause, whether metabolic, mechanical, or traumatic, which triggers the TH-positive neuron changes is still unclear. Thus, we examined whether changes to the number and intensity of TH-positive neurons exist in the lumbar DRG of db/db mice at 23 weeks. Our findings revealed a 3.69% and 4.42% increase in TH-positive neurons in L4 and L5 of diabetic mice, respectively; however, these were not statistically different (Figure 3.7). TH-positive neurons known as C-LTMRs (C-fibre low threshold mechanoreceptors), which are involved in the plausible touch and mechanical hypersensitivity. Changes in their number may indicate an adaptive or maladaptive response to an altered sensory environment in DPN (Le Pichon and Chesler, 2014).

Lee and Yoon (1998) also reported increased TH-positive fibres in the spinal nerve after ligation, suggesting a regenerative process in injured sympathetic fibres (Lee *et al.*, 1998). Whereas, in a study by McLachlan et al. (1993), they found a decrease in TH-positive fibres, which indicates signs of nerve degeneration (McLachlan *et al.*, 1993). Together, these findings imply that TH-positive fibres may have a capacity for regeneration and degeneration in response to injury, potentially restoring sympathetic innervation after damage. Thus, we examined if TH-positive fibre in the peripheral nerve showed changes in their number after diabetes. We found the number of TH-positive fibres in lean mice was (8 ±1.37, n=4) and in db/db mice was (11.25±3.25, n=4). This indicated a 3.25% slight increase in diabetic mice; however, this was not significantly difference (P= 0.0563) (Figure 3.6C). These TH-positive fibres were primarily located near the nerve edges, suggesting they may be the ones innervating blood vessels within the connective tissue surrounding the nerve rather than new growth (Winston P 2023). This minimal fibre count aligns with the conclusion that sympathetic sprouting is likely absent in diabetic DRG, indicating it may not be a feature of DPN.

Overall, in this chapter, our findings of a 3.69% increase in TH-positive neurons matched the 3.25% increase in TH-positive fibre, which might indicate that diabetes alteration at the axons site is equal to that at the DRG site. Our results indicate that diabetes does not induce sympathetic sprouting or basket formation in db/db mice, unlike what is typically observed in pain injury models. The possible explanation for this is that the type of damage caused by hyperglycaemia in our model may not be severe enough to trigger nerve injury, similar to other models.

In Chapter 4, we sought to build upon previous functional data (unpublished from Dr. Nassar's lab) that showed a reduction in large-dimeter cells and a corresponding increase in small-diameter cells in the DRG of t   db/db model (*in vitro*). Therefore, we investigated changes in the number and soma size of these neuronal populations in DRG neurons from the same db/db model (*in vivo*). Double IHC labelling peripherin (PRPH) for small-diameter neurons and neurofilaments (NF200) for large-diameter neurons in lumbar L4 and L5 DRGs were utilised to achieve this.

Our findings revealed a significant reduction in the percentage of NF200-positive neurons (large-diameter), accounting for 12.46% in db/db mice compared to lean mice (Figure 4.4A). Our in-vivo results align with the previous in-vitro results from the same model db/db, which revealed a significant reduction accounting for 22% in large-diameter cells (unpublished data from Nasar's group. By utilising DRG neurons in vivo, we offered structurally relevant perspective, in addition to the functionally reported findings, confirming that these neuronal changes are inherent to the diabetic condition itself rather than being influenced by external culture factors. Moreover, our finding agrees with the reduction reported by other studies on T1DM models. Similar declines were reported in STZ-rats by 18% and 40% at four weeks and 48 weeks, respectively (Sidenius and Jakobsen, 1980) (Kishi *et al.*, 2002). This agreement across experimental conditions strengthens the evidence that the reduction in large-diameter neurons is a key feature of diabetes. Large-diameter neurons detect proprioceptive and mechanical stimuli (touch and pressure) (Scroggs and Fox, 1992; Le Pichon and Chesler, 2014). Given the role of large-diameter neurons, their reduction might explain why patients with T2DM experience symptoms of loss of touch sense and pressure (Sosenko *et al.*, 1993; Rinkel *et al.*, 2018). In addition, according to behaviour studies, their loss in diabetic conditions contributed to hyposensitivity and hypoalgesia (Shi *et al.*, 2013). These findings, reported by

functional, morphological, and behavioural studies, underscore the importance of further research into strategies aimed at targeting large-diameter sensory neuron populations in diabetic patients.

In addition, we found a decrease in the soma size of large-diameter neurons in the lumbar DRG of db/db mice, which was more significant in lumbar L4 DRG than in L5 DRG (Figure 4.5). This is consistent with previous reports of soma size reduction in large-diameter neurons in STZ rats, indicating atrophy over time (Zochodne et al. (2001)). Morphological changes such as atrophy, demyelination, and apoptosis due to oxidative damage have been widely reported in large-diameter neurons in diabetic conditions, contributing to neuronal loss (Russell et al., 1999; Kishi et al., 2002).

Next, we examined changes to the number and soma size of PRPH-positive neurons in db/db mice. We found no changes to both parameters in PRPH-positive neurons (small diameter) in diabetic mice (Figures 4.6 and 4.7). Small-diameter neurons are known to be involved in pain perception. It is reported that half a percentage of diabetic patients suffer from pain sensations (Ko *et al.*, 2013; Lima *et al.*, 2017). Several studies reported discrepancies in the number of small-diameter neurons (not PRPH labelled). In BB/Wor rats, a 40% reduction in small-size neurons labelled SP (Substance P, marker for small-diameter neurons) was reported (Kamiya *et al.*, 2006). In STZ rats, the number of small-diameter neurons was not affected (Sidenius and Jakobsen, 1980). In addition, an increase of 40% in small-diameter neurons obtained from cultured DRG from db/db mice was found (Unpublished data from Nassar's group). Moreover, to our knowledge, there is only one study that compared the soma distribution of PRPH-positive neurons between rat and marmoset models and found that the distribution pattern was comparable in both species, which aligns with our findings (Kudo *et al.*, 2021). However, we found no changes affecting PRPH-positive neurons in our db/db model.

Lastly, we looked at whether changes to DRG neurons affect the number of non-neuronal cells; we found no changes in db/db mice (Figure 4.8). To our knowledge, no available studies examined the changes in the number of non-neuronal cells after diabetes. However, the available information about changes to the proportion of non-neuronal cells has been observed after nerve injury in CCD (specifically endothelial cells), which were activated in the form of angiogenesis, i.e., increased number of capillaries in the DRG (LaMotte and Ma, 2008).

In addition, activation of SGCs was observed in CCD rats, which contributed to neuronal excitability, leading to pain (Warwick and Hanani, 2013). These responses are typically associated with neuroinflammation, mediators release, and the attempt to support neuronal survival and repair. An interesting finding was the presence of vacuole-like structures in the cytoplasm of large-diameter neurons in both lean and db/db mice (Figure 5.3). This opened a new aim for our study, which will be discussed in the next chapter.

In Chapter 5, we characterised cytoplasmic vacuoles, which were observed in large-diameter neurons in db/db mice in the previous chapter (Chapter 4). We examined the origin of these vacuoles using general cellular markers for organelles dysfunction. In addition, we examined signs of stress and damage in vacuolated neurons.

To our knowledge, we were the first to confirm the existence of cytoplasmic vacuoles in the DRG of db/db mice (at 32 weeks). Our findings revealed a 1.2-fold increase in vacuolated neurons (VNs) in the lumbar DRG of db/db mice (Figure 5.3). This aligns with a study in T1DM models in BB/Wor rats, where VNs were found to be 4.6-fold higher from control rats (Kamiya, Zhang, and Sima, 2006) and the 1.19-fold increase in STZ rats (Sasaki et al., 1997; Kishi et al., 2002). These findings collectively indicate that vacuolation is a common pathological feature that increases due to diabetes. In addition to diabetic models, cytoplasmic vacuoles have been observed in the DRG neurons of neuropathy, such as peripheral nerve injury models which emphasise neuronal stress and degeneration conditions (Mourelatos et al., 1996; Nixon and Yang, 2011). Interestingly, while most studies observed vacuoles in small-diameter neurons in diabetic models (Kamiya, Zhang, and Sima, 2006), our study demonstrate vacuoles in large-diameter neurons, particularly NF200-positive neurons. Moreover, we found an increase in the number of vacuoles per VNs to be higher, exhibiting 4-8 vacuoles per neuron (Figure 5.3), suggesting that diabetes accelerates vacuole formation in this specific neuronal population. in diabetes. We were the first study that counted the number of vacuoles per neuron in lumbar DRG of db/db mice (32 weeks), so no comparison could be drawn with other studies.

The next aim was to examine the origin of vacuoles using cellular markers, including the Golgi apparatus (GM130), mitochondria (ATP5A), endoplasmic reticulum (Calreticulin), and phagosomes (ATG12). The origin of cytoplasmic vacuoles in DRG sensory neurons is thought to arise from intracellular organelle dysfunction, includes the fragmentation of the Golgi apparatus (Kamiya, Zhang, and Sima, 2006), mitochondrial swelling (Russell et al., 1999;

Cavaletti et al., 2007), autophagic pathway dysfunction (Nixon and Yang, 2011). Contrary to our expectations, we excluded cellular organelles as the origin of cytoplasmic vacuoles in large-diameter neurons of lumbar DRG of db/db mice since no specific markers were detected within or around the vacuole's rims. This is consistent with Corral-Pujol (2023), who observed a single-membrane vacuole in NOD diabetic rats, ruling out an autophagic origin as autophagosomes typically exhibit double membranes. Similarly, Jones and Cavanagh (1984) reported that single-membrane vacuoles are fluid-filled and likely originate from cellular components.

Finally, DRG neurons experience a wide array of stress conditions in diabetes, including oxidative stress, hypoxia, and inflammation, which damage cellular components like DNA, proteins, and lipids (Piras et al., 2016; Tay et al., 2019). Our final aim in this study was to investigate if vacuoles in lumbar DRG of db/db mice were signs of stress and damage using markers for DNA damage (53BP1), hypoxia (HIF1a), or neurodegeneration (Tau). Our findings showed changes in the distribution patterns of nuclear 53BP1 (in the form of foci) in VNs of db/db mice, indicating DNA damage (Figure 5.11). However, we did not observe any changes in HIF1a or Tau markers indicating no sign of hypoxia or neurodegeneration occurred (Figure 5.12 and 5.13).

Overall, our findings confirmed that diabetes accelerated the formation of cytoplasmic vacuoles in db/db models. Our findings could not specify the origin of cytoplasmic vacuoles using cellular markers; however, we show that DRG neurons in db/db undergo stress and DNA damage. Further investigation was rolled out due to time limitations.

6.2 Conclusion

In conclusion, the data presented in this thesis revealed an insight into the histological changes in lumbar DRG sensory neurons in db/db mice at 32 weeks. Our findings showed that diabetes did not cause sympathetic fibres sprouting in the lumbar DRG of db/db mice as contribution to pain symptoms in DPN. Then, our morphometric examinations of the DRG sensory neurons revealed that the number and soma size of large-diameter neurons, which are responsible for the sensation of touch (proprioception), were significantly reduced in db/db mice. In addition, we observed the formation of cytoplasmic vacuoles in large-diameter neurons, in which vacuolated neurons were higher, and the number of vacuoles per VNs was

also higher in db/db mice. These findings illustrate insights into the structural alterations in large-diameter neurons in DRG of db/db mice, that might explain their involvement in the loss of sensatio in DPN.

6.3 Future works

While this thesis provided some insights into the diabetes-induced changes to the sensory neurons in the lumbar DRG of the db/db mice at 32 weeks, future work might explore the the following avenues to address the current study's findings:

The present study demonstrated that a reduction had occurred in the proportion of (large-diameter) NF200-positive neurons in the lumbar DRG of the db/db mice. DRG neurons with large cell bodies are known as low-threshold mechanoreceptors (LTMR), which conduct proprioception and mechanoreception information (e.g., touch and body position) (Zochodne, Ramji and Toth, 2008; Berta *et al.*, 2017). Further characterisation using other subdivision markers, which can differentiate between proprioceptive and mechanoreceptive subtypes, might be essential. This includes the Tyrosine kinase receptor, including TrkC. The TrkC receptors bind to neurotrophin-3 (NT-3) and are crucial markers for the survival of proprioceptive neurons, which help to detect body position and movement (Ménard *et al.*, 2018). $NT-3^{-/-}$ Knockout mice (with deleted N 3 gene) demonstrated 70% sensory neuron loss due to apoptosis in the lumbar DRG (Elshamy and Ernfors, 1996). This indicates that NT-3 has an essential role in sensory neuronal development. Thus, it would be worth exploring whether altered NT-3 signalling contributes to the loss of NF200-positive neurons in db/db mice. Another approach might involve investigating neuronal death and oxidative injury in NF200-positive neurons by assessing the activated caspase 3 level and 8-Hydroxy-2†-deoxyguanosine. In experimental diabetic neuropathy (EDN) rats, a loss of large-diameter neurons was detected due to increased Caspase-3 labelled neurons, indicating apoptosis. They also found an increase in 8-Hydroxy-2†- deoxyguanosine labelled neurons, indicating oxidative injury (Schmeichel, Schmelzer and Low, 2003).

In addition, it would be possible to examine specific markers for non-neuronal various types. We only detected changes to the number of non-neuronal cells based on DAPI nuclear staining, so using markers for non-neuronal cell mediators might be fruitful. Several studies reported that under nerve injury conditions, non-neuronal cells are found to release different

mediators such as interleukin 1B (IL-1B), nerve growth factor (NGF), and tumour necrosis factor-a (TNF-a), which stimulates the nociceptive terminals in the peripheral axons leading to increasing pain sensation (Suter *et al.*, 2007; Song *et al.*, 2014; Ji, Chamessian and Zhang, 2016). Furthermore, studies on nerve injury on specific non-neuronal cells (endothelial and SGCs) observed increased activation, which led to neuronal excitability causing pain (Warwick and Hanani, 2013) or angiogenesis, i.e., an increased number of capillaries in the DRG (LaMotte and Ma, 2008). Therefore, using specific markers such as GFAP (Glial Fibrillary Acidic Protein) for SGCs or CD31 for endothelial cells might facilitate examining changes that occur in specific non-neuronal cell classes.

Furthermore, we are the first to confirm the existence of cytoplasmic vacuoles in the lumbar DRG of db/db models, although we could not specify their origin in cellular and secretory vesicle markers. Therefore, future investigation might explore the potential accumulation of sugar-related molecules such as sorbitol on these vacuoles by investigating their enzyme presence, which is Aldose reductase (AR), responsible for sorbitol production in the polyol pathway. Some research has explored therapeutic strategies targeting this pathway, specifically aldose reductase inhibitors (ARIs), which work by inhibiting the first step in sorbitol production. Promising findings have shown that ARIs can help mitigate early diabetic complications (Yapar, 2021). A key issue with the sorbitol pathway in diabetes is that specific tissues, such as the retina, kidneys, and Schwann cells, lack sorbitol dehydrogenase, leading to the toxic accumulation of sorbitol in diabetic tissue (Srikanth, 2022). Given that hyperglycaemia is a hallmark of diabetes, it is plausible that these vacuoles may contain accumulated sorbitol, which is linked to glucose metabolism.

In addition, employing advanced ultrastructural analysis using electron microscopy (EM) and similar cellular markers to explore the exact composition of these vacuoles to organelles might prove helpful. Finally, as the precise mechanism driving their formation remains unclear, it might be fruitful to establish functional experiments to assess whether vacuolated neurons exhibit altered sensory function or impairment in signal transmission.

7. Bibliography

Abbott, C.A. *et al.* (2011) 'Prevalence and characteristics of painful diabetic neuropathy in a large community-based diabetic population in the U.K', *Diabetes care*, 34(10), pp. 2220–2224. Available at: https://doi.org/10.2337/DC11-1108.

Abraira, V.E. and Ginty, D.D. (2013) 'The sensory neurons of touch', *Neuron*, 79(4), pp. 618–639. Available at: https://doi.org/10.1016/J.NEURON.2013.07.051.

Ahimsadasan, N. *et al.* (2022) 'Neuroanatomy, Dorsal Root Ganglion', *StatPearls* [Preprint]. Available at: https://www.ncbi.nlm.nih.gov/books/NBK532291/ (Accessed: 11 August 2024).

Akter, T. *et al.* (2020) 'Risk factors for peripheral neuropathy in patients with diabetes mellitus', *IMC Journal of Medical Science*, 13(2), pp. 40–44. Available at: https://doi.org/10.3329/imcjms.v13i2.45285.

Al-Saoudi, E. *et al.* (2022) 'Advanced glycation end-products are associated with diabetic neuropathy in young adults with type 1 diabetes', *Frontiers in Endocrinology*, 13, p. 891442. Available at: https://doi.org/10.3389/FENDO.2022.891442/FULL.

Amin, A. *et al.* (2020) 'Amyotrophic Lateral Sclerosis and Autophagy: Dysfunction and Therapeutic Targeting', *Cells*, 9(11), p. 2413. Available at: https://doi.org/10.3390/cells9112413.

Amin, N. and Doupis, J. (2016) 'Diabetic foot disease: From the evaluation of the "foot at risk" to the novel diabetic ulcer treatment modalities', *World journal of diabetes*, 7(7), p. 153. Available at: https://doi.org/10.4239/WJD.V7.I7.153.

Andrei Cristian, B. and Amorin Remus, P. (2018) 'Diabetic Neuropathy Prevalence and Its Associated Risk Factors in Two Representative Groups of Type 1 and Type 2 Diabetes Mellitus Patients from Bihor County', *Maedica*, 13(3), pp. 229–234. Available at: https://doi.org/10.26574/MAEDICA.2018.13.3.229.

Ang, L. *et al.* (2014) 'Glucose control and diabetic neuropathy: lessons from recent large clinical trials', *Current diabetes reports*, 14(9), pp. 1–15. Available at: https://doi.org/10.1007/S11892-014-0528-7.

Athie, M.C.P. *et al.* (2018) 'Transcriptome analysis of dorsal root ganglia's diabetic neuropathy reveals mechanisms involved in pain and regeneration', *Life Sciences*, 205, pp. 54–62. Available at: https://doi.org/10.1016/j.lfs.2018.05.016.

Ballatore, C., Lee, V.M.Y. and Trojanowski, J.Q. (2007) 'Tau-mediated neurodegeneration in Alzheimer's disease and related disorders', *Nature Reviews Neuroscience*, pp. 663–672. Available at: https://doi.org/10.1038/nrn2194.

Basbaum, A.I. *et al.* (2009) 'Cellular and Molecular Mechanisms of Pain', *Cell*, 139(2), pp. 267–284. Available at: https://doi.org/10.1016/j.cell.2009.09.028.

Bellier, J. *et al.* (2019) 'Methylglyoxal, a potent inducer of AGEs, connects between diabetes and cancer', *Diabetes Research and Clinical Practice*, 148, pp. 200–211. Available at: https://doi.org/10.1016/J.DIABRES.2019.01.002.

Biessels, G.J. *et al.* (2014) 'Phenotyping animal models of diabetic neuropathy: a consensus

statement of the diabetic neuropathy study group of the EASD (Neurodiab)', *Journal of the peripheral nervous system : JPNS*, 19(2), pp. 77–87. Available at: https://doi.org/10.1111/JNS5.12072.

Bondok, A.A. and Sansone, F.M. (1984) 'Retrograde and transganglionic degeneration of sensory neurons after a peripheral nerve lesion at birth', *Experimental Neurology*, 86(2), pp. 322–330. Available at: https://doi.org/10.1016/0014-4886(84)90190-0.

Boulton, A.J.M. (2010) 'What you can't feel can hurt you.', *Journal of the American Podiatric Medical Association*, 100(5), pp. 349–352. Available at: https://doi.org/10.7547/1000349.

Boulton, A.J.M. (2014) 'Diabetic neuropathy and foot complications', in, pp. 97–107. Available at: https://doi.org/10.1016/B978-0-444-53480-4.00008-4.

Boyle, J.P. *et al.* (2010) 'Projection of the year 2050 burden of diabetes in the US adult population: dynamic modeling of incidence, mortality, and prediabetes prevalence', *Population health metrics*, 8. Available at: https://doi.org/10.1186/1478-7954-8-29.

Bras, J.M. and Singleton, A. (2009) 'Genetic susceptibility in Parkinson's disease', *Biochimica et Biophysica Acta (BBA) - Molecular Basis of Disease*, 1792(7), pp. 597–603. Available at: https://doi.org/10.1016/J.BBADIS.2008.11.008.

Bruick, R.K. (2003) 'Oxygen sensing in the hypoxic response pathway: regulation of the hypoxia-inducible transcription factor', *Genes & development*, 17(21), pp. 2614–2623. Available at: https://doi.org/10.1101/GAD.1145503.

Brumovsky, P., Villar, M.J. and Hökfelt, T. (2006) 'Tyrosine hydroxylase is expressed in a subpopulation of small dorsal root ganglion neurons in the adult mouse', *Experimental neurology*, 200(1), pp. 153–165. Available at: https://doi.org/10.1016/J.EXPNEUROL.2006.01.023.

Bruun, C. *et al.* (2013) 'Amputations and foot ulcers in patients newly diagnosed with type 2 diabetes mellitus and observed for 19 years. The role of age, gender and co-morbidity', *Diabetic Medicine*, 30(8), pp. 964–972. Available at: https://doi.org/10.1111/dme.12196.

Burns, T.M. and Mauermann, M.L. (2011) 'The evaluation of polyneuropathies', *Neurology*, 76(7 Suppl 2). Available at: https://doi.org/10.1212/WNL.0B013E31820C3622.

Butt, M.T. (2010) 'Vacuoles in Dorsal Root Ganglia Neurons', *Toxicologic Pathology*, 38(6), pp. 999–999. Available at: https://doi.org/10.1177/0192623310378869.

Callaghan, B.C. *et al.* (2012) 'Diabetic neuropathy: clinical manifestations and current treatments', *The Lancet. Neurology*, 11(6), pp. 521–534. Available at: https://doi.org/10.1016/S1474-4422(12)70065-0.

Cataldo, A.M. *et al.* (1996) 'Properties of the endosomal-lysosomal system in the human central nervous system: Disturbances mark most neurons in populations at risk to degenerate in Alzheimer's disease', *Journal of Neuroscience*, 16(1), pp. 186–199. Available at: https://doi.org/10.1523/jneurosci.16-01-00186.1996.

Cavaletti, G. *et al.* (2007) 'Bortezomib-induced peripheral neurotoxicity: a neurophysiological and pathological study in the rat', *Experimental neurology*, 204(1), pp. 317–325. Available at: https://doi.org/10.1016/J.EXPNEUROL.2006.11.010.

Chae, C.W. *et al.* (2022) 'High glucose-mediated VPS26a down-regulation dysregulates neuronal amyloid precursor protein processing and tau phosphorylation', *British Journal of Pharmacology*, 179(15), pp. 3934–3950. Available at: https://doi.org/10.1111/bph.15836.

Chao, T. *et al.* (2008) 'Chronic nerve compression injury induces a phenotypic switch of neurons within the dorsal root ganglia', *The Journal of comparative neurology*, 506(2), pp. 180–193. Available at: https://doi.org/10.1002/CNE.21537.

Chelyshev, Y.A. and Raginov, I.S. (2002) 'Effect of stimulation of nerve regeneration on posttraumatic neuronal survival in dorsal root ganglia', *Bulletin of Experimental Biology and Medicine*, 134(6), pp. 597–599. Available at: https://doi.org/10.1023/A:1022929632535.

Chen, H. *et al.* (1996) 'Evidence That the Diabetes Gene Encodes the Leptin Receptor: Identification of a Mutation in the Leptin Receptor Gene in db/db Mice', *Cell*, 84(3), pp. 491–495. Available at: https://doi.org/10.1016/S0092-8674(00)81294-5.

Chen, S.-S. and Zhang, J.-M. (2015) 'Progress in Sympathetically Mediated Pathological Pain', *Journal of anesthesia and perioperative medicine*, 2(4), p. 216. Available at: https://doi.org/10.24015/JAPM.2015.0029.

Chien, S.Q. *et al.* (2005) 'Sympathetic Fiber Sprouting in Chronically Compressed Dorsal Root Ganglia Without Peripheral Axotomy', *Journal of Neuropathic Pain & Symptom Palliation*, 1(1), pp. 19–23. Available at: https://doi.org/10.3109/j426v01n01_05.

Chung, K. *et al.* (1996) 'Sympathetic Sprouting in the Dorsal Root Ganglia of the Injured Peripheral Nerve in a Rat Neuropathic Pain Model', *THE JOURNAL OF COMPARATIVE NEUROLOGY*, 376, pp. 241–252. Available at: https://doi.org/10.1002/(SICI)1096-9861(19961209)376:2.

Chung, K. and Chung, J.M. (2001) 'Sympathetic sprouting in the dorsal root ganglion after spinal nerve ligation: evidence of regenerative collateral sprouting', *Brain Research*, 895(1–2), pp. 204–212. Available at: https://doi.org/10.1016/S0006-8993(01)02092-3.

Ciglieri, E. *et al.* (2020) 'Cytoarchitectural analysis of the neuron-to-glia association in the dorsal root ganglia of normal and diabetic mice', *Journal of Anatomy*, 237(5). Available at: /pmc/articles/PMC7542191/ (Accessed: 9 September 2024).

Corral-Pujol, M. *et al.* (2023) 'NOD mouse dorsal root ganglia display morphological and gene expression defects before and during autoimmune diabetes development', *Frontiers in Endocrinology*, 14. Available at: https://doi.org/10.3389/FENDO.2023.1176566/PDF.

Davies, M. *et al.* (2006) 'The prevalence, severity, and impact of painful diabetic peripheral neuropathy in type 2 diabetes', *Diabetes Care*, 29(7), pp. 1518–1522. Available at: https://doi.org/10.2337/DC05-2228.

DeFronzo, R.A. *et al.* (2015) 'Type 2 diabetes mellitus', *Nature Reviews Disease Primers*, 1(July), pp. 1–23. Available at: https://doi.org/10.1038/nrdp.2015.19.

Dermatomes: What They Are & Locations (2024). Available at: https://my.clevelandclinic.org/health/body/24379-dermatomes (Accessed: 10 September 2024).

Derry, S. *et al.* (2014) 'Topical lidocaine for neuropathic pain in adults', *The Cochrane*

database of systematic reviews, 2014(7). Available at: https://doi.org/10.1002/14651858.CD010958.PUB2.

Derry, S. *et al.* (2019) 'Pregabalin for neuropathic pain in adults', *The Cochrane database of systematic reviews*, 1(1). Available at: https://doi.org/10.1002/14651858.CD007076.PUB3.

Didangelos, T., Doupis, J. and Veves, A. (2014) 'Painful diabetic neuropathy: clinical aspects', *Handbook of Clinical Neurology*, 126, pp. 53–61. Available at: https://doi.org/10.1016/B978-0-444-53480-4.00005-9.

Divisova, S. *et al.* (2012) 'Prediabetes/early diabetes-associated neuropathy predominantly involves sensory small fibres', *Journal of the peripheral nervous system : JPNS*, 17(3), pp. 341–350. Available at: https://doi.org/10.1111/J.1529-8027.2012.00420.X.

Djouhri, L. *et al.* (2006) 'Spontaneous pain, both neuropathic and inflammatory, is related to frequency of spontaneous firing in intact C-fiber nociceptors', *The Journal of neuroscience : the official journal of the Society for Neuroscience*, 26(4), pp. 1281–1292. Available at: https://doi.org/10.1523/JNEUROSCI.3388-05.2006.

Doupis, J. *et al.* (2009) 'Microvascular Reactivity and Inflammatory Cytokines in Painful and Painless Peripheral Diabetic Neuropathy', *The Journal of Clinical Endocrinology and Metabolism*, 94(6), p. 2157. Available at: https://doi.org/10.1210/JC.2008-2385.

Dubin, A.E. and Patapoutian, A. (2010) 'Nociceptors: the sensors of the pain pathway', *The Journal of Clinical Investigation*, 120(11), p. 3760. Available at: https://doi.org/10.1172/JCI42843.

Duehmke, R.M. *et al.* (2017) 'Tramadol for neuropathic pain in adults', *The Cochrane database of systematic reviews*, 6(6). Available at: https://doi.org/10.1002/14651858.CD003726.PUB4.

Eftekharpour, E. and Fernyhough, P. (2022) 'Oxidative Stress and Mitochondrial Dysfunction Associated with Peripheral Neuropathy in Type 1 Diabetes', *Antioxidants & Redox Signaling*, 37(7–9), pp. 578–596. Available at: https://doi.org/10.1089/ars.2021.0152.

Eid, S.A. *et al.* (2023) 'New perspectives in diabetic neuropathy', *Neuron*, 111(17), pp. 2623–2641. Available at: https://doi.org/10.1016/J.NEURON.2023.05.003.

Elafros, M.A. *et al.* (2022) 'Towards prevention of diabetic peripheral neuropathy: clinical presentation, pathogenesis, and new treatments', *The Lancet Neurology*, 21(10), pp. 922–936. Available at: https://doi.org/10.1016/S1474-4422(22)00188-0.

Emery, E.C. *et al.* (2016) 'In vivo characterization of distinct modality-specific subsets of somatosensory neurons using GCaMP', *Science Advances*, 2(11). Available at: https://doi.org/10.1126/SCIADV.1600990.

Entezari, M. *et al.* (2022) 'AMPK signaling in diabetes mellitus, insulin resistance and diabetic complications: A pre-clinical and clinical investigation', *Biomedicine and Pharmacotherapy*, 146, p. 112563. Available at: https://doi.org/10.1016/j.biopha.2021.112563.

Esposito, M.F. *et al.* (2019) 'Unique Characteristics of the Dorsal Root Ganglion as a Target for Neuromodulation', *Pain Medicine*, 20(Supplement_1), pp. S23–S30. Available at: https://doi.org/10.1093/pm/pnz012.

Feldman, E.L. *et al.* (2019) 'Diabetic neuropathy', *Nature reviews. Disease primers*, 5(1). Available at: https://doi.org/10.1038/S41572-019-0092-1.

Fornaro, M. *et al.* (2008) 'Neuronal intermediate filament expression in rat dorsal root ganglia sensory neurons: An in vivo and in vitro study', *Neuroscience*, 153(4), pp. 1153–1163. Available at: https://doi.org/10.1016/j.neuroscience.2008.02.080.

Fowler, M.J. (2008) 'Microvascular and Macrovascular Complications of Diabetes', *Clinical Diabetes*, 26(2), pp. 77–82. Available at: https://doi.org/10.2337/DIACLIN.26.2.77.

Franco-Iborra, S. *et al.* (2018) 'Defective mitochondrial protein import contributes to complex I-induced mitochondrial dysfunction and neurodegeneration in Parkinson's disease', *Cell Death & Disease 2018 9:11*, 9(11), pp. 1–17. Available at: https://doi.org/10.1038/s41419-018-1154-0.

Gasser, H.S. (1941) 'The classification of nerve fibers.', *Ohio Journal of Science* [Preprint].

Gasser, H.S. and Erlanger, J. (1929) 'The Action Potential in Fibers of Slow Conduction in Spinal Roots and Somatic Nerves.', *https://doi.org/10.3181/00379727-26-4441*, 26(8), pp. 647–649. Available at: https://doi.org/10.3181/00379727-26-4441.

Geraldes, P. and King, G.L. (2010) 'Activation of protein kinase C isoforms and its impact on diabetic complications', *Circulation research*, 106(8), pp. 1319–1331. Available at: https://doi.org/10.1161/CIRCRESAHA.110.217117.

Gold, M.S. and Gebhart, G.F. (2010) 'Nociceptor sensitization in pain pathogenesis', *Nature medicine*, 16(11), pp. 1248–1257. Available at: https://doi.org/10.1038/NM.2235.

De Gregorio, C. *et al.* (2018) 'Characterization of diabetic neuropathy progression in a mouse model of type 2 diabetes mellitus', *Biology Open*, 7(9). Available at: https://doi.org/10.1242/BIO.036830.

Groves, M.J. *et al.* (1997) 'Axotomy-induced apoptosis in adult rat primary sensory neurons', *Journal of neurocytology*, 26(9), pp. 615–624. Available at: https://doi.org/10.1023/A:1018541726460.

Groves, M.J. *et al.* (2003) 'Profile of adult rat sensory neuron loss, apoptosis and replacement after sciatic nerve crush', *Journal of Neurocytology*, 32(2), pp. 113–122. Available at: https://doi.org/10.1023/B:NEUR.0000005596.88385.ec.

Guest, P.C. and Rahmoune, H. (2019) 'Characterization of the db/db Mouse Model of Type 2 Diabetes', *Methods in Molecular Biology*, 1916, pp. 195–201. Available at: https://doi.org/10.1007/978-1-4939-8994-2_18/TABLES/1.

Hamano, T. *et al.* (2021) 'Autophagy and Tau Protein', *International Journal of Molecular Sciences*, 22(14), p. 7475. Available at: https://doi.org/10.3390/ijms22147475.

Hammond, D.L. *et al.* (2004) 'Effects of spinal nerve ligation on immunohistochemically identified neurons in the L4 and L5 dorsal root ganglia of the rat', *The Journal of comparative neurology*, 475(4), pp. 575–589. Available at: https://doi.org/10.1002/CNE.20209.

Harper, A.A. and Lawson, S.N. (1985) 'Conduction velocity is related to morphological cell

type in rat dorsal root ganglion neurones', *The Journal of physiology*, 359(1), pp. 31–46. Available at: https://doi.org/10.1113/JPHYSIOL.1985.SP015573.

Herradon, G. *et al.* (2008) 'Noradrenergic and opioidergic alterations in neuropathy in different rat strains', *Neuroscience Letters*, 438(2), pp. 186–189. Available at: https://doi.org/10.1016/j.neulet.2008.03.095.

Herweijer, G. *et al.* (2014) 'Characterisation of primary afferent spinal innervation of mouse uterus', *Frontiers in Neuroscience*, 8(8 JUN), pp. 1–6. Available at: https://doi.org/10.3389/fnins.2014.00202.

Huang, B., Li, X. and Zhu, X. (2021) 'The Role of GM130 in Nervous System Diseases', *Frontiers in Neurology*, 12, p. 743787. Available at: https://doi.org/10.3389/FNEUR.2021.743787.

Hummel, K.P., Dickie, M.M. and Coleman, D.L. (1966) 'Diabetes, a New Mutation in the Mouse', *Science*, 153(3740), pp. 1127–1128. Available at: https://doi.org/10.1126/SCIENCE.153.3740.1127.

Ibrahim, F. and Megahed, A.-L. (2013) 'Quality of life of type 2 diabetic patients attending family medicine outpatient clinic of Suez Canal university hospitals in Ismailia city'. Available at: https://www.researchgate.net/publication/328228639 (Accessed: 19 July 2024).

Iqbal, Z. *et al.* (2018) 'Diabetic Peripheral Neuropathy: Epidemiology, Diagnosis, and Pharmacotherapy', *Clinical therapeutics*, 40(6), pp. 828–849. Available at: https://doi.org/10.1016/J.CLINTHERA.2018.04.001.

Jang, H.N. and Oh, T.J. (2023) 'Pharmacological and Nonpharmacological Treatments for Painful Diabetic Peripheral Neuropathy', *Diabetes & Metabolism Journal*, 47(6), pp. 743–756. Available at: https://doi.org/10.4093/dmj.2023.0018.

Jende, J.M.E. *et al.* (2020) 'Diabetic Polyneuropathy Is Associated With Pathomorphological Changes in Human Dorsal Root Ganglia: A Study Using 3T MR Neurography', *Frontiers in Neuroscience*, 14. Available at: https://doi.org/10.3389/fnins.2020.570744.

Ji, R.R., Chamessian, A. and Zhang, Y.Q. (2016) 'Pain regulation by non-neuronal cells and inflammation', *Science (New York, N.Y.)*, 354(6312), pp. 572–577. Available at: https://doi.org/10.1126/SCIENCE.AAF8924.

Ji, Y. *et al.* (2022) 'Effect of sympathetic sprouting on the excitability of dorsal root ganglion neurons and afferents in a rat model of neuropathic pain', *Biochemical and Biophysical Research Communications*, 587, pp. 49–57. Available at: https://doi.org/10.1016/j.bbrc.2021.11.096.

Johnson, P.C. (1983) 'Thickening of the human dorsal root ganglion perineurial cell basement membrane in diabetes mellitus', *Muscle & Nerve*, 6(8), pp. 561–565. Available at: https://doi.org/10.1002/mus.880060805.

Jolivalt, C.G. *et al.* (2008) 'Defective insulin signaling pathway and increased glycogen synthase kinase-3 activity in the brain of diabetic mice: Parallels with Alzheimer's disease and correction by insulin', *Journal of Neuroscience Research*, 86(15), pp. 3265–3274. Available at: https://doi.org/10.1002/JNR.21787.

Joshi, G. *et al.* (2014) 'Aβ-induced Golgi fragmentation in Alzheimer's disease enhances Aβ production', *Proceedings of the National Academy of Sciences of the United States of America*, 111(13). Available at: https://doi.org/10.1073/PNAS.1320192111.

Kamiya, H. *et al.* (2006) 'C-Peptide reverses nociceptive neuropathy in type 1 diabetes', *Diabetes*, 55(12), pp. 3581–3587. Available at: https://doi.org/10.2337/DB06-0396.

Kamiya, H., Zhang, W. and Sima, A.A. (2006) 'Degeneration of the Golgi and neuronal loss in dorsal root ganglia in diabetic BioBreeding/Worcester rats.', *Diabetologia*, 49(11), pp. 2763–2774. Available at: https://doi.org/10.1007/s00125-006-0379-0.

Kavakiotis, I. *et al.* (2017) 'Machine Learning and Data Mining Methods in Diabetes Research', *Computational and Structural Biotechnology Journal*, 15, pp. 104–116. Available at: https://doi.org/10.1016/J.CSBJ.2016.12.005.

Kim, H.J. *et al.* (1996) 'Sprouting of sympathetic nerve fibers into the dorsal root ganglion following peripheral nerve injury depends on the injury site', *Neuroscience Letters*, 212(3), pp. 191–194. Available at: https://doi.org/10.1016/0304-3940(96)12811-1.

Kishi, M. *et al.* (2002) *Morphometry of Dorsal Root Ganglion in Chronic Experimental Diabetic Neuropathy*, *Diabetes*. Diabetes. Available at: https://doi.org/10.2337/DIABETES.51.3.819.

Ko, M.J. *et al.* (2013) 'Postprandial blood glucose is associated with generalized pruritus in patients with type 2 diabetes', *European journal of dermatology : EJD*, 23(5), pp. 688–693. Available at: https://doi.org/10.1684/EJD.2013.2100.

Kobayashi, M. *et al.* (2017) 'Diabetic polyneuropathy, sensory neurons, nuclear structure and spliceosome alterations: a role for CWC22', *Disease models & mechanisms*, 10(3), pp. 215–224. Available at: https://doi.org/10.1242/DMM.028225.

Kudo, M. *et al.* (2021) 'Distribution of Large and Small Dorsal Root Ganglion Neurons in Common Marmosets', *Frontiers in Systems Neuroscience*, 15. Available at: https://doi.org/10.3389/FNSYS.2021.801492.

LaMotte, R.H. and Ma, C. (2008) 'Hyperexcitable neurons and altered non-neuronal cells in the compressed spinal ganglion', *Sheng li xue bao : [Acta physiologica Sinica]*, 60(5), p. 597. Available at: /pmc/articles/PMC2669673/ (Accessed: 8 August 2024).

Lee, B.H. *et al.* (1998) 'Comparison of sympathetic sprouting in sensory ganglia in three animal models of neuropathic pain', *Experimental Brain Research*, 120(4), pp. 432–438. Available at: https://doi.org/10.1007/S002210050416/METRICS.

Lee, S.M. and Bressler, R. (1981) 'Prevention of diabetic nephropathy by diet control in the db/db mouse', *Diabetes*, 30(2), pp. 106–111. Available at: https://doi.org/10.2337/DIAB.30.2.106.

Li, C. *et al.* (2018) 'Somatosensory Neuron Typing with High-Coverage Single-Cell RNA Sequencing and Functional Analysis', *Neuroscience bulletin*, 34(1), pp. 200–207. Available at: https://doi.org/10.1007/S12264-017-0147-9.

Li, X.L. *et al.* (2002) 'Impairment of long-term potentiation and spatial memory in leptin receptor-deficient rodents', *Neuroscience*, 113(3), pp. 607–615. Available at:

https://doi.org/10.1016/S0306-4522(02)00162-8.

Liem, L. *et al.* (2015) 'One-Year Outcomes of Spinal Cord Stimulation of the Dorsal Root Ganglion in the Treatment of Chronic Neuropathic Pain', *Neuromodulation: Technology at the Neural Interface*, 18(1), pp. 41–49. Available at: https://doi.org/10.1111/NER.12228.

Like, A.A. *et al.* (1972) 'Studies in the Diabetic Mutant Mouse: VI. Evolution of Glomerular Lesions and Associated Proteinuria', *The American Journal of Pathology*, 66(2), p. 193. Available at: /pmc/articles/PMC2032492/?report=abstract (Accessed: 1 October 2024).

Lima, A.L. *et al.* (2017) 'Cutaneous Manifestations of Diabetes Mellitus: A Review', *American journal of clinical dermatology*, 18(4), pp. 541–553. Available at: https://doi.org/10.1007/S40257-017-0275-Z.

Lu, J., Wu, M. and Yue, Z. (2020) 'Autophagy and Parkinson's Disease', in, pp. 21–51. Available at: https://doi.org/10.1007/978-981-15-4272-5_2.

Lunn, M.P.T., Hughes, R.A.C. and Wiffen, P.J. (2014) 'Duloxetine for treating painful neuropathy, chronic pain or fibromyalgia', *The Cochrane database of systematic reviews*, 2014(1). Available at: https://doi.org/10.1002/14651858.CD007115.PUB3.

Ma, W. and Bisby, M.A. (1999) 'Partial sciatic nerve transection induced tyrosine hydroxidase immunoreactive axon sprouting around both injured and spared dorsal root ganglion neurons which project to the gracile nucleus in middle-aged rats', *Neuroscience Letters*, 275(2), pp. 117–120. Available at: https://doi.org/10.1016/S0304-3940(99)00746-6.

Madani, S. and Doughty, C. (2020) 'Lower extremity entrapment neuropathies', *Best Practice & Research Clinical Rheumatology*, 34(3), p. 101565. Available at: https://doi.org/10.1016/J.BERH.2020.101565.

Magliano, D.J. and Boyko, E.J. (2021) 'IDF DIABETES ATLAS', *IDF DIABETES ATLAS [Internet]. Brussels*, pp. 1–141. Available at: https://www.ncbi.nlm.nih.gov/books/NBK581934/ (Accessed: 22 July 2024).

Mai, S. *et al.* (2012) 'Autophagy proteins LC3B, ATG5 and ATG12 participate in quality control after mitochondrial damage and influence life span', *Autophagy*, 8(1), pp. 47–62. Available at: https://doi.org/10.4161/auto.8.1.18174.

Martin, C.L., Albers, J.W. and Pop-Busui, R. (2014) 'Neuropathy and related findings in the diabetes control and complications trial/epidemiology of diabetes interventions and complications study', *Diabetes care*, 37(1), pp. 31–38. Available at: https://doi.org/10.2337/DC13-2114.

McCarthy, C.J. *et al.* (2016) 'Axotomy of tributaries of the pelvic and pudendal nerves induces changes in the neurochemistry of mouse dorsal root ganglion neurons and the spinal cord', *Brain structure & function*, 221(4), p. 1985. Available at: https://doi.org/10.1007/S00429-015-1019-6.

McHugh, J.M. and McHugh, W.B. (2004) 'Diabetes and Peripheral Sensory Neurons', *AACN Clinical Issues: Advanced Practice in Acute and Critical Care*, 15(1), pp. 136–149. Available at: https://doi.org/10.1097/00044067-200401000-00012.

McLachlan, E.M. *et al.* (1993) 'Peripheral nerve injury triggers noradrenergic sprouting

within dorsal root ganglia', *Nature*, 363(6429), pp. 543–546. Available at: https://doi.org/10.1038/363543A0.

Michalak, M. *et al.* (2009) 'Calreticulin, a multi-process calcium-buffering chaperone of the endoplasmic reticulum', *Biochemical Journal*, 417(3), pp. 651–666. Available at: https://doi.org/10.1042/BJ20081847.

Mohan, A.G. *et al.* (2023) 'The Golgi Apparatus: A Voyage through Time, Structure, Function and Implication in Neurodegenerative Disorders', *Cells*, 12(15). Available at: https://doi.org/10.3390/CELLS12151972.

Moore, R.A. *et al.* (2015) 'Amitriptyline for neuropathic pain in adults', *The Cochrane database of systematic reviews*, 2015(7). Available at: https://doi.org/10.1002/14651858.CD008242.PUB3.

Mourelatos, Z. *et al.* (1996) 'The Golgi apparatus of spinal cord motor neurons in transgenic mice expressing mutant Cu,Zn superoxide dismutase becomes fragmented in early, preclinical stages of the disease', *Proceedings of the National Academy of Sciences of the United States of America*, 93(11), pp. 5472–5477. Available at: https://doi.org/10.1073/PNAS.93.11.5472.

Murtazina, A. and Adameyko, I. (2023) 'The peripheral nervous system', *Development (Cambridge, England)*, 150(9). Available at: https://doi.org/10.1242/DEV.201164.

Niimi, N. *et al.* (2021) 'Aldose Reductase and the Polyol Pathway in Schwann Cells: Old and New Problems', *International journal of molecular sciences*, 22(3), pp. 1–14. Available at: https://doi.org/10.3390/IJMS22031031.

Nixon, R.A. and Yang, D.S. (2011) 'Autophagy failure in Alzheimer's disease--locating the primary defect', *Neurobiology of disease*, 43(1), pp. 38–45. Available at: https://doi.org/10.1016/J.NBD.2011.01.021.

Noorafshan, A., Ebrahimpoor, M.R. and SADEGHI, Y. (2001) 'Stereological study of the cells of dorsal root ganglia in male diabetic rats', *APMIS*, 109(11), pp. 762–766. Available at: https://doi.org/10.1034/j.1600-0463.2001.d01-143.x.

Obrosova, I.G. *et al.* (2007) 'High-fat diet induced neuropathy of pre-diabetes and obesity: effects of "healthy" diet and aldose reductase inhibition', *Diabetes*, 56(10), pp. 2598–2608. Available at: https://doi.org/10.2337/DB06-1176.

Ohtori, S. *et al.* (2007) 'Characteristics of Sensory Dorsal Root Ganglia Neurons Innervating the Lumbar Vertebral Body in Rats', *Journal of Pain*, 8(6), pp. 483–488. Available at: https://doi.org/10.1016/j.jpain.2007.01.004.

Pannese, E. (2010) 'The structure of the perineuronal sheath of satellite glial cells (SGCs) in sensory ganglia', *Neuron Glia Biology*, 6(1), pp. 3–10. Available at: https://doi.org/10.1017/S1740925X10000037.

Pelletier, C. *et al.* (2012) 'Report summary. Diabetes in Canada: facts and figures from a public health perspective.', *Chronic diseases and injuries in Canada*, 33(1), pp. 53–54. Available at: https://doi.org/10.24095/hpcdp.33.1.07.

Peltier, A., Goutman, S.A. and Callaghan, B.C. (2014) 'Painful diabetic neuropathy', *BMJ*

(Clinical research ed.), 348. Available at: https://doi.org/10.1136/BMJ.G1799.

Le Pichon, C.E. and Chesler, A.T. (2014) 'The functional and anatomical dissection of somatosensory subpopulations using mouse genetics', *Frontiers in Neuroanatomy*, 8(APR). Available at: https://doi.org/10.3389/FNANA.2014.00021.

Piras, A. *et al.* (2016) 'Autophagic and lysosomal defects in human tauopathies: analysis of post-mortem brain from patients with familial Alzheimer disease, corticobasal degeneration and progressive supranuclear palsy', *Acta neuropathologica communications*, 4, p. 22. Available at: https://doi.org/10.1186/S40478-016-0292-9.

Pop-Busui, R., Sima, A. and Stevens, M. (2006) 'Diabetic neuropathy and oxidative stress', *Diabetes/Metabolism Research and Reviews*, 22(4), pp. 257–273. Available at: https://doi.org/10.1002/DMRR.625.

Price, J. (1985) 'An immunohistochemical and quantitative examination of dorsal root ganglion neuronal subpopulations', *The Journal of neuroscience : the official journal of the Society for Neuroscience*, 5(8), pp. 2051–2059. Available at: https://doi.org/10.1523/JNEUROSCI.05-08-02051.1985.

Ramer, M.S. and Bisby, M.A. (1997) 'Rapid sprouting of sympathetic axons in dorsal root ganglia of rats with a chronic constriction injury', *Pain*, 70(2–3), pp. 237–244. Available at: https://doi.org/10.1016/S0304-3959(97)03331-9.

Ramer, M.S. and Bisby, M.A. (1998) 'Differences in sympathetic innervation of mouse DRG following proximal or distal nerve lesions', *Experimental Neurology*, 152(2), pp. 197–207. Available at: https://doi.org/10.1006/exnr.1998.6855.

Ramer, M.S., Thompson, S.W.N. and McMahon, S.B. (1999) 'Causes and consequences of sympathetic basket formation in dorsal root ganglia', *Pain*, 82(SUPPL.1), pp. S111–S120. Available at: https://doi.org/10.1016/S0304-3959(99)00144-X.

Rees, D.A. and Alcolado, J.C. (2005) 'Animal models of diabetes mellitus', *Diabetic medicine : a journal of the British Diabetic Association*, 22(4), pp. 359–370. Available at: https://doi.org/10.1111/J.1464-5491.2005.01499.X.

Rinkel, W.D. *et al.* (2018) 'Grading the loss of sensation in diabetic patients: A psychometric evaluation of the rotterdam diabetic foot study test battery', *Muscle and Nerve*, 58(4), pp. 559–565. Available at: https://doi.org/10.1002/MUS.26192.

Rogers-Cotrone, T. *et al.* (2010) 'Vacuolation of sensory ganglion neuron cytoplasm in rats with long-term exposure to organophosphates', *Toxicologic Pathology*, 38(4), pp. 554–559. Available at: https://doi.org/10.1177/0192623310369343.

Rossi, R. *et al.* (2022) 'Synaptic Vesicle Glycoprotein 2A: Features and Functions', *Frontiers in Neuroscience*, 16. Available at: https://doi.org/10.3389/FNINS.2022.864514.

Ruscheweyh, R. *et al.* (2007) 'Modification of classical neurochemical markers in identified primary afferent neurons with Abeta-, Adelta-, and C-fibers after chronic constriction injury in mice', *The Journal of comparative neurology*, 502(2), pp. 325–336. Available at: https://doi.org/10.1002/CNE.21311.

Russell, J.W. *et al.* (1999) 'Neurons undergo apoptosis in animal and cell culture models of

diabetes', *Neurobiology of Disease*, 6(5), pp. 347–363. Available at: https://doi.org/10.1006/nbdi.1999.0254.

Sahin, G.S., Lee, H. and Engin, F. (2021) 'An accomplice more than a mere victim: The impact of β-cell ER stress on type 1 diabetes pathogenesis', *Molecular Metabolism*, 54, p. 101365. Available at: https://doi.org/10.1016/j.molmet.2021.101365.

Said, G. (2007) 'Diabetic neuropathy--a review', *Nature clinical practice. Neurology*, 3(6), pp. 331–340. Available at: https://doi.org/10.1038/NCPNEURO0504.

Sandireddy, R. *et al.* (2014) 'Neuroinflammation and Oxidative Stress in Diabetic Neuropathy: Futuristic Strategies Based on These Targets Reddemma', 2014(1), p. 674987. Available at: https://doi.org/10.1155/2014/674987.

Sango, K. *et al.* (2006) 'Cultured Adult Animal Neurons and Schwann Cells Give Us New Insights into Diabetic Neuropathy', *Current Diabetes Reviews*, 2(2), pp. 169–183. Available at: https://doi.org/10.2174/157339906776818613.

Sasaki, H. *et al.* (1997) 'Neuropathology and blood flow of nerve, spinal roots and dorsal root ganglia in longstanding diabetic rats', (5001), pp. 118–128.

Schmeichel, A.M., Schmelzer, J.D. and Low, P.A. (2003) 'Oxidative injury and apoptosis of dorsal root ganglion neurons in chronic experimental diabetic neuropathy', *Diabetes*, 52(1), pp. 165–171. Available at: https://doi.org/10.2337/diabetes.52.1.165.

Schreiber, A.K. (2015) 'Diabetic neuropathic pain: Physiopathology and treatment', *World Journal of Diabetes*, 6(3), p. 432. Available at: https://doi.org/10.4239/wjd.v6.i3.432.

Scroggs, R.S. and Fox, A.P. (1992) 'Calcium current variation between acutely isolated adult rat dorsal root ganglion neurons of different size.', *The Journal of Physiology*, 445(1), pp. 639–658. Available at: https://doi.org/10.1113/JPHYSIOL.1992.SP018944.

Shadfar, S. *et al.* (2023) 'Redox dysregulation as a driver for DNA damage and its relationship to neurodegenerative diseases', *Translational Neurodegeneration*, 12(1). Available at: https://doi.org/10.1186/S40035-023-00350-4.

Shi, T.J.S. *et al.* (2013) 'Coenzyme Q10 prevents peripheral neuropathy and attenuates neuron loss in the db-/db- mouse, a type 2 diabetes model', *Proceedings of the National Academy of Sciences of the United States of America*, 110(2), pp. 690–695. Available at: https://doi.org/10.1073/PNAS.1220794110/-/DCSUPPLEMENTAL/PNAS.201220794SI.PDF.

Sidenius, P. and Jakobsen, J. (1980) 'Reduced Perikaryal Volume of Lower Motor and Primary Sensory Neurons in Early Experimental Diabetes', *Diabetes*, 29(3), pp. 182–187. Available at: https://doi.org/10.2337/DIAB.29.3.182.

Sierra-Fonseca, J.A. and Gosselink, K.L. (2018) 'Tauopathy and neurodegeneration: A role for stress', *Neurobiology of Stress*. Elsevier Inc, pp. 105–112. Available at: https://doi.org/10.1016/j.ynstr.2018.08.009.

Sima, A.A.F. and Robertson, D.M. (1978) 'Peripheral neuropathy in mutant diabetic mouse [C57BL/Ks (db/db)]', *Acta neuropathologica*, 41(2), pp. 85–89. Available at: https://doi.org/10.1007/BF00689757.

Simpson, D.M. *et al.* (2017) 'Capsaicin 8% Patch in Painful Diabetic Peripheral Neuropathy: A Randomized, Double-Blind, Placebo-Controlled Study', *The journal of pain*, 18(1), pp. 42–53. Available at: https://doi.org/10.1016/J.JPAIN.2016.09.008.

Singh, R., Kishore, L. and Kaur, N. (2014) 'Diabetic peripheral neuropathy: current perspective and future directions', *Pharmacological research*, 80, pp. 21–35. Available at: https://doi.org/10.1016/J.PHRS.2013.12.005.

Song, D.D. *et al.* (2014) 'Neuron-glial communication mediated by TNF-α and glial activation in dorsal root ganglia in visceral inflammatory hypersensitivity', *American journal of physiology. Gastrointestinal and liver physiology*, 306(9). Available at: https://doi.org/10.1152/AJPGI.00318.2013.

Sosenko, J. *et al.* (1993) 'A Prospective Study of Sensory Function in Patients with Type 2 Diabetes', *Diabetic Medicine*, 10(2), pp. 110–114. Available at: https://doi.org/10.1111/J.1464-5491.1993.TB00026.X.

Soundararajan, M. *et al.* (2021) 'Prevalence of Diabetic Peripheral Neuropathy among Type 2 Diabetes Mellitus Patients in an urban area of Puducherry'. Available at: https://doi.org/10.26727/NJRCM.2021.10.2.41-044.

Spallone, V. and Greco, C. (2013) 'Painful and painless diabetic neuropathy: one disease or two?', *Current diabetes reports*, 13(4), pp. 533–549. Available at: https://doi.org/10.1007/S11892-013-0387-7.

Sperry, Z.J. *et al.* (2020) 'Spatial models of cell distribution in human lumbar dorsal root ganglia', *The Journal of comparative neurology*, 528(10), p. 1644. Available at: https://doi.org/10.1002/CNE.24848.

Srinivasan, S., Stevens, M. and Wiley, J.W. (2000) 'Evidence for Apoptosis and Associated Mitochondrial Dysfunction', *Diabetes*, 49(11), pp. 1932–1938. Available at: https://doi.org/10.2337/DIABETES.49.11.1932.

Sulzer, D. *et al.* (2008) 'Neuronal pigmented autophagic vacuoles: lipofuscin, neuromelanin, and ceroid as macroautophagic responses during aging and disease', *Journal of Neurochemistry*, 106(1), pp. 24–36. Available at: https://doi.org/10.1111/j.1471-4159.2008.05385.x.

Sun, H. *et al.* (2022) 'IDF Diabetes Atlas: Global, regional and country-level diabetes prevalence estimates for 2021 and projections for 2045', *Diabetes Research and Clinical Practice*, 183, pp. 1–23. Available at: https://doi.org/10.1016/j.diabres.2021.109119.

Suriano, F. *et al.* (2021) 'Novel insights into the genetically obese (ob/ob) and diabetic (db/db) mice: two sides of the same coin', *Microbiome*, 9(1), pp. 1–20. Available at: https://doi.org/10.1186/S40168-021-01097-8/FIGURES/7.

Suter, M.R. *et al.* (2007) 'Do glial cells control pain?', *Neuron Glia Biology*, 3(3), pp. 255–268. Available at: https://doi.org/10.1017/S1740925X08000100.

Tandrup, T. (1993) 'A method for unbiased and efficient estimation of number and mean volume of specified neuron subtypes in rat dorsal root ganglion', *Journal of Comparative Neurology*, 329(2), pp. 269–276. Available at: https://doi.org/10.1002/CNE.903290208.

Tandrup, T., Woolf, C. and Coggeshall, R. (2000) 'Delayed loss of small dorsal root ganglion cells after transection of the rat sciatic nerve', *Journal of Comparative Neurology* [Preprint]. Available at: https://doi.org/10.1002/(SICI)1096-9861(20000626)422:2.

Tang, Z.Y. *et al.* (2009) 'Changes of cervical dorsal root ganglia induced by compression injury and decompression procedure: a novel rat model of cervical radiculoneuropathy', *Journal of neurotrauma*, 26(2), pp. 289–295. Available at: https://doi.org/10.1089/NEU.2008.0506.

Tay, V.S.Y. *et al.* (2019) 'Increased double strand breaks in diabetic β-cells with a p21 response that limits apoptosis', *Scientific Reports*, 9(1). Available at: https://doi.org/10.1038/S41598-019-54554-8.

Tesfaye, S. *et al.* (2005) 'Vascular risk factors and diabetic neuropathy', *The New England journal of medicine*, 352(4), pp. 341–350. Available at: https://doi.org/10.1056/NEJMOA032782.

Tesfaye, S. and Kempler, P. (2005) 'Painful diabetic neuropathy', *Diabetologia*, 48(5), pp. 805–807. Available at: https://doi.org/10.1007/S00125-005-1721-7/TABLES/1.

Tomlinson, D.R. and Gardiner, N.J. (2008) 'Glucose neurotoxicity', *Nature Reviews Neuroscience 2008 9:1*, 9(1), pp. 36–45. Available at: https://doi.org/10.1038/nrn2294.

Usman, U.Z. *et al.* (2015) 'A Review on Experimental Methods of Diabetic Research: Advantages and Limitations', *Annual Research & Review in Biology*, 7(2), pp. 100–108. Available at: https://doi.org/10.9734/ARRB/2015/17404.

Usoskin, D. *et al.* (2015) 'Unbiased classification of sensory neuron types by large-scale single-cell RNA sequencing', *Nature Neuroscience*, 18(1), pp. 145–153. Available at: https://doi.org/10.1038/nn.3881.

Vanderweyde, T. *et al.* (2016) 'Interaction of tau with the RNA-Binding Protein TIA1 Regulates tau Pathophysiology and Toxicity', *Cell Reports*, 15(7), pp. 1455–1466. Available at: https://doi.org/10.1016/j.celrep.2016.04.045.

Wang, K. *et al.* (2023) 'Somatosensory neuron types and their neural networks as revealed via single-cell transcriptomics', *Trends in Neurosciences*, 46(8), pp. 654–666. Available at: https://doi.org/10.1016/j.tins.2023.05.005.

Ward, I.M. *et al.* (2003) 'p53 Binding Protein 53BP1 Is Required for DNA Damage Responses and Tumor Suppression in Mice', *Molecular and Cellular Biology*, 23(7), pp. 2556–2563. Available at: https://doi.org/10.1128/MCB.23.7.2556-2563.2003.

Warwick, R.A. and Hanani, M. (2013) 'The contribution of satellite glial cells to chemotherapy-induced neuropathic pain', *European journal of pain (London, England)*, 17(4), pp. 571–580. Available at: https://doi.org/10.1002/J.1532-2149.2012.00219.X.

Welch, G. and Tsai, L. (2022) 'Mechanisms of DNA damage-mediated neurotoxicity in neurodegenerative disease', *EMBO Reports*, 23(6). Available at: https://doi.org/10.15252/EMBR.202154217.

Wiffen, P.J. *et al.* (2017) 'Gabapentin for chronic neuropathic pain in adults', *The Cochrane database of systematic reviews*, 6(6). Available at:

https://doi.org/10.1002/14651858.CD007938.PUB4.

Wua, J. *et al.* (2013) 'The research applications of db/db mouse', *europepmc.orgJ Wua, HM Wang, J Li, XL MenSheng li ke xue jin zhan [Progress in physiology], 2013•europepmc.org* [Preprint]. Available at: https://europepmc.org/article/med/23671994 (Accessed: 25 September 2024).

Xie, W., Strong, J.A. and Zhang, J.-M. (2020) 'Localized sympathectomy reduces peripheral nerve regeneration and pain behaviors in 2 rat neuropathic pain models', *Pain*, 161(8), pp. 1925–1936. Available at: https://doi.org/10.1097/j.pain.0000000000001887.

Xie, W., Strong, J.A. and Zhang, J.M. (2010) 'Increased excitability and spontaneous activity of rat sensory neurons following in vitro stimulation of sympathetic fiber sprouts in the isolated dorsal root ganglion', *Pain*, 151(2), pp. 447–459. Available at: https://doi.org/10.1016/J.PAIN.2010.08.006.

Yu, Y. (2021) 'Gold Standard for Diagnosis of DPN', *Frontiers in Endocrinology*, 12. Available at: https://doi.org/10.3389/FENDO.2021.719356.

Z, Y. *et al.* (2018) 'Scoring systems to screen for diabetic peripheral neuropathy', *The Cochrane Database of Systematic Reviews*, 2018(7). Available at: https://doi.org/10.1002/14651858.CD010974.pub2.

Zang, Y. *et al.* (2023) 'Changes in the central nervous system in diabetic neuropathy', *Heliyon*, 9(8), p. e18368. Available at: https://doi.org/10.1016/j.heliyon.2023.e18368.

Zeisel, A. *et al.* (2018) 'Molecular Architecture of the Mouse Nervous System', *Cell*, 174(4), pp. 999-1014.e22. Available at: https://doi.org/10.1016/J.CELL.2018.06.021.

Zhang, S.-S.C. and J.-M. (2017) 'Progress in Sympathetically Mediated Pathological Pain Si-Si', *Physiology & behavior*, 176(3), pp. 139–148. Available at: https://doi.org/10.24015/JAPM.2015.0029.Progress.

Zhu, X. *et al.* (2022) 'Sympathectomy decreases pain behaviors and nerve regeneration by downregulating monocyte chemokine CCL2 in dorsal root ganglia in the rat tibial nerve crush model', *Pain*, 163(1), pp. e106–e120. Available at: https://doi.org/10.1097/j.pain.0000000000002321.

Ziegler, D. *et al.* (1999) 'Treatment of symptomatic diabetic polyneuropathy with the antioxidant alpha-lipoic acid: a 7-month multicenter randomized controlled trial (ALADIN III Study). ALADIN III Study Group. Alpha-Lipoic Acid in Diabetic Neuropathy', *Diabetes care*, 22(8), pp. 1296–1301. Available at: https://doi.org/10.2337/DIACARE.22.8.1296.

Zochodne, D.W. *et al.* (2001) 'Does diabetes target ganglion neurones? Progressive sensory neurone involvement in long-term experimental diabetes', *Brain : a journal of neurology*, 124(Pt 11), pp. 2319–2334. Available at: https://doi.org/10.1093/BRAIN/124.11.2319.